Pharmacological disruption of the microtubule array to determine the role of Golgi-nucleated microtubules in cancer cell migration

A Thesis

Presented to

The College of Graduate Studies

Austin Peay State University

In Partial Fulfillment

Of the Requirements for the Degree

Master of Science in Biology

Briar Bell

January, 2020

(This page is left intentionally blank.)

January, 2020

To the College of Graduate Studies:

We are submitting a thesis written by Briar Bell entitled "Pharmacological disruption of the microtubule array to determine the role of Golgi-nucleated microtubules in cancer cell migration". We have examined the final copy of this thesis for form and content. We recommend that it be accepted in partial fulfillment of the requirements for the degree of Master of Science in Biology.

Dr. Sarah Lundin-Schiller

Research/Committee Advisor/Chair

Dr. Amy Thompson

Committee Member

Dr. Marcia Schilling

Committee Member

Dr. Chad Brooks

Associate Provost and Dean, College of Graduate Studies

(Original signatures are on file with official student records.)

Statement of Permission to Use

In presenting this thesis in partial fulfillment of the requirements for the Masters of Science in Biology at Austin Peay State University, I agree that the library shall make it available to borrowers under the rules of the library. Brief quotations from this field study are allowable without special permission, provided that accurate acknowledgement of the source is made. Permissions for extensive quotation or reproduction of this field study may be granted by my major professor, or in his/her absence, by the Head of the Interlibrary Services when, in the opinion of either, the proposed use of the material is for scholarly purposes. Any copying or use of the material in this thesis for financial gain shall not be allowed without my written permission.

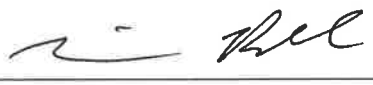

Briar Bell

1/10/2020

Date

ABSTRACT

Breast cancer is an increasingly common disease, with 1 in 10 women in the United States receiving a diagnosis of the disease during their lifetime. Taken alone, cancer of the breast is not particularly dangerous, however the tendency of this cancer to metastasize and move to other areas of the body greatly increase its mortality rate. The availability of breast cancer cell lines with varying migratory behavior make these cells useful models for studying molecular mechanisms of cellular motility.

One mechanism hypothesized to contribute to this motility has been increasingly studied in the past two decades. The discovery of a specific subset of microtubules in the cell which originate, or nucleate, at the Golgi have been the focus of this research. These structures have been linked to the transport of signaling molecules and proteins which interact with the extra cellular matrix. Due to their ability to polarize, these microtubules can deliver intracellular cargo directly to the leading edge of the cell, implicating them in directed cell migration.

Recent work by Laura Zahn in our lab has revealed an increased presence of these microtubules nucleated at the Golgi in cells with aggressive migratory behavior and cells treated with the chemotactic epidermal growth factor (EGF). Immunofluorescence microscopy was utilized for these observations. The objective of this thesis was to continue testing this hypothesis by observing the role of these microtubules in cell migration. This was accomplished utilizing pharmacological agents targeting the Golgi and microtubules to determine their effects on migration with a scratch wound assay. A secondary objective of this study was to determine if the morphology of the cells or organization of the Golgi and microtubules within the cell correlated to migratory behavior.

The migratory behavior of the less invasive MCF7 cell line was slightly reduced by the disruption of its Golgi with brefeldin-A (BFA) treatment, but not depolymerization of its microtubules with nocodazole treatment. However, the more invasive MDA-MB-231 cell line was significantly impacted by both of these disruptions. Supplementation with the chemotactic factor EGF had mixed effects. This treatment returned Golgi-disrupted migratory behaviors to levels nearly that of control cells. However, this treatment was unable to rescue the cells from their inhibited migratory behavior caused by global microtubule depolymerization induced by nocodazole treatment.

The morphology of the MDA-MB-231 cells was also affected by disruption of these structures. Treatment with either pharmacological reagent caused cells to lose adhesion to the matrix beneath the cells, causing them to round. This change in morphology, which was rescued with EGF supplementation, is associated with a significant reduction in migratory behavior

The results of this study build support for the current hypothesis that the Golgi-nucleated subset of microtubules play a critical role in directed cell migration, especially in a highly invasive cell type. It is likely that the disruption of these structures prevents polarized delivery of intracellular cargo, including the EGF receptor, affecting directional migration.

TABLE OF CONTENTS

LIST OF FIGURES

FIGURE PAGE

LIST OF TABLES

TABLE PAGE

CHAPTER I

Introduction

Written records of the occurrence of breast cancer date to the 30th century B.C. Early accounts describe the look and feel of the breast afflicted with this cancer (Lakhtakia, 2014). With invention of the microscope, descriptions of the cellular pathology of breast cancer developed in the 19th and 20th centuries (Lakhtakia and Chinoy, 2014). In 1713, Bernandino Ramazzini published his work on occupational related afflictions, observing that the incidence of cervical cancer in nuns was almost non-existent, however the incidence of breast cancer was very high in this same population (Ramazzini, 2001; Louis et al., 2015). This would later be ascribed to the fact that the nuns were not childbearing, so higher levels of estrogen in their bodies likely resulted in an increased incidence of breast cancer, as compared to the child-bearing women of the time. The foundation for elucidating the molecular mechanism of many forms of breast cancer was the discovery of estrogen receptors in certain breast cancers by Elwood Jensen (Jensen, 1975).

The formation of a cellular mass at the breast is not especially dangerous, however the metastatic potential of these cancers greatly increases their rates of mortality due to the alteration of the function of the organs to which they migrate. Many factors influence the ability of cells to travel in this way, including growth factors, hormones and other signaling molecules within the body.

With recent major advancements in cellular and molecular biology, scientists are better equipped to solve more narrowly focused questions about this disease. A number of discoveries within the last two decades have suggested that microtubules nucleated at the Golgi likely play a role in cell motility through the control of intracellular transport of signals, molecular motors and

the structures on which they operate (Bretscher and Velasco, 1998; Krendel et al., 2002; Mingle et al., 2005; Etiemme-Manneville, 2013). Interestingly, Laura Zahn recently observed the nucleation of microtubules at the Golgi in MDA-MB-231 cells, especially those that were migratory (Zahn and Lundin-Schiller, 2016). This observation suggests a potential mechanism which is targeted in this study to determine if these structures are in fact a major component of cellular motility, particularly in two breast cancer lines.

What follows in this chapter is a literature review highlighting a number of statistics about breast cancer, as well as a review of the molecular mechanisms causing cancer. Other topics are reviewed in this chapter, including the molecular mechanisms of cell motility, metastasis, intracellular transport and the nucleation of microtubules at the Golgi. The second chapter provides a brief explanation and history of the cell types utilized in this study. The third chapter follows with a review of the materials and methods of the study, while the fourth chapter presents results from experiments of the study. Finally, the fifth chapter is a discussion of the results that were obtained throughout the study.

Literature Review

Breast Cancer Statistics

With an estimated total annual economic cost reaching well over a trillion dollars, the impact of cancer is increasing every year, even as risk factors associated with the disease are identified (WHO, 2017). In the United States, cancer is the second leading cause of death, narrowly following heart disease by a difference of only 10 deaths per 100,000 people. While the mortality rate of each of these diseases has decreased over the last 40 years, the mortality of heart disease has decreased nearly three-fold compared to that of cancer (National Center for Health Statistics, 2017). Of the numerous types of cancers, lung, liver, colorectal, stomach and breast cancers account for the most common causes of death (WHO, 2017).

Approximately 12.4 percent of women from the United States will be diagnosed with breast cancer during their lifetime (SEER, 2015). In 2015 alone, there were 571,000 deaths due to breast cancer worldwide (WHO, 2017). However, the chances of survival in women with breast cancer strongly correlates to the stage of the cancer at diagnosis. Women with breast cancer that is diagnosed as localized have a high five-year survival rate at 98.7%, while this percentage drops to 27% in women with breast cancer that has migrated to another part of the body, even with current treatments (SEER, 2015). It is estimated that 30% of all new cases of cancers in 2018 will be cancer of the breast. This rate is almost three times as high as the rate of colorectal cancer, the next highest incidence of cancer (Stewart and Wild, 2014).

Breast Anatomy

The breast is an anatomical structure containing the mammary gland, adipose tissue, connective tissue, blood vessels, nerves and portions of the lymphatic system. Located just outside of the muscle of the chest and arm are lymph nodes, joined together by a system of lymph ducts that run throughout various of areas of the body. These work to remove harmful

compounds and molecules from the body. Also running along the muscles of the chest are arteries and capillaries, which transport oxygen-carrying blood cells toward and away from the breast. Directly beneath the breast is a layer of muscle, separating the structure from the ribs and inner body cavity. Outside of the muscle, and throughout the breast, are adipose tissue, ligaments and a number of connective tissues, retaining the shape of and protecting the mammary gland. Finally, the gland is organized into lobules, composed of many hollow sacs known as alveoli. When necessary, these sacs fill with milk, which is then transported from the lobule, through a duct, to the areola, which ends in the nipple. These ducts join together, forming larger ducts and delivering milk through the end of the nipple.

Cancer of the Breast

Breast cancer is the term describing a subset of over 20 different diseases affecting the breast (Lakhani et al., 2005). The majority of these cancers originate from the epithelial cells which line the lobules and ducts of the breast (Wellings et al., 1975). These cancers are known as carcinomas. A very small minority of breast cancers originate from other surrounding tissues, these are known as sarcomas (Berg and Hutter, 1995). Finally, a subset of cancer can arise in the lymphatic system located at the breast, known as a lymphoma. Breast cancer can exist as a non-invasive tumor consisting of epithelial-type cells that form from the duct or lobe. However, these cells can become more invasive, through mechanisms which will be described in more detail in this manuscript, and travel to other areas of the body.

Environmental Factors Contributing to Cancer

While mutations that cause cancer can be spontaneous, environmental factors affect the rate at which mutations occur. Substances that contribute to an increased incidence of mutations leading to cancer are known as carcinogens (Yamagiwa and Ichikawa, 1918; Kennaway, 1930;

Cook et al., 1933; Boveri, 2008). However, many of these substances will not affect the genome without the presence of downstream molecular mechanisms in the body, which will be addressed later in this chapter (Miller and Miller, 1947; Conney et al., 1956).

Tobacco is a major source of carcinogens still widely used worldwide, although its use in the United States has declined (Stewart and Wild, 2014). The smoke from tobacco contains a considerable number of compounds that are known carcinogens, including arsenic, benzene and formaldehyde. A more recent meta-analysis, considering 24 studies that represent nearly 98,000 women over 30 years, suggests that there is a positive correlation between smoking and breast cancer incidence (Gaudet et al., 2013). While more evidence is required to explain the mechanisms, these carcinogens potentially play a role in the development of breast cancer in smokers.

Alcohol is another source of carcinogens commonly consumed and abused throughout the world (IARC, 2010). Alcoholic beverages contain carcinogenic compounds in the form of acetylaldehyde and ethanol, among others (Lachenmeier et al., 2012). Acetylaldehyde can interact directly with DNA, while ethanol metabolites can cause oxidative damage, increase estrogen concentrations, which will upregulate the activity of estrogen-receptor positive cells, and affect DNA repair mechanisms (Barnes et al., 2000; Singletary et al., 2001). There are a number of studies that suggest a correlation between large levels of alcohol consumption and increased incidence of breast cancer. This is likely due to mammary gland developmental damage and increased cell proliferation, either through the activation of estrogen receptors or loss of cell cycle fidelity (Singletary and Gatspur, 2001; IARC, 2010).

Some infectious agents have strong positive correlations with many different forms of cancer, including *Heliobacter pylori* and gastric cancer, the hepatitis B and C viruses and liver

cancer, and finally human papillomavirus (Parsonnet et al., 1994; Donato et al., 1998; Herrero et al., 2003). In relation to breast cancer in particular, it appears that presence of human mammary tumor virus (HMTV) is highly associated with breast cancers within some populations and is passed from mother to offspring through breast milk (Holland, 2014).

Reproduction and, consequentially, hormonal influences are the major factors affecting cancers of the breast, cervix and ovaries (Stewart and Wild, 2014). Childbirth and age at conception, age at menarche and menopause, and breast feeding contribute to the likelihood of a number of these cancers (Bernstein, 2002; Collaborative Group on Hormonal Factors in Breast Cancer, 2012). The hormonal variation of these events has been suggested as the basis for increased incidence of cancers. For breast cancer in particular, any event that induces an increase in endogenous or exogenous estrogen to the body has a chance to increase the activity of estrogen receptor positive cancerous cells (Heldring et al., 2007).

The physical fitness and associated diet of an individual can contribute to the incidence of cancer (Stewart and Wild, 2014). There are studies linking diet to the incidence of a number of cancers. However, there is not conclusive evidence that it directly increases the incidence of breast cancer, especially after adolescence (American Institute for Cancer Research, 2007; Linos et al., 2008; Lee et al., 2009; Liu et al., 2011; Aune et al., 2012). Poor diet is linked to increased body mass due to adipose tissue deposits throughout the body. Obesity has been linked to a higher incidence of cancer, especially those of the breast and endometrium (IARC, 2002; American Institute for Cancer Research, 2007). The current hypothesis is that the presence of adipose tissue is responsible for an increase in circulating estrogen due to the presence and storage of cholesterol, a hormone precursor, in these tissues (Angel and Farkas, 1974; Stewart and Wild, 2014).

Radiation from the environment has been linked to a number of cancers, particularly melanomas, carcinomas and leukemias. The source of this radiation includes the sun, electromagnetic commercial and personal devices and radioactive medicine; however, conflicting results suggest a necessity for more evidence before a causative relationship can be supported, especially regarding electromagnetic radiation (Whiteman et al., 2003; Schüz and Albom, 2008; Muirhead et al, 2009; MacKie et al., 2009; Pearce et al, 2012; Stewart and Wild, 2014). Currently, a robust relationship between radiation and breast cancer is unsupported; however, there are studies that suggest patients with melanomas have an increased likelihood of breast cancer incidence (Wassberg et al., 1999; Borg et al., 2000).

There are many other environmental carcinogens, which come from manufacturing and other anthropogenic activities not listed above, that are responsible for common cancers, especially those of the skin, bladder and the lungs (HEI Asbestos Literature Review Panel, 1991; IARC, 2004, A; IARC, 2004, B; Samet and Cohen, 2006; HEI Air Toxics Review Panel, 2007; Claxton and Woodall, 2007; Lewtas, 2007; IARC, 2013; Loomis et al., 2013). One of these carcinogens, bisphenol-A, is hypothesized to correlate with an increased incidence of breast cancer. It is a loosely bound monomer used in plastic manufacturing (Brede et al., 2003). This compound mimics estrogen, binding and activating both estrogen receptor α and β, as well as other targets on the membrane and within the cell (Melzer et al., 2011; Delfosse et al., 2012; Pupo et al., 2012). It is likely that the estrogen mimicking behavior of this compound contributes to the incidence of breast cancer through the same mechanism as increased endogenous estrogen levels.

Molecular Mechanisms of Cancer

Cancer cells possess mutations in their genomes. These mutations can occur in the form of base addition, deletion or substitution. In cancerous cells, these mutations typically occur in genes that control cell growth and proliferation. When properly functioning, tumor suppressors inhibit the cell's ability to proliferate. Opposite of these genes are proto-oncogenes, which regularly promote the propagation of cells (Hanahan and Weinberg, 2011).

In an unaffected cell there are a number of factors controlling the progression of the cell cycle, however the majority of the cycle is controlled by cyclin proteins (cyclin A, B, D and E) and cyclin-dependent kinases (Cdks; Cdk 1, 2, 4 and 6) (Girard et al., 1991; van den Heuvel and Harlow, 1993; Nigg, 1995; Stern and Nurse, 1996). Cyclin proteins were named because of the cyclical nature through which they are present throughout the cell cycle. (Evans et al., 1983; Mathews et al., 1984; Celis and Celis, 1985; Nielsen et al., 1987). There are three major types of cyclins in the cell, G_1-, S- and M-cyclins, indicating in which phase they are active. The G_1-cyclins bind Cdks at the end of the G_1 phase and commit the cells to DNA replication (Nielsen et al., 1987; Wittenberg and Reed, 1988; Richardson et al., 1989). S-cyclins bind Cdks during the S phase and are required to initiate DNA replication (Celis and Celis, 1985; Girard et al., 1991). Finally, M-cyclins binding to Cdks promotes mitosis (Swinson et al., 1986; Fang and Newport, 1991; Johnston and Sloboda, 1992). Regulation of these complexes is done through the use of kinases (such as Wee1), phosphatases (such as Cdc25) and Cdk inhibitor proteins (CKIs) (Russell and Nurse, 1987; Sadhu et al., 1990; Harper et al., 1993; Gu et al., 1993; Xiong et al., 1993). Not only are the concentration of specific cyclins within the cell at any one-time ubiquitin dependent, but also transcriptionally controlled for differential expression, often by previously expressed cyclin-Cdk complexes. (Desai et al., 1992).

During proliferation, cyclin D is first activated when the cell receives a growth factor signal, which binds at the epidermal growth factor receptor (EGFR), a transmembrane protein. Growth factor binding to its receptor results in homodimerization, causing autophosphorylation of tyrosine residues of the cytoplasmic domain of the EGFR (Downward et al., 1984; Yarden and Schlessinger, 1987). Proteins bound to the receptor, such as growth factor receptor-bound proteins (Grbs), interact with another set of proteins, such as Son of Sevenless (SOS), that are activated and promote the exchange of guanosine diphosphate (GDP) to guanosine triphosphate (GTP) in Ras proteins (Schulze et al., 2005; Zarich et al., 2006). The activated Ras protein activates another cascade of proteins known as mitogen-activated protein kinases (MAPKs), beginning with c-Raf, or MAP Kinase, and ending with MAPK. Finally, MAPK can activate transcription factors, such as c-myc and c-fos, which contribute to cell cycle regulation by activating the transcription of other genes, including cyclin D (Campisi et al., 1984; Gruda et al., 1994).

Cyclin D binds to a constitutively expressed Cdk4, activating the retinoblastoma susceptibility protein (Rb) (Reed et al, 1991). This activation decouples Rb from a number of transcription factor genes, activating the expression of many cyclins, DNA polymerase and kinases. One of these products, cyclin E, binds to Cdk2, advancing the cell from G_1 to S phase (Dutta et al, 1991; Skotheim et al, 2008). At this point, the cycle can be arrested if there is detection of DNA damage. Either ataxia telangiectasia mutated (ATM, for double-strand breaks) or ataxia telangiectasia and Rad 3 related (ATR, for single-strand breaks) kinases are activated. These proteins activate Chk1 and 2, which are responsible for activating a number of DNA repair machinery, including p53 and breast cancer 1 (BRCA1) (Bartek and Lukas, 2001).

After DNA synthesis, there is expression and accumulation of another cyclin, cyclin B, which complexes with Cdk1 (Jackman et al., 2003). Sufficient accumulation initiates nuclear envelope breakdown and mitosis begins (Nurse, 1990). A subsequent checkpoint occurs during metaphase when the chromosomes should be aligned at the middle of the cell. Correct tension across the cell due to this alignment activates an anaphase-promoting complex (APC), which degrades cyclin B in the cell (Saxton and McIntosh, 1987; King et al., 1995; Gorbsky et al., 1999). APC activation is also responsible for the degradation of securin, which subsequently activates separase (Ciosk et al., 1998). Separase removes cohesins, which are keeping sister chromatids in close proximity (Michaelis et al., 1997; Waizenegger et al., 2000). Completion of this cascade allows the sister chromatids to separate, moving the cell into anaphase (Uhlmann et al., 1999; Uhlmann et al., 2000).

As a consequence of a very involved proliferative process, cells are susceptible to a number of mutations which can completely halt cell division or activate uncontrolled cell division. These mutations are the foundation for cancers and subsequent tumors that develop. Often, tumors consist of subsets of cells with their own set of mutations and accompanying proteomics. Examination of a number of breast cancers suggests that among them, there are a wide range of genes affected. Also, the number of genes in each of these cancers varies dramatically (Stephens et al., 2012). A select number of tumor suppressor genes commonly found to have mutations in incidences of breast cancer include cyclin proteins, *BRCA1*, *BRCA2*, *PTEN*, and *p53* (Keyomarsi and Pardee, 1993; Wooster et al., 1994; Hollstein et al., 1995; Ford et al., 1995; Mills et al., 2001). These proteins are responsible for controlling cell division, especially when there is damage to the DNA, which prevents an accurate replication. A number of proto-oncogenes with increased incidence of mutation associated with breast cancer include

human epithelial growth factor receptor 2 (*HER-2*), the cyclin family and *c-myc* (Slamon et al., 1987; Nass and Dickson, 1997; Steeg and Zhou, 1998). Mutations occurring in these sets of genes will often cause uncontrolled proliferation of the cell, resulting in the formation of a tumor, known as a primary tumor.

Metastasis

The migration of cancer occurs through a process known as metastasis. Metastatic development begins with a number of cellular mutations from which a primary tumor arises. The mutations are responsible for letting a single cell divide unimpeded. From here, a cell or cells from the primary tumor travel to another area of the body and form secondary tumors in this new location. While a number of factors affect the efficiency of metastatic cell movement, including microenvironment, a basic mechanism is shared among cancerous cell types (Hunter et al., 2008). Initially, cells separate from the primary tumor and invade surrounding tissues or basement membrane, eventually arriving at the blood or lymphatic circulatory system. The cells travel through these systems to another area of the body and adhere to vessels located on the organ in that area. Finally, these cells extravasate from their new location at the vessel into the adjoining organ tissue. At this point, the cells proliferate and form a secondary tumor, relatively far from the primary tumor (Beatson, 1912).

For metastatic cells to survive through this entire process, they must be able to traverse, survive and proliferate in a number of microenvironments, again provided by a number of genetic mutations (Fidler, 1989). From primary tumor proliferation, traveling through the circulatory system, and adherence and proliferation at a new site, these cells must contend with a number of immune responses from the body. Not only must the cells survive during this time, but they must also have the ability to respond to signaling molecules contained within the

microenvironments in which they are located, as well as other more broadly located environments. Because of the concentrated presence of these molecules in specific organs, breast cancer is much more likely to metastasize to the lymph nodes, bones and lungs than other organs (Mukherjee and Zhao, 2013).

Cell Migration

Cell movement is a foundational trait of metastatic cancer cells. As eluded to in the preceding subsection, cells move as a consequence of responding to the environment around them. A migratory response of a cell to a chemical or molecular signal from its environment is known as chemotaxis (Harris, 1954). One form of these signals are chemokines. These are a type of cytokines, or extracellular signal proteins or peptides active in cell-cell communication, which are expressed by tissues and bind to receptors on target cells. Breast cancer cells in particular respond to two known chemokines, C-X-C chemokine ligand 12 (CXCL12), also known as stromal derived factor-1 (SDF-1), and epidermal growth factor (EGF) (Voldborg et al., 1997; Muller et al., 2001). EGF specifically is known to be a major regulator in cell growth and proliferation (Cohen, 1965; Rose et al., 1975; Carpenter and Cohen, 1976). Interestingly, cells that are in a group can release and respond to EGF in an autocrine fashion (Wiley et al., 1998). There is evidence that the cellular response of migrating epithelial cells to this signaling is modulated through the previously discussed MAPK pathway (Joslin et al., 2007). Furthermore, cell migration has been confirmed to be modulated cooperatively by gradients of SDF-1 and EGF in a breast cancer cell line (Kim et al., 2013). A recent, unpublished study from our lab supports that a 10 ng/mL treatment of MCF7 and MDA-MB-231 cells is sufficient for increased cellular motility (Grady and Lundin-Schiller, personal communication).

It is hypothesized that the chemotactic response of these cells to EGF is due to its effect on downstream focal adhesion kinase (FAK) expression, which is also a consequence of estrogen signaling (Brunton et al., 1997; Harder et al., 1998; Sieg et al., 2000; Hauck 2001). The specific mechanism of estrogen action is currently unknown, however EGF treatment has been observed to phosphorylate the FAK, targeting it to the area of focal adhesions and increasing cell migration (Lu et al., 2001). It has been suggested that these responses are dissociated from proliferative pathways in the MDA-MB-231 cell line, solely affecting migration (Price et al., 1999). Migratory response to estrogen relies on many different components, including estrogen receptor α, FAK, paxillin, phosphatidylinositol 3 kinase (PI3K) and MAPK, although the specific interplay between these pathways, if one exists, is unclear (Li et al., 2010). The components within the cell on which these signals traverse is a potential target for determining the mechanism in which these signals function to affect motility.

Cells also have the ability to respond to mechanical and electrical stimuli in their environment, in processes called mechanotaxis and electrotaxis, respectively (Zhao, 2009; Roca-Cusachs et al., 2013). During mechanotaxis, cells recognize physical forces in the environment and respond through a biochemical pathway within the cell, resulting in an associated movement (Roca-Cusachs et al., 2012). These forces can occur through a number of avenues: cell movement due to substrate stiffness, manipulation of the extra-cellular matrix (ECM) and collective modulation of intracellular forces have been observed (Lo et al., 2000; Reinhart-King et al., 2005; Tambe, 2011). One mechanism for sensing this gradient is the ability of force to cause conformational changes in a number of molecules, resulting in a signaling cascade which is expressed as movement (Roca-Cusachs et al., 2012). Force responses to the environment begin with integrin binding to the extracellular matrix (ECM). With the application of force, integrins

will unbind and rebind with components of the ECM, while also interacting with the varied structures to which they are bound, known as adapters, including α-actinin, filamin and tensin, each of which can interact with the actin cytoskeletal structure (Pavalko et al., 1991; Lo et al., 1994; Loo et al., 1998). The activation of the adaptor proteins can activate guanine exchange factors (GEFs), which affect a number of other downstream processes (Rottner et al., 1999; Tomar and Schlepfer, 2009; Guilluy et al., 2011).

Interestingly, cells can communicate cell movement as a group, resulting in the movement of an entire cluster of cells, as is the case in an invasive cancer (Friedl et al., 2012). In recent studies, preference for perpendicular intercellular forces and substrate with deformations was observed (Angelini et al., 2010; Tambe, 2011). Although the exact mechanism is currently unknown, it is likely that cancer cells use these mechanosensory traits to migrate *in vivo*.

As human breast cancer cells are eukaryotic cells, there are a number of components involved in the molecular mechanism of cell motility. The major contributor to cell movement is the array of protein filaments that are located throughout the cell that are known collectively as the cytoskeleton. These three filaments are actin filaments, intermediate filaments and microtubules (Tilney and Gibbins, 1969; Menko et al., 1983; Tanaka et al., 1995). Motor proteins are required for the function of these arrays. Often, epithelial cells, including those that are non-cancerous in the breast, maintain a stable structure (Asch et al., 1979; Fey et al., 1984). However, many of the filamentous components comprising this structure are dynamic and will be recycled regularly. The filament cytoskeleton structure organization is responsible for the polarization, or directionality, of these cells that are motile (Allen and Borisy, 1974; Small et al., 1978). While this chapter will briefly review the motor proteins and actin filaments, the microtubules are of most concern to this project.

Motor Proteins

One set of accessory proteins that are involved in cell motility are known as motor proteins (Vale, 2003). These proteins, responding to intra- and extracellular signaling, utilize the energy available in ATP hydrolysis reactions to move components of the cell along the filamentous cytoskeleton. The effect of these proteins on the filaments produces the cellular-wide movement observed during migration.

Motor proteins function by binding to a molecule, undergoing a conformational change and then moving along from that molecule to another nearby. Motor proteins can vary in structure and location, from the mitochondrial membrane-located ATP-synthase motor, to those located in the nucleus that function in the replication of genetic material, such as polymerases and helicases (Gelles and Landick, 1998; Rondelez et al., 2005). However, the most relevant category of motor proteins to this study are cytoskeletal filament motor proteins. These include dyneins, kinesins and myosins, each of which travel along microtubules or actin filaments.

Two major classes of motor proteins are kinesins and dyneins. The majority of kinesins transport membrane-enclosed organelles by "walking" toward the plus end of the microtubule, however some transport cargo in the opposite direction (Scholey et al., 1985; Vale et al., 1985a; Vale 1985b). Dyneins are responsible for movement in the minus direction of the microtubule (Gibbons and Rowe, 1965; Haimo et al., 1979). This family of proteins is responsible for the organization of the nucleus and centrosome during migration, as well as mRNA and organelle trafficking, and the molecular movement required for beating flagella and cilia (Gibbons and Rowe, 1965; Renaud et al., 1968; Muhua et al., 1994; Xiang et al., 1994; Langford, 1995; Durrbach et al., 1996). The formation of the endoplasmic reticulum (ER) and the Golgi apparatus (Golgi) rely on these motor protein and microtubule interactions. Kinesins are responsible for the

positioning of the ER throughout the cell, while dyneins are responsible for the positioning of the Golgi near the centrosome at the center of the cell (Vale and Hotani, 1988; Harada et al., 1998; Bannai et al., 2004)

The other major class of motor proteins is myosin. There are many myosin proteins that have been identified; however, myosin I is involved in the transport of cargo throughout the cell (Adams and Pollard, 1986; Adams and Pollard, 1989; Fath et al., 1993; Fath et al., 1994, Bose et al., 2002). Myosin consists of three different domains: head, neck and tail (Baryiko et al., 1992). The head domain of the myosin is an ATPase that undergoes a conformational change and exerts force along the actin of the cell (Jontes et al., 1995; Veigel et al., 1999). The tail domain is the portion of the myosin that is attached to the membrane-bound vesicle transporting cargo in the cell (Hayden et al., 1990; Doberstein and Pollard, 1992; Brzeska et al, 2010).

Actin

The actin subunit is highly conserved across eukaryotes (Stoddard et el., 2017). It is globular as a free subunit; however multiple subunits polymerize to form a helical structure known as filamentous actin (Straub, 1942; Pantaloni et al., 1984; Pantaloni et al., 1985; Kabsch et al., 1990). While this structure is rather fragile on its own, a number of accessory proteins cause the filament to interact and bundle together, forming a larger, more durable structure (Wessells et al., 1971; Rosenberg et al., 1981). Because the subunits organize in a polarized fashion, the filamentous actin structure contains both a quickly elongating, “plus” end, and a more slowly elongating, “minus” end (Hitchcock-DeGregori, 1980). At a large scale, this behavior can associate polarity to an entire cell.

The actin filaments organize in arrays, forming higher-order structures which allow for motility (Anderson, 1977). Specifically, the actin filaments can be organized in loosely packed

structures known as contractile bundles. The spacing of the bundles allows them to interact with motor proteins, including myosin, to create tension between, and as a result, movement of the actin filaments (Mooseker, 1976). These structures can also adhere adjacent cells together through adherens junctions, especially between epithelial cells (Rodewald et al., 1976; Hull and Staehelin, 1979).

One important actin-based structure that cells utilize to migrate are lamellipodia. These are actin projections that protrude from the leading edge of cells (Taylor et al., 1973; Edds, 1977). This structure is a result of the nucleation of actin at the plasma membrane, and the polarization of these structures allow for a tread-milling effect of the actin, resulting in cell crawling (Edds, 1977; Kirschner, 1980; Herman et al., 1981; Wang, 1985). Ahead of the lamellipodia are filopodia, which act as a leading point as cells encounter their environment and associated molecular cues (Albrecht-Buehler, 1976).

Microtubules

Microtubules are another integral actor in the cytoskeleton network. Much like actin subunits, free subunits of α-tubulin and β-tubulin found throughout the cell exist in the globular form (Feit et al., 1971, Erickson, 1974; Snyder and McIntosh, 1975; Cleveland et al., 1978). The monomer subunits each have a binding site for the GTP molecule, which is utilized in their dimerization (Feit et al., 1971; Shelanski et al., 1973; Kobayahi, 1975). The α-tubulin and β-tubulin subunits polymerize as dimers, in an alternating pattern, to form protofilaments that interact in parallel to form hollow tubes (Warfield and Bouck, 1974; Bryan, 1976; Langford, 1980). The subunit organization provides polarization to the microtubule structure (Heidemann and McIntosh, 1980).

Microtubules exhibit a quality known as dynamic instability in which they can quickly alternate from an extending activity to a shrinking activity due to GTP- and GDP-bound tubulin dynamics (Mitchison and Kirschner, 1984). Tubulin subunits with a bound GTP are likely to polymerize with the leading subunit of the protofilament, meanwhile the subunits with a converted GDP molecule will have a weakened bond and likely dissociate (Carlier and Pantaloni, 1981; Hill and Carlier, 1983; Carlier et al., 1984). While the plus end of the microtubule is usually occupied by a GTP-bound subunit, the addition of a GDP-bound subunit will prevent the addition of a new subunit, causing the dissociation of the end of the microtubule, also known as catastrophe (Mitchison and Kirschner, 1984). After a free GTP-bound subunit is able to polymerize with the collapsing end, the microtubule is "rescued" and growth can continue in the plus end direction (Mitchison and Kirschner, 1984; Cassimeris et al., 1988; Billger et al., 1996).

Proteins that bind to and modulate these structural changes of the microtubules are generally known as microtubule associated proteins (MAPs) (Sloboda et al., 1975; Murphy and Borisy, 1975; Sloboda et al., 1976). Examples of each include XMAP215, which promotes microtubule nucleation, and kinesin-13, which promotes destabilization of the growing microtubule (Gard and Kirschner, 1987; Vasquez et al., 1994; Walczak et al., 1996; Desai et al., 1999). The frequency of the interactions of MAPs with the microtubules controls the dynamics of these structures observed throughout the cell.

The ER and Golgi organelles form the cellular hub from which proteomic and molecular cargo are sorted and distributed throughout the cell (Porter, 1964). Membrane-bound and soluble proteins that are to be secreted are manufactured in the rough ER, then mature as they travel through the Golgi (Porter 1964; Caro and Palade, 1964). From here, this cargo is sent to the plasma membrane from the *cis*-Golgi or sent back to the ER from the *trans*-Golgi (Pelltier,

1974). The importance of these structures for cargo transport, which includes the components required for cell motility, make them potential candidates of interest for studies based on disrupted migration.

Golgi-Nucleated Microtubules

To function, microtubules nucleate at specific regions of the cell. These areas are known as microtubule organizing centers (MTOCs) (Slautterback, 1963; Frankel F, 1976; Osborn and Weber, 1976; Stearns and Brown, 1979). Typically, this occurs at the centrosome of the cell; however, the Golgi has also been implicated as another MTOC (Slautterback, 1963; Kupfer et al., 1982; Wehland et al., 1983; Rogalski and Singer, 1984). Before microtubules can form, a template must be recruited to the Golgi (Kollman et al., 2011). This precursor is a ring complex known as the γ-tubulin ring complex (γTuRC) (Mortiz et al., 1995; Zheng et al., 1995). The complex consists of a smaller ring complex known as the γ-tubulin small complex (γTuSC), itself made of a spiral ring of multiple γ-tubulin and γ-tubulin complex proteins (GCP2 and GCP3), as well as other γ-tubulin complex proteins (GCP4, GCP5, GCP6) (Murphy et al., 1998; Murphy et al., 2001; Kollman et al., 2008). GCP4, GCP5 and GCP6 stabilize the γTuSC, while GCP3 regulates α-tubulin and β-tubulin subunit binding, nucleating microtubule formation (Janski et al., 2012; Nakamura et al., 2012). Currently, microtubule nucleation at the Golgi has not been observed without an associated γTuRC recruitment. A number of proteins have been implicated in the recruitment of the γTuRC to the Golgi, however two of them appear to be vital (Takahashi et al., 2002; Rivero et al., 2009). GM130 (Golgi matrix protein of 130 kD), a Golgi peripheral protein, recruits a large signaling protein, AKAP450 (A-kinase anchor protein 450) to the *cis*-Golgi compartment. In turn, the γTuRC is recruited and tethered to the AKAP450, allowing newly formed microtubules to nucleate at the Golgi (Rivero et al., 2009).

An immortalized human pigment epithelial cell line (hTer-RPE1) was the model system used in experiments to identify the components that localized the microtubule nucleation to the Golgi (Rivero et al., 2009). More recently, our lab utilized two breast cancer cell lines (MDA-MB-231 and MCF7) to perform co-localization studies of two components of the nucleation complex described above, GM130 and γ-tubulin (Zahn and Lundin-Schiller, 2016). These studies used microscopic analysis of fluorescently labeled co-localizations and found that these same proteins co-localize in both novel cell lines. The study also used microscopy to visualize microtubule depolymerization and reassembly at the Golgi, as well as EGF induced migrations. It was found that co-localization was increased in cells induced to migrate, as well as the highly invasive cell line (MDA-MB-231), marking the potential impact of the microtubules on directed migration activity. This is in agreement with other groups who have suggested a unique role for Golgi-nucleated microtubules in cell motility, including modulation of exocytosis toward the leading edge and crosstalk between the cytoskeletal pathways of actin and microtubules (Schmoranzer et al., 2003; Kaverina and Straube, 2011). The contribution of this population of microtubules to cellular migration in both cancer cell lines is going to be considered further in the current study.

Current Drugs/ Targets for Breast Cancer Treatment

Historically, medical doctors have used surgery to remove cancer within the body, with recurrence very likely (Madden et al., 1972; Allen, 2005; Lakhtakia, 2014). In the latter half of the twentieth century, the addition of chemotherapy expanded the tools available to fight cancer (Goodman et al., 1984; Wickerman et al., 2008). While these are still very valuable tools, the methods for targeting cancer have changed dramatically in the modern era of oncology (Ades et al., 2017).

Today, breast cancers are designated by the molecular components they express, including a number of receptors and cytoskeletal or mechanical components (Perou et al., 2000; Sørlie et al., 2001). Hormone receptors on these breast cancers, when expressed, remain a major therapeutic target (Tryfonidis et al., 2016). Trastuzumab, an antibody for HER-2, is a drug currently available that utilizes an immunological relationship to deliver chemotherapy to HER-2 overexpressing cells (Coussens, 1985; Baselga, 1986). Neratinib and lapatinib are two tyrosine-kinase inhibitors that are currently FDA-approved for the treatment of breast cancer (Xia et al., 2002; Rabindran, 2004). Many other targets are under review and include proteins involved in the cell-cycle (Verzenio) and DNA repair (Tate et al., 2014; Gelbert et al., 2014). One final treatment that is growing in potential is the use of immunotherapies, which utilize the body's immune system to identify and destroy cancerous cells within the body.

Drugs Targeting the Golgi and Microtubules

Pharmacological agents can be utilized to determine if the Golgi-nucleated microtubules are implicated in the control of cellular migration. One candidate, nocodazole, is a potent antineoplastic and microtubule inhibitor. In non-transformed embryonic mouse cells, nocodazole completely depolymerizes microtubules, with only diffuse staining of microtubules evident after treatment (de Brabander et al., 1977). This occurs through the binding of nocodazole to free tubulin dimers, preventing further polymerization (Hoebeke et al., 1976). In addition, evidence from previous experiments show that nocodazole treatment is accompanied by a decrease in migration in invasive cell types, including mouse fibroblasts and macrophages (Mareel and de Brabander, 1978; Storme and Mareel, 1980; Cheung and Terry, 1980; Bershadsky and Futerman, 1994). Along with a reduction in the motility of cells treated with nocodazole, this treatment also reduces the secretion and transport of proteins within the cell, while also diminishing or

eliminating the polarity of the presence of these proteins (Birkett et al., 1981; Rogalski et al., 1984; Johnson and Maro, 1985; Rindler et al., 1987; Sinha and Wagner, 1987). Nocodazole appears to affect other structures in the cell as well, eliminating the endocytic delivery of lysosomal cargo (Deng and Storrie, 1988).

The second pharmacological agent used in treatments during this study is brefeldin-A (BFA). This compound is a metabolite, produced by the fungus *Eupenicillium brefeldianum*, which acts on the flow of cargo from the *trans*-Golgi network (TGN) to the cell membrane (Singleton et al., 1958; Misumi et al., 1986). The mechanism through which this molecule functions is by preventing exchange of GDP for GTP on the ADP-ribosylation factor (ARF), preventing COP-β from binding to secretory vesicles, and subsequent loss of the Golgi structure. This binding is a requirement for stable vesicles which bind to the Golgi and allow for delivery of the cargo elsewhere in the cell, outside of the ER (Magner and Papagiannes, 1988; Lippincott-Schwartz et al., 1989; Ulmer and Palade, 1989; Donaldson et al., 1990; Serafini et al., 1991; Orci et al., 1991; Miller et al., 1992; Donaldson et al., 1992; Hendricks et al., 1992). Notably, BFA treatment prevents proper protein secretion to the polarized ends of the cell as a consequence of an inhibited trafficking system, resulting in accumulation of secretory protein at the ER (Fujiwara et al., 1988; Low et al., 1991; Hunziker et al., 1991; Rosa et al., 1992). This phenomenon is conserved in invertebrates as well, with similar effects observed in *Candida albicans* (Arioka et al., 1991).

A number of studies have utilized both drugs, to determine their effect on trafficking and migration. The data support that BFA and nocodazole had comparable effects on cell shape and protrusion, with similar reductions in cell motility (Bershadsky and Futerman, 1994; Tseng et al., 2014). However, one current hypothesis is that BFA affects sorting solely, while nocodazole

attenuates delivery of intracellular cargo to the plasma membrane (Cid-Arregui et al., 1995; Porowska et al., 2008). Utilizing these compounds to determine the role of Golgi-nucleated microtubules in breast cancer cell migration is novel, as the contribution of each subset in this particular cancer is currently unknown.

Study Objectives

The first objective of this study was to determine if pharmacological agents known to alter the Golgi or microtubules were sufficient for inhibiting the migration of MCF7 or MDA-MB-231 breast cancer cell lines in a wound healing scratch assay. Inhibition of this movement suggests a role for these molecular components in the process of cell migration.

The second objective of the study was to determine if the inhibited migration was correlated with a morphological change accompanying pharmacological agent treatment. This was studied by utilizing pharmacological reagents and light microscopy.

The third objective of the study was to determine if the morphological change in these cells correlated with a change in the organization of the Golgi and the microtubules. This was studied by tracking these structures through immunofluorescence of their components, specifically GM130 and α-tubulin.

The final objective of the study was to determine if exogenous growth factors could rescue the cells from an inhibited migratory state, with an accompanying morphological change. This study utilized the addition of EGF and FBS to treatments, as well as all other previously discussed methods of observation.

CHAPTER II

Cell Types

MCF7 Breast Cancer Cell Line

The MCF7 cell line was isolated by Herbert Soule at the Michigan Cancer Foundation from the pleural effusion of a 69-year-old nun, Sister Catherine Frances Mallon (Soule et al., 1973). Interestingly, she was a member of the same occupational population in whom Ramazzini had observed higher rates of cancer of the breast (Ramazzini, 2001; Louis et al., 2015). After attempting to culture metastatic breast cancer cells from both Sister Mallon's chest wall and lungs, Soule observed a recurring culture of those cells from the lungs (Soule et al., 1973). This cell line gets its name from the location that the work was done, the Michigan Cancer Foundation, and because this was Soule's seventh attempt to cultivate a cancer cell line. The popularity of this cell line for research has been robust, with 25,000 published papers using this cell line (Lee et al., 2015).

The isolation of these cells was a major discovery and laid the foundation for future breast cancer research. While Soule observed estrogen receptors in the cells, researchers also observed the efficacy of tamoxifen, a selective estrogen receptor modulator, on treating breast cancer that same year (Brooks et al., 1973; Ward, 1973). Over the next two decades, the results of numerous studies supported estrogen as the driving component in breast cancer tumor growth (Levenson and Jordan, 1997). Further studies have supported the presence of estrogen and progesterone receptors on these cells, making them viable candidates for targeted therapy (Lippman and Bolan, 1975; Horwitz et al., 1975). In this same time span, tamoxifen use with MCF7 cells was studied extensively (Osborne et al., 1983; Sutherland et al., 1983).

The first antibodies for estrogen receptors were created using receptors isolated from MCF7 cells, giving insight into their mechanism of action in the cell (Greene et al. 1980; King

and Greene, 1984). Lines of both estrogen receptor-positive and estrogen receptor-negative MCF7 cells have since been produced, while the discovery of tamoxifen-induced proliferation has also been observed (Osborne, 1996; Gottardis and Jordan, 1988; Jeng et al., 1998; Oesterreich et al, 2001; Sweeney et al., 2012). In addition to the presence of estrogen receptors, EGFR and HER-2 receptors have been observed in the cell line, although most agree that the parental cell line is HER-2 negative (Baguley and Leung, 2011).

The phenotype of these cells is epithelial, with robust expression of typical epithelial molecular products, while lacking the expression of mesenchymal products. The cells exist in small, compact colonies with some cells on the edge of the colony expressing an altered morphology (Pérez-Yépez et al., 2012; D'Anselmi et al., 2013). Because of the organization of these colonies, MCF7 cells have low migratory potential (Gest et al., 2013). No metastasis has been observed with transplantation of these cells into a mouse model (Perrot-Applanat and Di Benedetto, 2012). While estradiol increases proliferation of these cells, they are hardy enough to survive in the absence of serum, albeit with reduced proliferation as a consequence (Barabutis et al., 2007).

MDA-MB-231 Breast Cancer Cell Line

Throughout the 1970's, nineteen breast cancer carcinoma cells lines were established at the M.D. Anderson Hospital and Tumor Institute, including the MDA-MB-231 cell line. This cell line originated from the pleural effusion of a 51-year-old female patient with a metastatic adenocarcinoma, who died within one year of cell culturing (Cailleau et al., 1978).

Immunohistochemical analysis of this cell line has suggested that it is triple-negative for estrogen receptors, progesterone receptors (PRs) and HER-2. However, EGFR is overexpressed in this same cell type (Subik et al., 2010). Because MDA-MB-231 cells lack the expression of these receptors, they are not a viable candidate for the popular therapeutic targets that currently exist (Chen and Russo, 2009).

MDA-MB-231 cells form loosely cohesive groups of cells, with individual cells being highly migratory and invasive (Gordon et al., 2003; Bozzuto et al., 2015). The difference in migratory potential between MCF7 and MDA-MB-231 cells make them viable candidates for comparison in this study. The over-expression of EGFR in MDA-MB-231, as compared to MCF7 cells, is another useful difference for the purpose of this study.

CHAPTER III

Materials and Methods

Cell Culture

MDA-MB-231 and MCF7 cells (MDA-MB-231: American Type Culture Collection (ATCC), catalog #HTB-26 and MCF-7: ATCC, catalog #HTB-22) were grown in Dulbecco's Modified Eagle's Medium (DMEM) (ATCC, catalog #30-2002) supplemented with 10% fetal bovine serum (FBS: ThermoFisher Scientific, catalog #10082-139) and 2% antibiotic/ antimycotic (ThermoFisher Scientific, catalog #15240-096) and incubated at 37 °C in an atmosphere of 5% CO_2 in air. To ensure genetic continuity between cells used during experimentation, an initial aliquot of cells was grown to confluence in 25-cm^2 seed flasks (Falcon, catalog #353109), approximately 7 days for MDA-MB-231 cells and 10 days for MCF7 cells. Media was replaced every other day for cell viability and proliferation. Upon confluence, cells were harvested by incubation in 3 mL 0.5% trypsin-EDTA in PBS (phosphate buffered saline: Gibco, catalog # 15400-054) for 5 minutes. After this incubation period, 2 mL fresh DMEM was added to quench the reaction. This solution was centrifuged for 10 minutes, pelleting the cells.

The trypsin-EDTA-DMEM solution was decanted and pellets were suspended in fresh media. Cells were counted as follows: a 200 µL aliquot of cell suspension was suspended in 300 µL Hanks' Balanced Salts Solution (HBSS: ATCC, catalog #30-2213) and 500 µL 0.4% Trypan Blue (Trypan Blue Solution: Sigma, catalog #T8154-100mL). The solution was then thoroughly mixed and incubated for 10 minutes at room temperature. After incubation, a 20 µL aliquot of the solution was pipetted into the chambers of a hemocytometer and observed using a Meiji inverted phase contrast microscope. Cells were counted within the middle and corner squares

located in the chambers of the hemocytometer. The number of cells was then multiplied by a dilution factor of 5 and an extrapolation factor of 10^4. The result of this equation was equivalent to the total number of viable cells per milliliter (mL) in the solution.

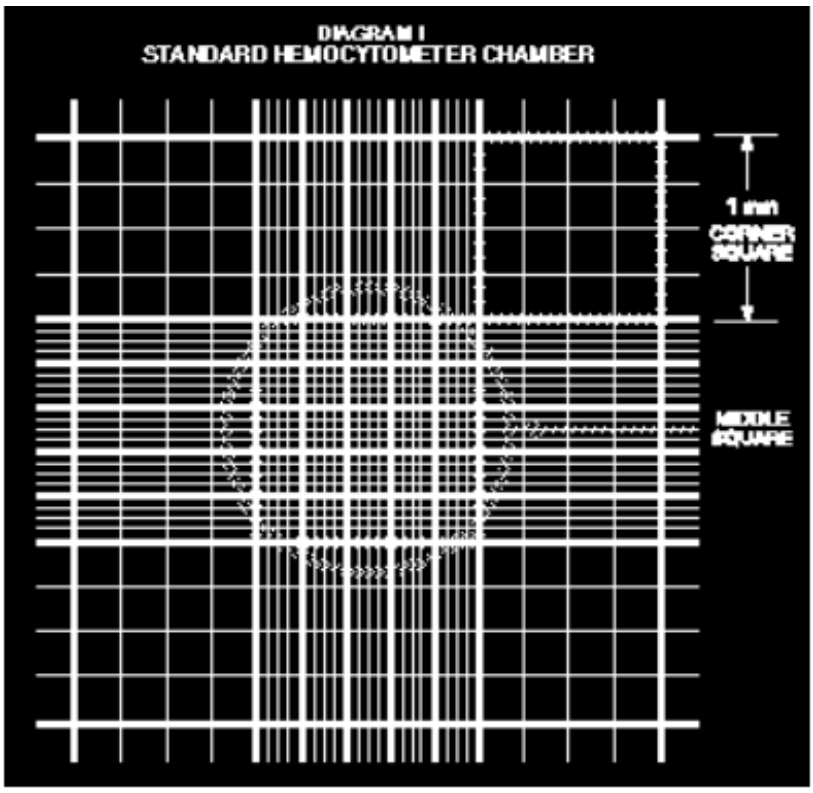

Figure 1. Hemocytometer grid used for counting viable cells from culture.

These cells were then separated into aliquots containing 100,000 cells diluted with 1 mL DMEM. Each of the aliquots was frozen at -80 °C, over a 24-hour period. After 24 hours, all aliquots were moved to liquid nitrogen until needed.

Once cells were required, the frozen aliquot was moved from liquid nitrogen to a sterile fume-hood at 20 °C. After the aliquot had thawed, the cells were transferred to a sterile 15-mL conical and diluted with 4 mL of DMEM. To re-suspend the cells into the media, the conical was agitated until the media was homogenous. The cells were then spun at 1000 x g for 10 minutes to pellet cells. The pellet was resuspended in 5 mL fresh media and cells were counted and diluted with DMEM to the appropriate concentration for experimentation.

Migration Study

To determine the effect of pharmacological treatments on the migration potential of cells, treatments were applied and cell migration was analyzed. Cells were plated on a 24-well plate at a density of 80,000 cells per well for MCF7 experiments and 40,000 cells per well for MDA-MB-231 experiments. Cells were then incubated in 500 µL DMEM, supplemented with 10% FBS and 2% antibiotic/ antimycotic, at 37 °C in an atmosphere of 5% CO_2 in air for 7 days. Media was replaced every other day. After 6 days, the cells were starved to force all cells into interphase and remove the effect of any potential endogenous signaling between cells, by replacement of the media with 500 µL serum-free DMEM. After 24 hours, an approximately 800 µm scratch was made through the middle of the well using a P-200 micropipette tip. A line was drawn perpendicular to the scratch with a permanent marker, this served as a reference for the field of view of the scratch. The serum-free media was removed, and the wells were rinsed with serum-free media to remove any cellular debris. After rinsing, the media was decanted and 500 µL treatments were added to the wells.

Images of the assay were acquired immediately after the application of the treatment, as well as at 12 and 24 hours, using an Olympus IX71 Inverted Phase Contrast Microscope and QCapture software. Scratch assays were analyzed using ImageJ software. A line was measured across a reference distance and this scale was applied globally to all pictures of the experiment. Five equidistant points, within the reference line, were selected along the top edge of the scratch, and straight lines were drawn to the bottom edge. These lines were then measured in micrometers using the software. To calculate an initial gap distance, the mean distance of the five lines was determined. To determine the change in gap distance at subsequent times, each of

the five lines at the next time point were subtracted from the initial gap distance. These differences were averaged for a calculated change in gap distance.

Statistical analyses of the scratches were done using JMP Pro 12 statistical software. Differences in gap distances between time points were analyzed by a *t-test*, while differences in gap distances between treatments were analyzed using a *t-test* or an ANOVA.

Morphology Study

To determine the effect of pharmacological treatment on the morphology of cells, treatments were applied and images were collected. Thirty-five mm glass-bottom dishes were pre-treated with poly-L-lysine for 2 hours to promote cell adherence. After this pre-treatment period, cells were plated at a density of 25,000 cells/mL using a total volume of 2 mL per plate. Cells were incubated for 24 hours at 37 °C in an atmosphere of 5% CO_2 in air. After 24 hours, the DMEM was removed and replaced with serum-free DMEM and incubated for 24 hours in the same conditions. Finally, the serum-free medium was removed and replaced with the pharmacological treatment. Images of the cells were obtained immediately after addition of the treatment, then every 2 hours over the subsequent 12 hours and again at 24 hours.

Representative morphologies for each time point and treatment were determined with images obtained using a Nikon Eclipse Ti2 microscope with differential interference contrast (DIC) imaging and NIS-Elements Advanced Research Version 5 software. Morphologies of cells in 10 fields of view were compared. Those morphologies with at least 51% consistency were considered the predominant phenotype.

Immunofluorescence Study

To visually determine the effect of pharmacological treatment on the Golgi and microtubule array of the cells, treatments were applied and images were collected. Two mL of

cell suspension was plated on a 35-mm glass bottom dish at a density of 25,000 cells/mL. Cells were incubated for 24 hours at 37 °C in an atmosphere of 5% CO_2 in air. After 24 hours, the DMEM was removed and replaced with serum-free DMEM and incubated for 24 hours in the same conditions. After starvation, the cells were incubated for 12 hours, also in the same conditions, with the pharmacological treatment.

Fixation of the cells was required for immunofluorescence. After the 12-hour treatment, enough ice-cold anhydrous methanol (Sigma-Aldrich, catalog # 322415-100mL) to cover the bottom of the dish was added and the plates were incubated at -20 °C for 5 minutes. After this fixing period, the dishes were washed three times with sterile PBS (Cellgro, catalog #21-040-CV) at 20 °C and then left in 2 mL PBS overnight at 5 °C to rehydrate the cells.

The following day, the PBS was removed from the dishes and replaced with 2 mL blocking buffer (5% horse serum, ThermoFisher Scientific, catalog #16050-130; 1% bovine serum albumin, BSA: Sigma-Aldrich, catalog #A7034; and PBS). After blocking, the buffer was removed and 2 mL α-tubulin 1° antibody (Ab) (1:800 monoclonal rat α-tubulin 1° Ab: ThermoFisher Scientific, catalog #MA1-80017; 5% horse serum, 1% bovine serum albumin, PBS) was added and cells incubated for one hour at 20 °C. After incubating, the cells were rinsed with PBS three times for five minutes each. Then, cells were incubated with 2 mL GM130 1° Ab (1:800 polyclonal rabbit GM130 1° Ab: ThermoFisher Scientific, catalog #PA1-077; 5% horse serum, 1% bovine serum albumin, PBS) for one hour at 20 °C. Again, cells were washed with PBS three times for five minutes each. After 1° Ab incubation, the cells were incubated with 2 mL Alexa-Flour 568 (anti-rat Alexa-Flour 568 2° Ab: Thermofisher Scientific, catalog #A-11077) and Alexa-Flour 488 (anti-rabbit Alexa-Flour 488 2° Ab: Thermofisher Scientific, catalog #A-21206) in 5% horse serum, 1% bovine serum albumin and PBS for one hour at 20 °C.

After the incubation period, the 2° Ab solution was removed, and 2 mL sterile PBS was added for storage. Plates were kept at 20 °C in the dark while not in use.

After the addition of sterile PBS, images of the cells were obtained using a Nikon Eclipse Ti2 microscope with multi-channel fluorescence imaging and NIS-Elements Advanced Research Version 5 software. Areas of the cell expressing GM130 fluoresced green, while α-tubulin fluoresced red. The red color was synthetically changed to blue using the NIS-Elements Advanced Research software. The distributions of these structures within cells were analyzed in 10 fields of view. Those distributions with at least 51% consistency were considered the predominant phenotype.

Pharmacological Treatments

Control Treatment

All experiments utilized a control condition during experiments to determine the effects of the pharmacological agents. All control treatments consisted of DMEM, trehalose (Fisher Scientific, catalog #BP2687100) and DMSO (Sigma Aldrich, catalog #276855-100ML). Working concentrations for each of these reagents matched those of the pharmacological agent treatments.

EGF Treatment

To promote cellular motility, EGF treatments were added to the cells. EGF was added to a solution of trehalose and PBS, stabilizing the EGF in the stock solution. To create the stock solution, 100 µg EGF (Gibco, catalog #PHG0313) was added to 990 µL of a 15% solution of trehalose in PBS. This resulted in a 100 µg/mL EGF stock solution. This solution was separated into aliquots of 10 µL and stored at -20 °C until needed. When required, the stock solution aliquot was thawed and diluted further into 9990 µL of DMEM, resulting in a new stock solution

of 100 ng/mL. The working solution of EGF in treatments was 10 ng/mL (Grady and Lundin-Schiller, personal communication).

Golgi Disruption Treatment

To disrupt the Golgi, cells were treated with BFA. The original stock of 1 mg BFA (EMD Millipore, catalog #20-372-91MG) was diluted with 2 mL DMSO, resulting in a 500 µg/mL BFA stock solution. This solution was separated into 10 µL aliquots and kept at -20 °C until needed. The working concentration of the treatment for experiments was 50 ng/mL (Bershadsky and Futerman, 1994). This solution was made by diluting 10 µL of the BFA stock solution into 9985 µL DMEM. An additional 5 µL of DMSO was added to the solution to control for the DMSO required in the nocodazole solution. For those treatments requiring EGF, 500 µL of stock EGF solution was added to 4500 µL of BFA solution. To control for the trehalose in the EGF working solution, 1.1 µL of trehalose was added to the remaining 5000 µL of BFA solution. The final working solution of the BFA/EGF solution was 50 ng/mL BFA and 10 ng/mL EGF.

Microtubule Disruption Treatment

Microtubules were disrupted during experimentation using nocodazole. A stock solution was made by diluting 2 mg of nocodazole (Sigma Aldrich, catalog #M1404-2MG) into 1 mL of DMSO, resulting in a 2000 µg/mL stock solution. The stock solution was separated into 15 µL aliquots and stored at -20 °C until needed. The working concentration of the treatment for experiments was 3 µg/mL (Zahn and Lundin-Schiller, 2016). This solution was made by diluting 15 µL of the nocodazole stock solution into 9985 µL DMEM. For those treatments requiring EGF, 500 µL of stock EGF solution was added to 4500 µL of nocodazole solution. To control for the trehalose in the EGF working solution, 1.1 µL of trehalose was added to the remaining

5000 µL of nocodazole solution. The final working solution of the nocodazole/EGF solution was 3 µg/mL nocodazole and 10 ng/mL EGF.

Endogenous Molecule Treatment

To determine the effect of potential endogenous signaling, which occurs in a physiological environment, heat inactivated fetal bovine serum (HI FBS: Gibco, catalog #16140-063) was included in some treatments. Except for the immunofluorescence study, cells were starved and then treatments were given that included or omitted the presence of 10% FBS, for each of the experiments.

CHAPTER IV

Results

Comparing the Cell Types

Establishing Control Behavior

The two cell types have very different migratory behaviors. In the absence of FBS, the scratch separating the MDA-MB-231 cell fronts narrows by 250 µm greater than MCF7 cells (Figure 2, $p<0.0001$). This variation in migratory potential is even more apparent in the presence of FBS, with a difference of 400 µm in gap distance (Figure 2, $p<0.0001$).

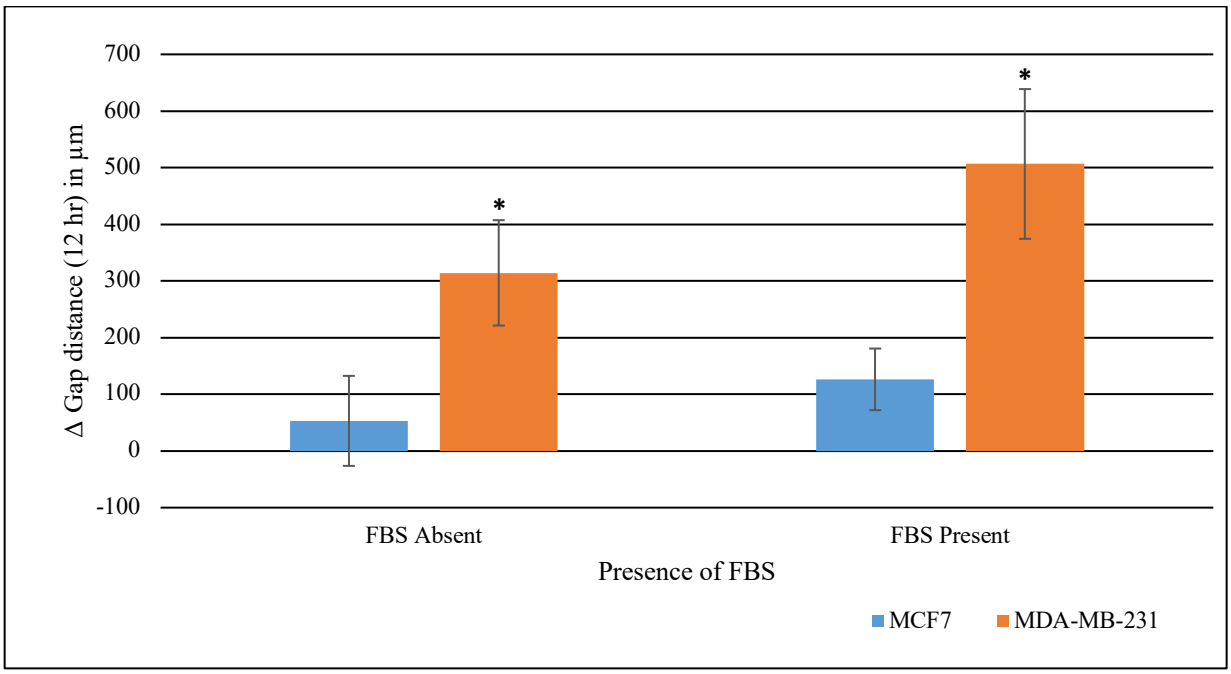

Figure 2. Comparing migration between the two cell types, in the presence or absence of FBS. Average (n=40 for MCF7 FBS absent and present, ± STD; n=60 for MDA-MB-231 FBS absent, ± STD; n=45 for MDA-MB-231, ± STD; MCF7 vs. MDA-MB-231 FBS Absent: $p<0.0001$; MCF7 vs. MDA-MB-231 FBS Present: $p<0.0001$) change in gap distance of each cell type after 12 hours. Experiments were conducted after FBS starvation, with or without the presence of additional FBS (10%) during wound healing. Asterisk (*) represents significance.

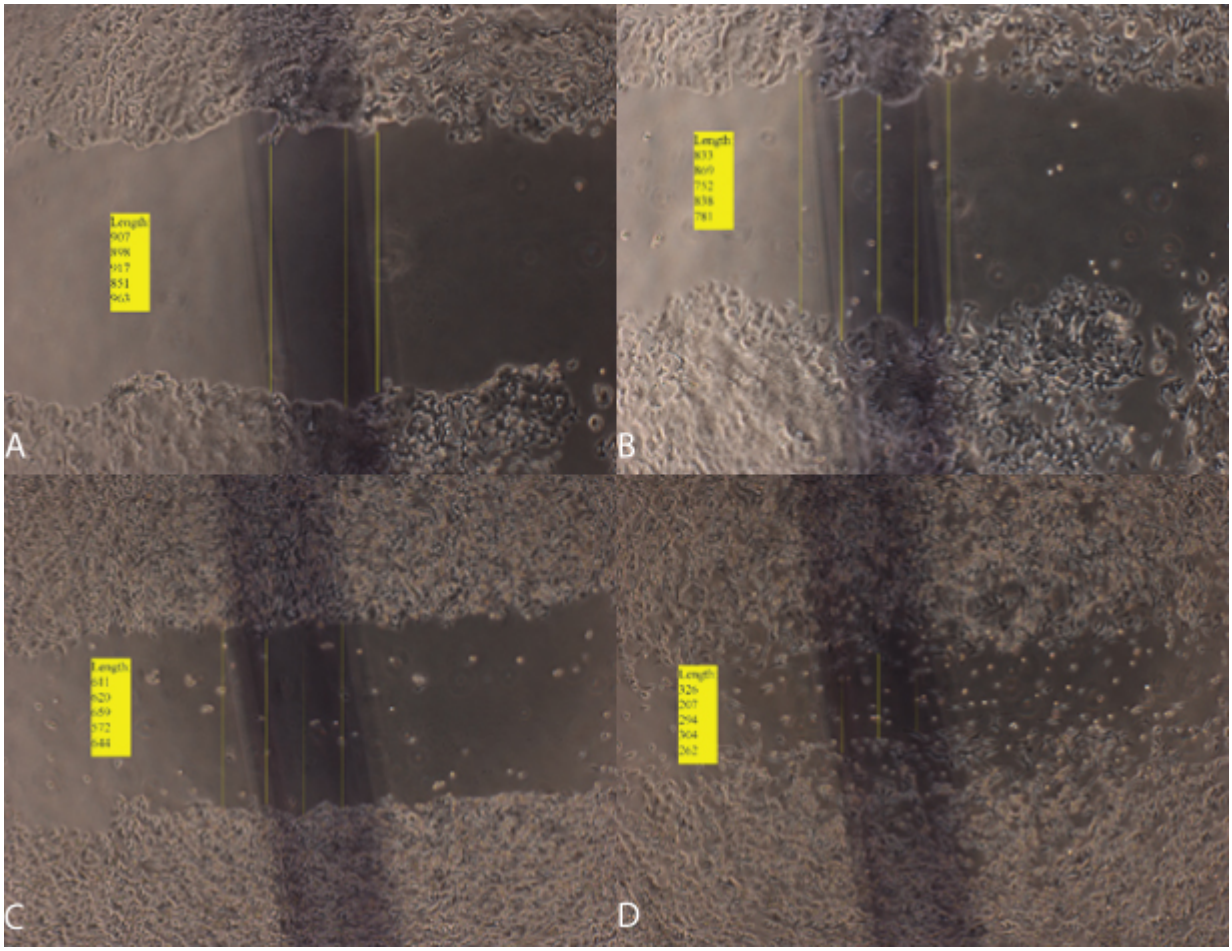

Figure 3. Images of scratch wound assay and associated scratch width measurements. Images were collected with bright-field microscopy using a 4x objective. A) Scratch wound assay using MCF7 cells, immediately after scratch. Experiments were conducted after FBS starvation. Scratch width measurements (μm) are reported in the yellow key. B) Scratch wound assay using MCF7 cells, 12 hours after scratching. Experiments were conducted after FBS starvation. Scratch width measurements (μm) are reported in the yellow key. C) Scratch wound assay using MDA-MB-231 cells, immediately after scratch. Experiments were conducted after FBS starvation. Scratch width measurements (μm) are reported in the yellow key. D) Scratch wound assay using MDA-MB-231 cells, 12 hours after scratching. Experiments were conducted after FBS starvation. Scratch width measurements (μm) are reported in the yellow key.

The morphology of each cell type also differs. MCF7 cells in control conditions, in the absence of FBS, have an epithelial morphology and cluster more closely than MDA-MB-231 cells (Figure 4A; Table 1). Instead, MDA-MB-231 cells have a mesenchymal morphology and are organized more sparsely (Figure 4C; Table 1). In the presence of FBS, the morphology of the cells does not vary greatly. The cell bodies of MCF7 cells present a more mesenchymal morphology than when FBS is absent, however they are still more rounded than MDA-MB-231 cells (Figures 4B, 4C). In the presence of FBS, MDA-MB-231 cells appear to lose the linear shape that they normally display, and instead have much wider leading edges (Figure 4D).

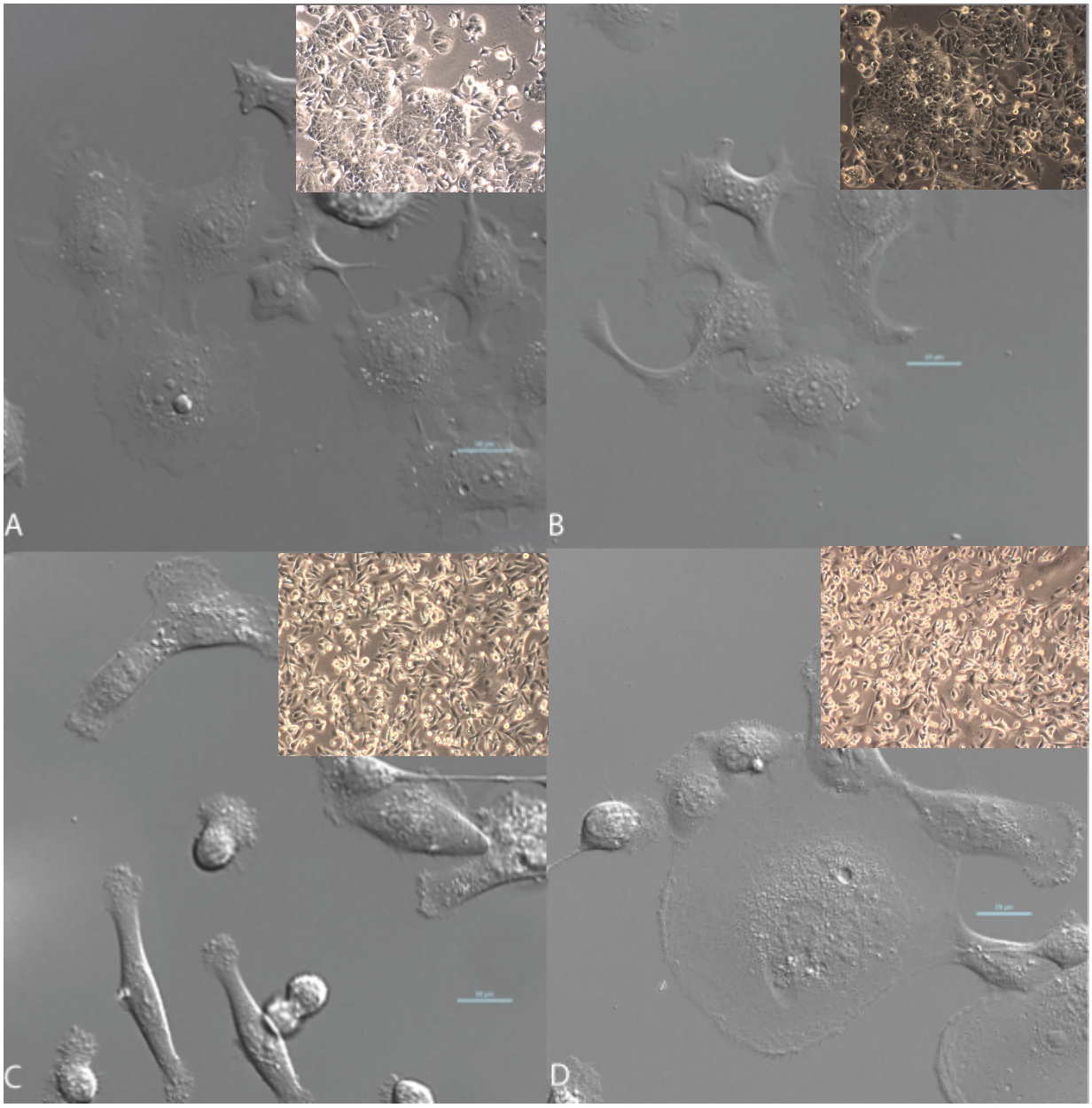

Figure 4. Morphology of each cell type, in the presence or absence of FBS. Images were collected with DIC microscopy using a 40x objective. Inset pictures collected with 10x objective. Scale bar is representative of 10 µm. Figure is representative of 10 fields of view. A) Morphology of MCF7 cell after 12 hours of treatment. Experiments were conducted after FBS starvation. B) Morphology of MCF7 cell after 12 hours of treatment. Experiments were conducted after FBS starvation, with supplemental FBS (10%) after starving. C) Morphology of MDA-MB-231 cell after 12 hours of treatment. Experiments were conducted after FBS starvation. D) Morphology of MDA-MB-231 cell after 12 hours of treatment. Experiments were conducted after FBS starvation, with supplemental FBS (10%) after starving.

Table 1. Morphology of each cell type, with or without FBS (10%), observed from 10 fields of view with DIC microscopy using a 40x objective.

Cell Type	Treatment	Cell Morphology	# of Cells
MCF7	Control	Epithelial Mesenchymal	71 16
	Control + FBS	Epithelial Mesenchymal	80 12
MDA-MB-231	Control	Epithelial Mesenchymal	17 63
	Control + FBS	Epithelial Mesenchymal	13 60

When cellular components of each cell type are analyzed through the use of immunofluorescence, there are a few notable differences. The GM130, indicative of the Golgi and labeled green, of control MCF7 cells is heavily concentrated at the nucleus (Figure 5A; Table 2). This same structure appears to be more diffuse in control MDA-MB-231 cells; however, the leading edge of these cells also displays a fairly concentrated presence of GM130 (Figure 5B; Table 2).

The nuclear area of control MCF7 cells is mostly devoid of α-tubulin, labeled blue (Figure 5A; Table 2). This same phenomenon is not as drastic in control MDA-MB-231 cells (Figure 5B; Table 2). In both control cell types, α-tubulin is present throughout the rest of the cell, including the leading edge.

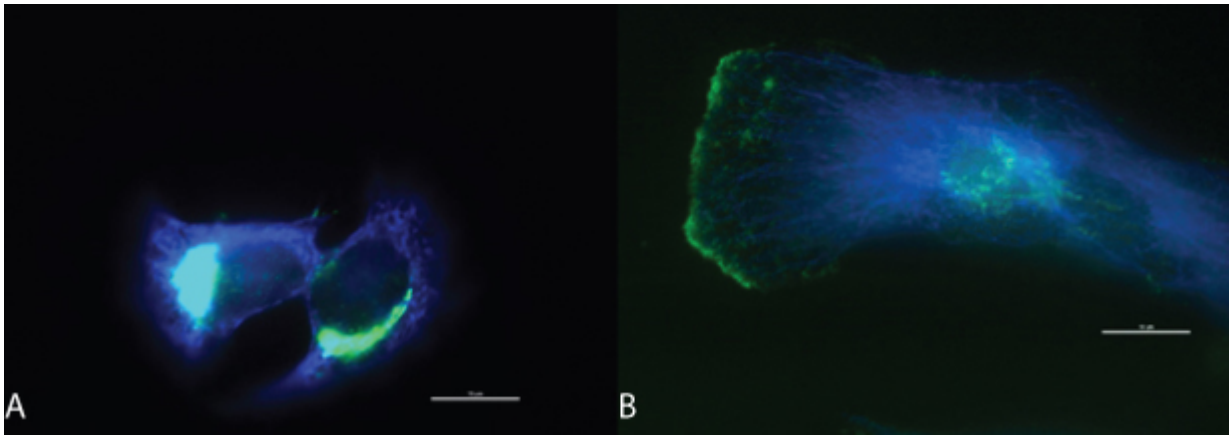

Figure 5. Immunofluorescence of GM130 (green) and α-tubulin (blue) in each cell type. Images were collected with multi-channel fluorescence microscopy using a 60x objective. Scale bar is representative of 10 µm. Figure is representative of 10 fields of view. A) Organization of the Golgi and microtubules within the MCF7 cell at 12 hours after treatment. Experiments were conducted after FBS starvation. B) Organization of the Golgi and microtubules within the MDA-MB-231 cell at 12 hours after treatment. Experiments were conducted after FBS starvation.

Table 2. Organization of the microtubules (MT) and Golgi distribution of each cell type, with or without FBS (10%), observed from 10 fields of view with multi-channel fluorescence microscopy using a 60x objective.

Cell Type	**Treatment**	**MT Organization**	**# of Cells**	**Golgi Distribution**	**# of Cells**
MCF7	Control	Heavily Concentrated Diffuse	16 23	Compact Diffuse	33 6
MDA-MB-231	Control	Heavily Concentrated Diffuse	10 24	Compact Diffuse	23 11

Addition of EGF

Those cells that are treated with EGF have a greater migratory behavior, in both cell types (Figures 6, 7; both cell types: $p<0.0001$).

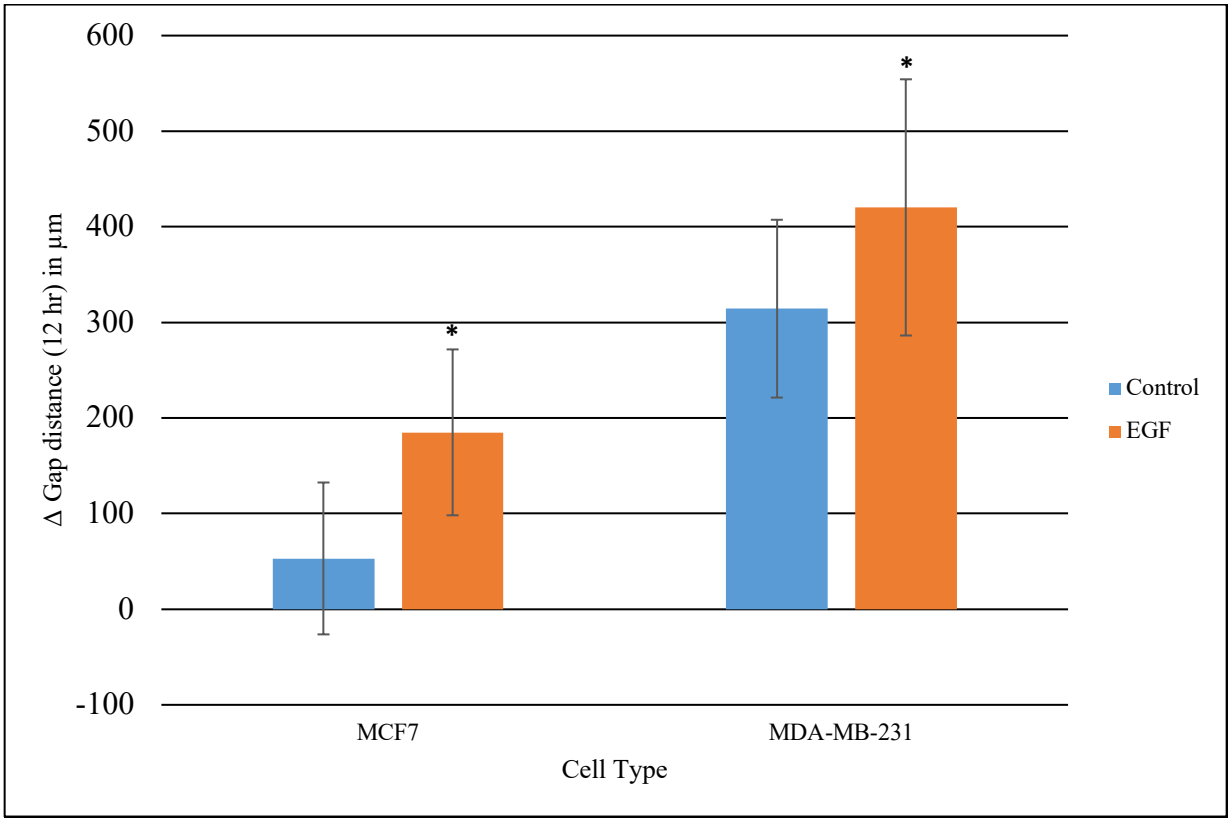

Figure 6. Comparing EGF-induced migration in each cell type. Average (MCF7 Control n=40, ± STD; MCF7 EGF Present n=45, ± STD; MDA-MB-231 Control n=60, ± STD; MDA-MB-231 EGF Present n=45, ± STD; MCF7 Control vs. MCF7 EGF Present: $p<0.0001$; MDA-MB-231 Control vs. MDA-MB-231 EGF Present: $p=<0.0001$) change in gap distance of each cell type after 12 hours. Experiments were conducted after FBS starvation with EGF (10 ng/mL) supplementation. Asterisk (*) represents significance compared to the control.

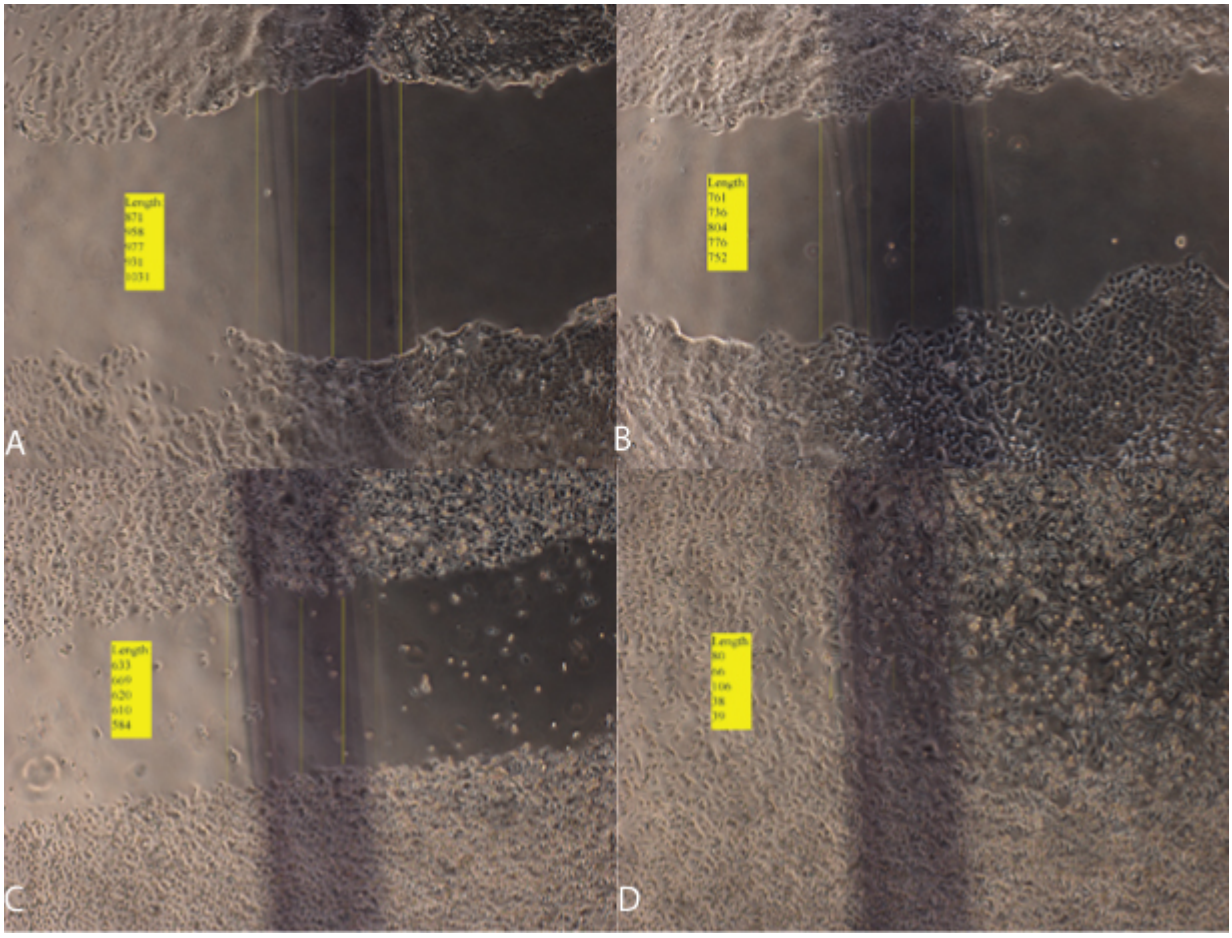

Figure 7. Images of EGF-induced scratch wound assay and associated scratch width measurements. Images were collected with bright-field microscopy using a 4x objective. A) Scratch wound assay using MCF7 cells, immediately after scratch. Experiments were conducted after FBS starvation, with supplemental EGF (10 ng/mL) after starving. Scratch width measurements (µm) are reported in the yellow key. B) Scratch wound assay using MCF7 cells, 12 hours after scratching. Experiments were conducted after FBS starvation, with supplemental EGF (10 ng/mL) after starving. Scratch width measurements (µm) are reported in the yellow key. C) Scratch wound assay using MDA-MB-231 cells, immediately after scratch. Experiments were conducted after FBS starvation, with supplemental EGF (10 ng/mL) after starving. Scratch width measurements (µm) are reported in the yellow key. D) Scratch wound assay using MDA-MB-231 cells, 12 hours after scratching. Experiments were conducted after FBS starvation, with supplemental EGF (10 ng/mL) after starving. Scratch width measurements (µm) are reported in the yellow key.

The presence of EGF increases the likelihood that cells of either type migrate more closely to one another (Figure 8). MCF7 cells, specifically, migrate toward one another and maintain an epithelial state, forming dense masses of cells (Figure 8B; Table 3). MDA-MB-231 cells treated with EGF also migrate toward one another, however they also produce very long, thin cell projections leading from one cell to another (Figure 8D). These cells retain the mesenchymal morphology that control MDA-MB-231 cells exhibit (Figures 8C, 8D; Table 3).

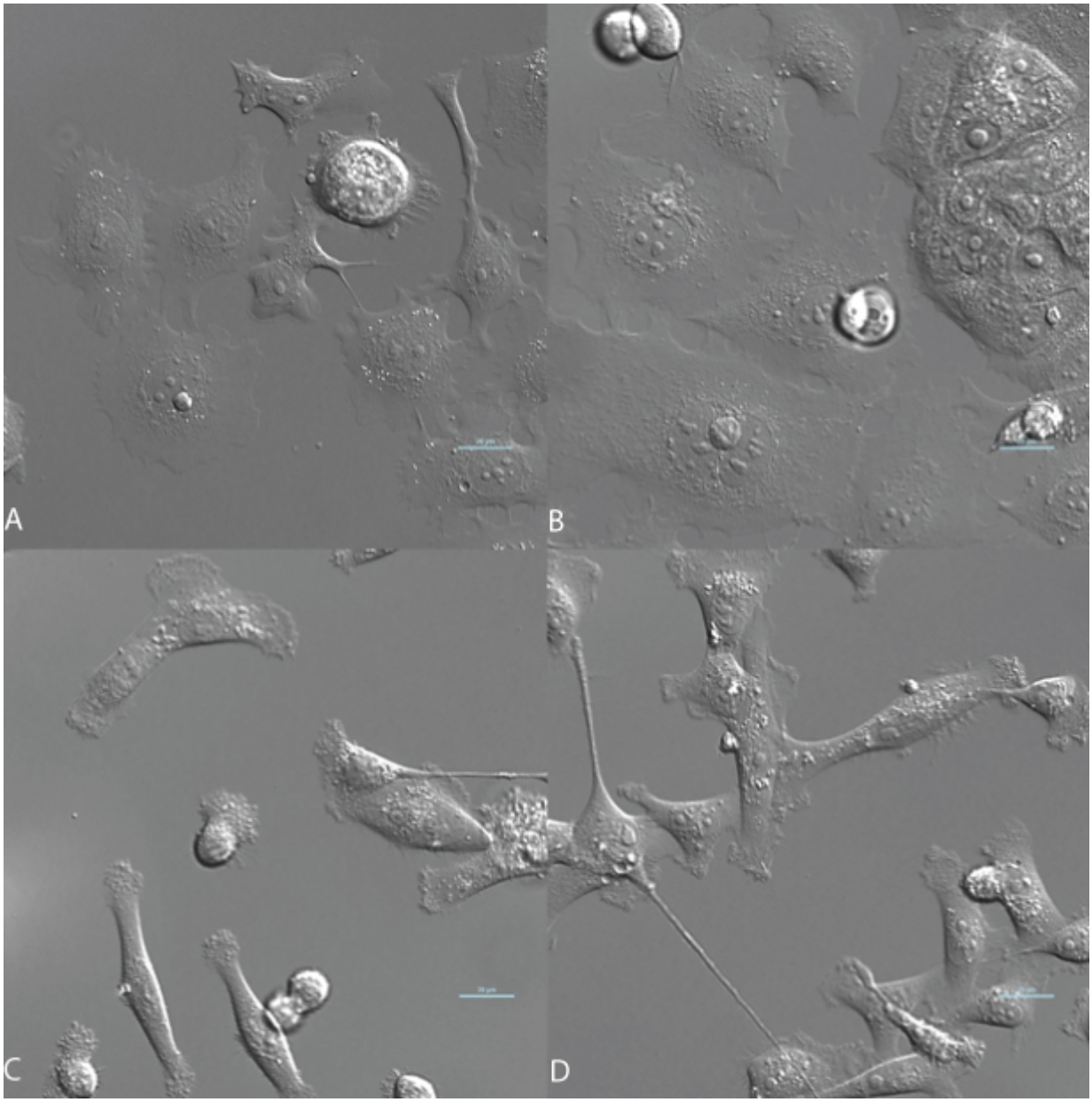

Figure 8. EGF-induced morphology of each cell type. Images were collected with DIC microscopy using a 40x objective. Scale bar is representative of 10 µm. Figure is representative of 10 fields of view. A) Morphology of MCF7 cell after 12 hours of treatment. Experiments were conducted after FBS starvation. B) Morphology of MCF7 cell after 12 hours of treatment. Experiments were conducted after FBS starvation, with supplemental EGF (10 ng/mL) after starving. C) Morphology of MDA-MB-231 cell after 12 hours of treatment. Experiments were conducted after FBS starvation. D) Morphology of MDA-MB-231 cell after 12 hours of treatment. Experiments were conducted after FBS starvation, with supplemental EGF (10 ng/mL) after starving.

Table 3. Morphology of each cell type, with or without EGF (10 ng/mL), observed from 10 fields of view with DIC microscopy using a 40x objective.

Cell Type	Treatment	Cell Morphology	# of Cells
MCF7	Control	Epithelial Mesenchymal	71 16
	EGF	Epithelial Mesenchymal	72 6
MDA-MB-231	Control	Epithelial Mesenchymal	17 63
	EGF	Epithelial Mesenchymal	4 60

The immunofluorescence images captured of cells treated with EGF indicate increased microtubule presence in each cell type (Figures 9B, D; Table 4). In MCF7 cells, the Golgi is diffused around the nucleus (Figure 9B). In MDA-MB-231 cells, GM130 expression is increased at the leading edges (Figure 9D).

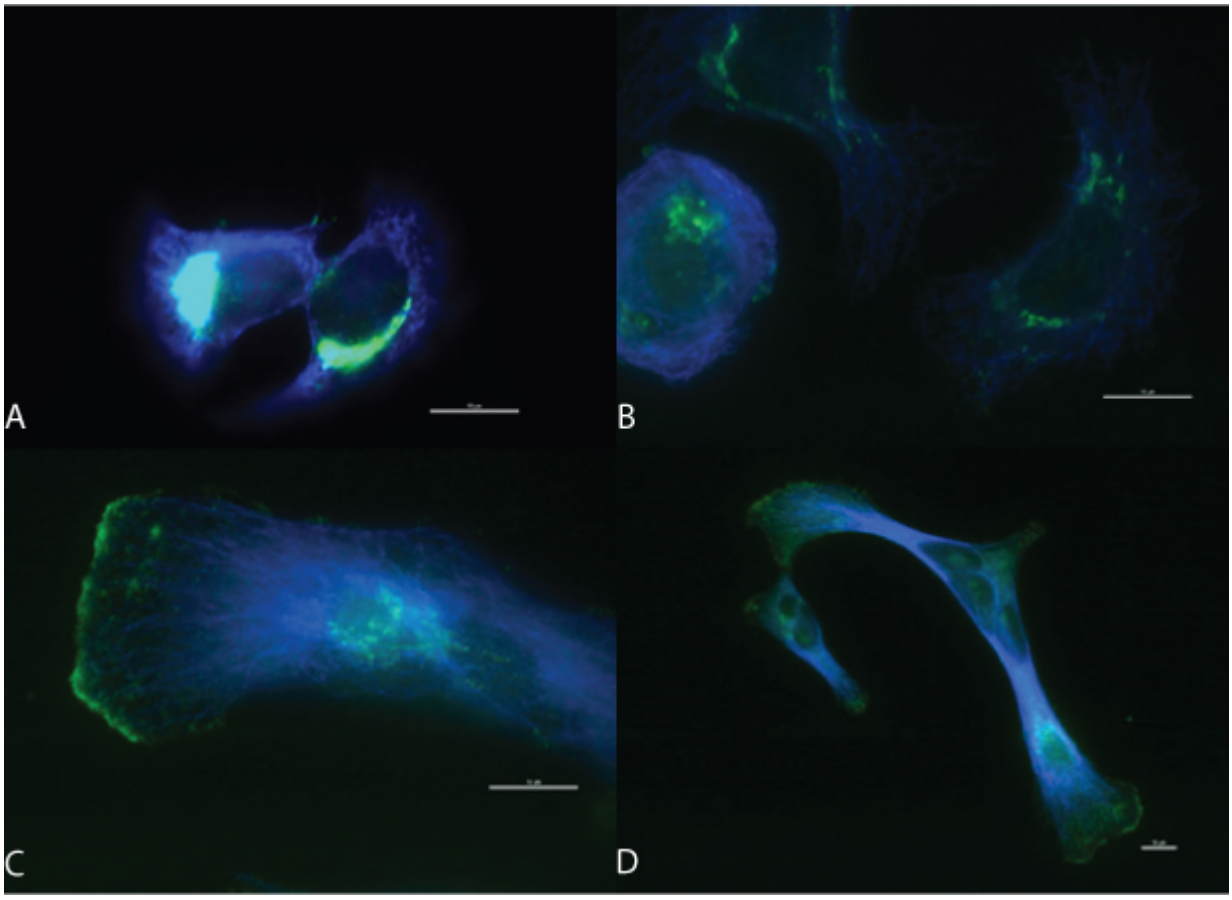

Figure 9. EGF-induced immunofluorescence of GM130 (green) and α-tubulin (blue) in each cell type. Images were collected with multi-channel fluorescence microscopy using a 60x objective. Scale bar is representative of 10 μm. Figure is representative of 10 fields of view. A) Organization of the Golgi and microtubules within the MCF7 cell at 12 hours after treatment. Experiments were conducted after FBS starvation. B) Organization of the Golgi and microtubules within the MCF7 cell at 12 hours after treatment. Experiments were conducted after FBS starvation, with supplemental EGF (10 ng/mL) after starving. C) Organization of the Golgi and microtubules within the MDA-MB-231 cell at 12 hours after treatment. Experiments were conducted after FBS starvation. D) Organization of the Golgi and microtubules within the MDA-MB-231 cell at 12 hours after treatment. Experiments were conducted after FBS starvation, with supplemental EGF (10 ng/mL) after starving.

Table 4. Organization of the microtubule (MT) and Golgi distribution in each cell type, with or without EGF (10 ng/mL), observed from 10 fields of view with multi-channel fluorescence microscopy using a 60x objective.

Cell Type	Treatment	MT Organization	# of Cells	Golgi Distribution	# of Cells
MCF7	Control	Heavily Concentrated Diffuse	16 23	Compact Diffuse	33 6
MCF7	EGF	Heavily Concentrated Diffuse	20 15	Compact Diffuse	3 32
MDA-MB-231	Control	Heavily Concentrated Diffuse	10 24	Compact Diffuse	23 11
MDA-MB-231	EGF	Heavily Concentrated Diffuse	30 7	Compact Diffuse	7 30

Addition of EGF & FBS

Because the microenvironment of these cells *in vivo* possesses many other molecules involved in cellular processes, which are often produced at other sites throughout the body and transported by serum, supplemental FBS was given to the cells during treatment to replicate the presence of these molecules. There was a significant increase in the migration of both cell types when supplemented with EGF and FBS (Figure 10; MCF7: p=0.0035, MDA-MB-231: p=0.0023).

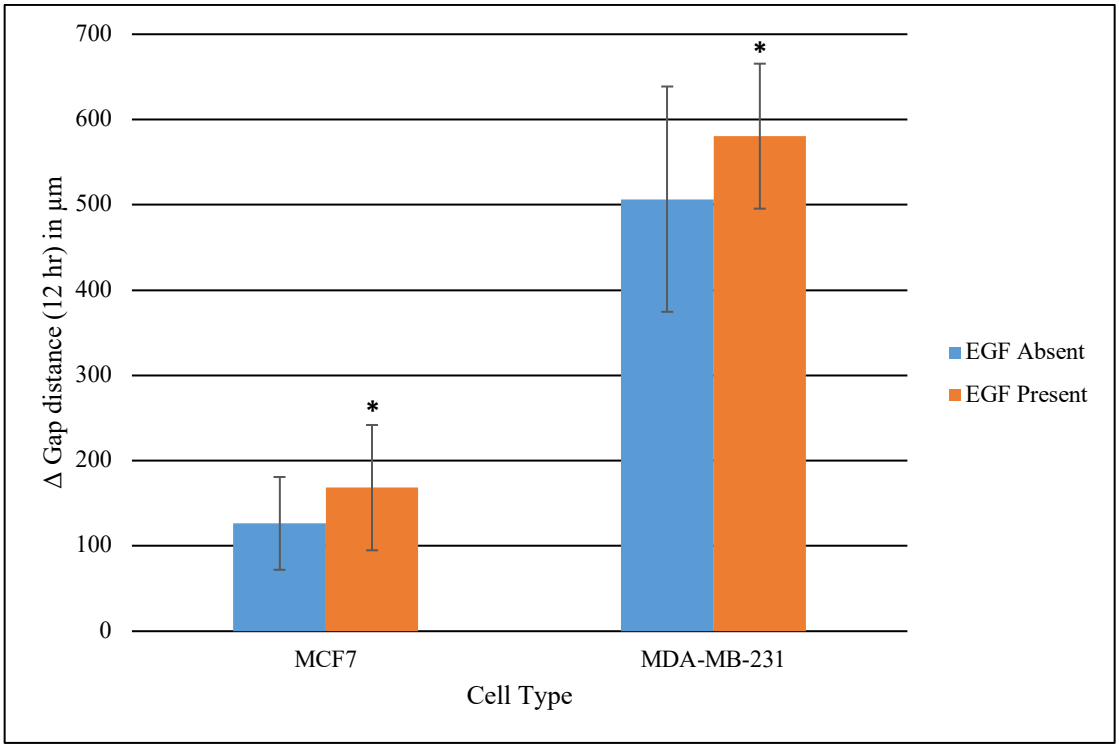

Figure 10. Comparing EGF-induced migration in each cell type supplemented with FBS. Average (MCF7 Control n=40, ± STD; MCF7 EGF Present n=45; MDA-MB-231 Control and EGF Present n=45; MCF7 Control vs. EGF Present: p=0.0035; MDA-MB-231 Control vs. EGF Present: p=0.0023) change in gap distance of each cell type after 12 hours. Experiments were conducted after FBS starvation with supplementation of EGF (10 ng/mL), as well as the presence of additional FBS (10%) during wound healing. Asterisk (*) represents significance compared to the control.

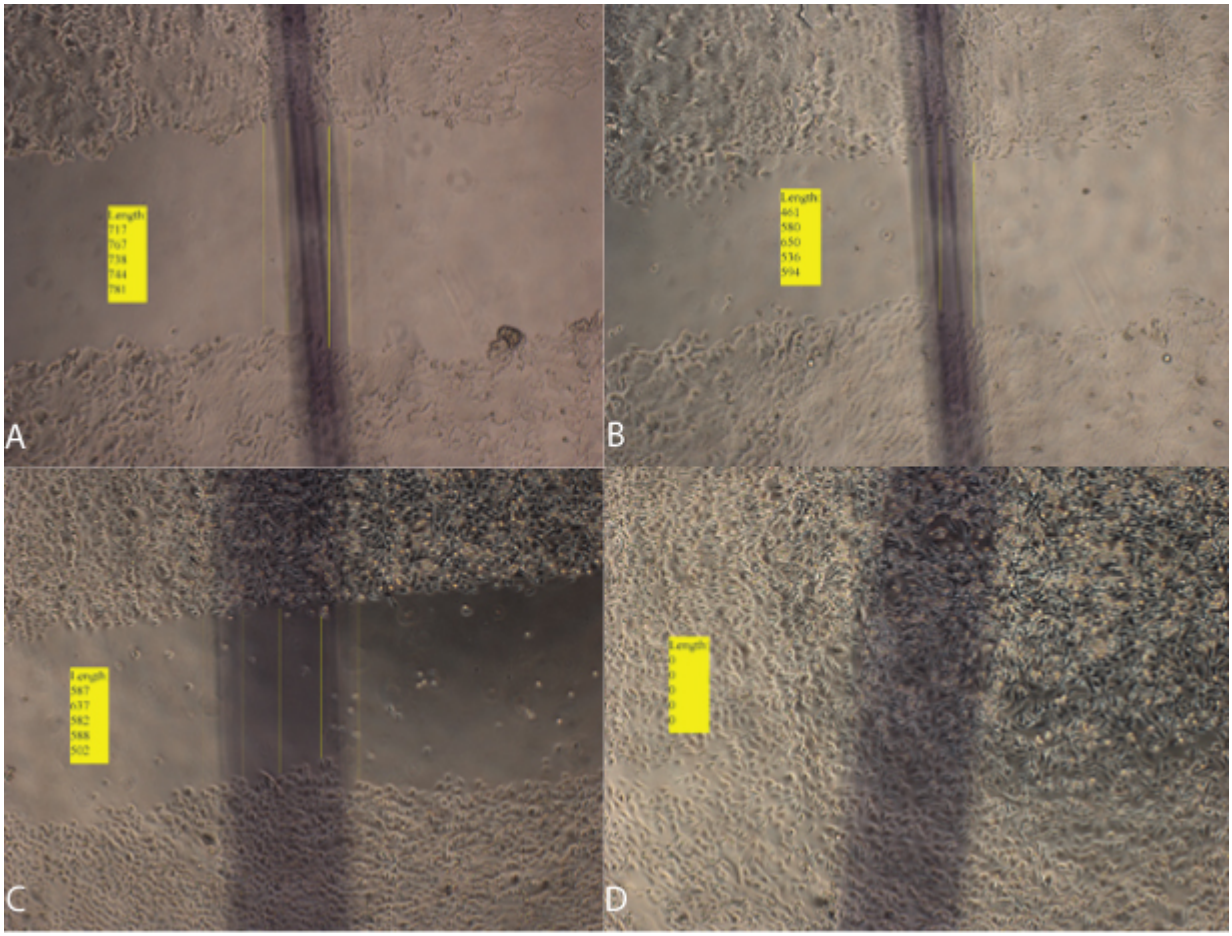

Figure 11. Images of EGF- and BFA-induced scratch wound assay and associated scratch width measurements, supplemented with FBS. Images were collected with bright-field microscopy using a 4x objective. A) Scratch wound assay using MCF7 cells, immediately after scratch. Experiments were conducted after FBS starvation, with supplemental EGF (10 ng/mL) and FBS (10%) after starving. Scratch width measurements (µm) are reported in the yellow key. B) Scratch wound assay using MCF7 cells, 12 hours after scratching. Experiments were conducted after FBS starvation, with supplemental EGF (10 ng/mL) and FBS (10%) after starving. Scratch width measurements (µm) are reported in the yellow key. C) Scratch wound assay using MDA-MB-231 cells, immediately after scratch. Experiments were conducted after FBS starvation, with supplemental EGF (10 ng/mL) and FBS (10%) after starving. Scratch width measurements (µm) are reported in the yellow key. D) Scratch wound assay using MDA-MB-231 cells, 12 hours after scratching. Experiments were conducted after FBS starvation, with supplemental EGF (10 ng/mL) and FBS (10%) after starving. Scratch width measurements (µm) are reported in the yellow key.

The morphology of each cell type when treated with EGF and FBS resembled the morphology of cells treated solely with EGF (Figures 8, 12; Tables 3, 5). The MDA-MB-231 cells treated with both reagents had slightly longer and slender projections than EGF only treated MDA-MB-231 cells (Figure 12).

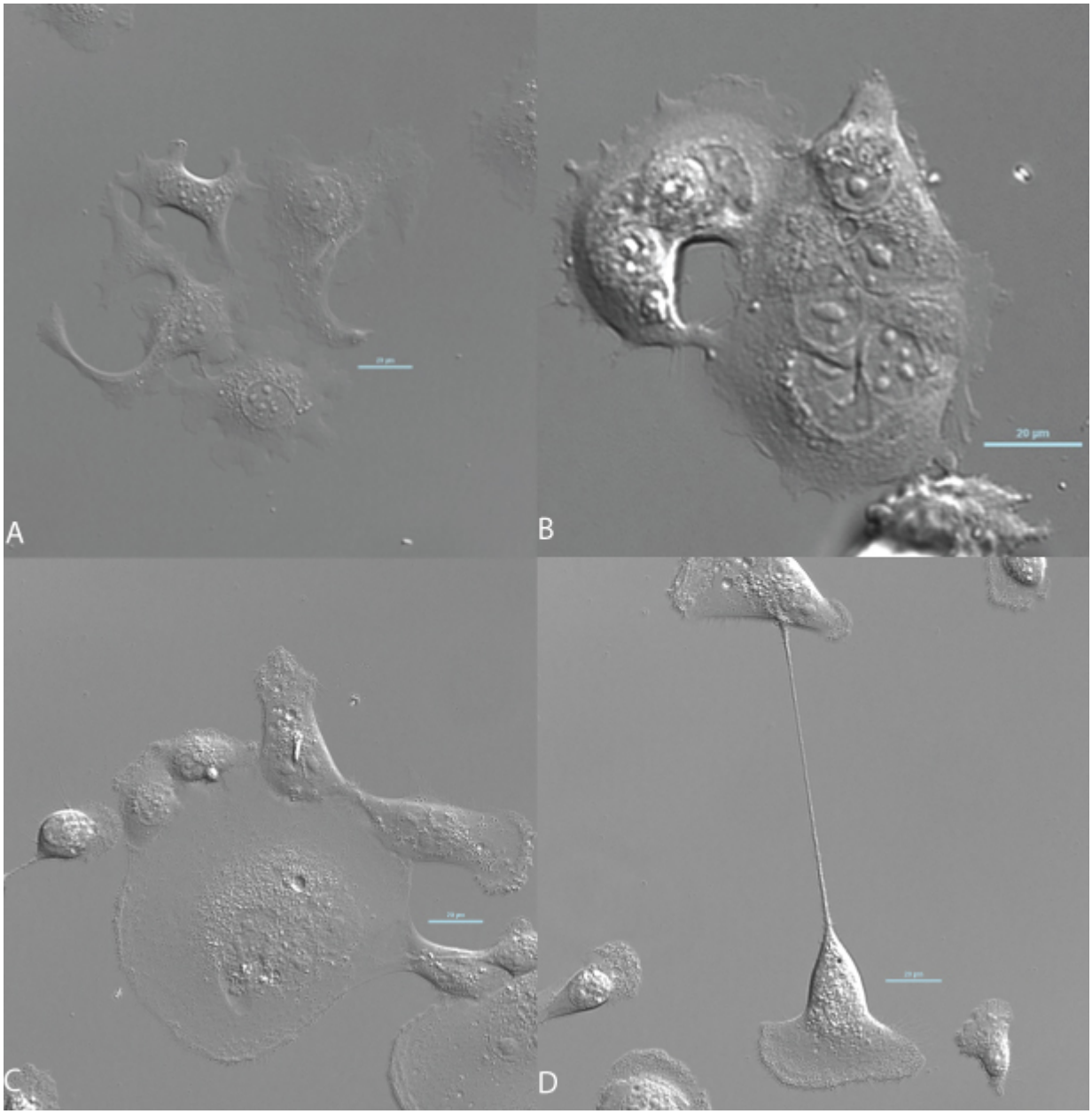

Figure 12. EGF-induced morphology of each cell type, with FBS supplementation. Images were collected with DIC microscopy using a 40x objective. Scale bar is representative of 10 µm. Figure is representative of 10 fields of view. A) Morphology of MCF7 cell after 12 hours of treatment. Experiments were conducted after FBS starvation, with supplemental FBS (10%) after starving. B) Morphology of MCF7 cell after 12 hours of treatment. Experiments were conducted after FBS starvation, with supplemental EGF (10 ng/mL) and FBS (10%) after starving. C) Morphology of MDA-MB-231 cell after 12 hours of treatment. Experiments were conducted after FBS starvation, with supplemental FBS (10%) after starving. D) Morphology of MDA-MB-231 cell after 12 hours of treatment. Experiments were conducted after FBS starvation, with supplemental EGF (10 ng/mL) and FBS (10%) after starving.

Table 5. Morphology of each cell type supplemented with FBS (10%), with or without EGF (10 ng/mL), observed from 10 fields of view with DIC microscopy using a 40x objective.

Cell Type	Treatment	Cell Morphology	# of Cells
MCF7	Control + FBS	Epithelial	80
		Mesenchymal	12
	EGF + FBS	Epithelial	60
		Mesenchymal	9
MDA-MB-231	Control + FBS	Epithelial	13
		Mesenchymal	60
	EGF + FBS	Epithelial	7
		Mesenchymal	51

EGF treatment produced a significantly larger change in gap distance than the control condition for both cell types (Figures 13, 14; both cell types: $p<0.0001$). There was no significant difference in the change in gap distance between EGF treatment and the addition of FBS to this treatment in MCF7 cells (Figure 13; $p=0.8217$). However, there was a significant difference with the addition of FBS in the MDA-MB-231 cell type (Figure 14; $p<0.0001$).

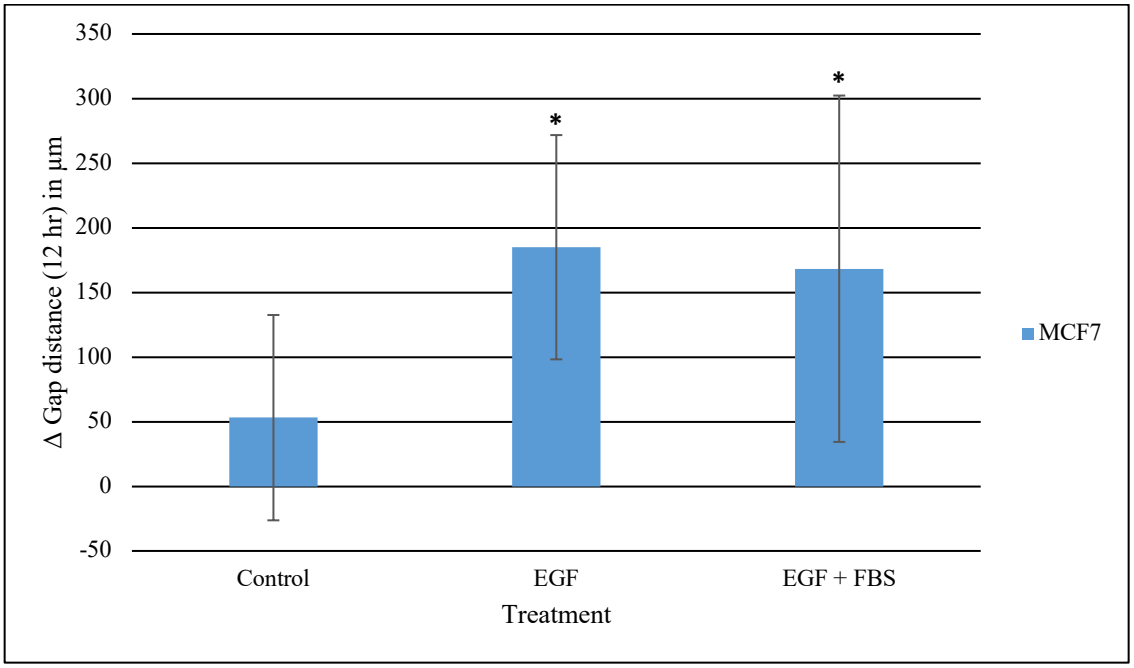

Figure 13. Comparing EGF-induced MCF7 cell migration, with or without supplementation of FBS. Average (MCF7 Control n=40, ± STD; MCF7 EGF Present n=45, ± STD; MCF7 EGF and FBS Present n=45, ± STD; Control vs. EGF: $p<0.0001$; Control vs EGF+ FBS: $p<0.001$; EGF vs EGF + FBS: $p=0.8217$) change in gap distance for control and treated cells after 12 hours. Experiments were conducted after FBS starvation, with or without the presence of additional EGF (10 ng/mL) and FBS (10%) during wound healing. Asterisk (*) represents significance compared to the control.

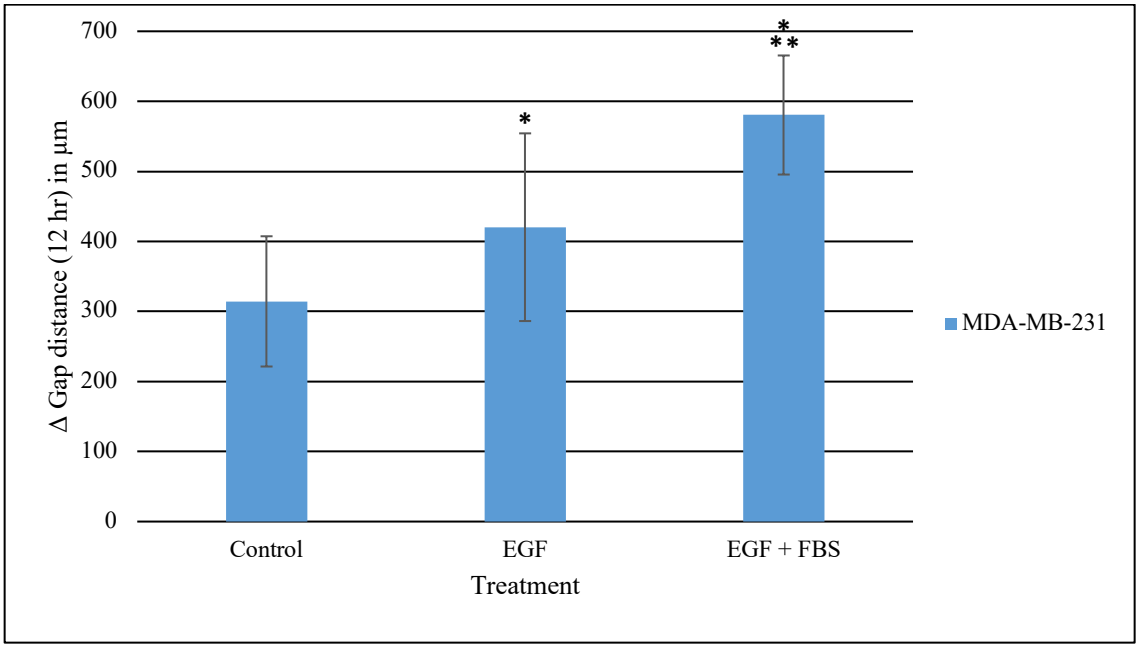

Figure 14. Comparing EGF-induced MDA-MB-231 cell migration, with or without supplementation of FBS. Average (MDA-MB-231 Control n=60, ± STD; MDA-MB-231 EGF Present n=45, ± STD; MDA-MB-231 EGF and FBS Present n=45, ± STD; Control vs. EGF: $p<0.0001$; Control vs EGF and FBS: $p<0.0001$; EGF vs EGF and FBS: $p<0.0001$) change in gap distance for control and treated cells after 12 hours. Experiments were conducted after FBS starvation, with or without the presence of additional EGF (10 ng/mL) and FBS (10%) during wound healing. Asterisk (*) represents significance compared to the control. Double asterisks (**) represent significance compared to EGF treatment.

Pharmacological Treatments

Disruption of the Golgi

Disruption of the Golgi, through the treatment of cells with BFA, produced varying differences in the change in gap distance. For MCF7 cells, migration appeared to be, but was not significantly different, when treated with BFA (Figure 15; $p=0.0572$). The addition of BFA and EGF did produce a significant change in gap distance as compared to the control or solely BFA treated cells (Figure 15; $p<0.0001$). Unexpectedly, supplementing BFA and EGF with FBS produced a significantly lower change in gap distance than BFA and EGF treatment; however, this change was significantly higher than control or solely BFA treated cells (Figure 15; BFA and EGF: $p=0.0302$, control: $p=0.0145$, BFA: $p=0.0007$).

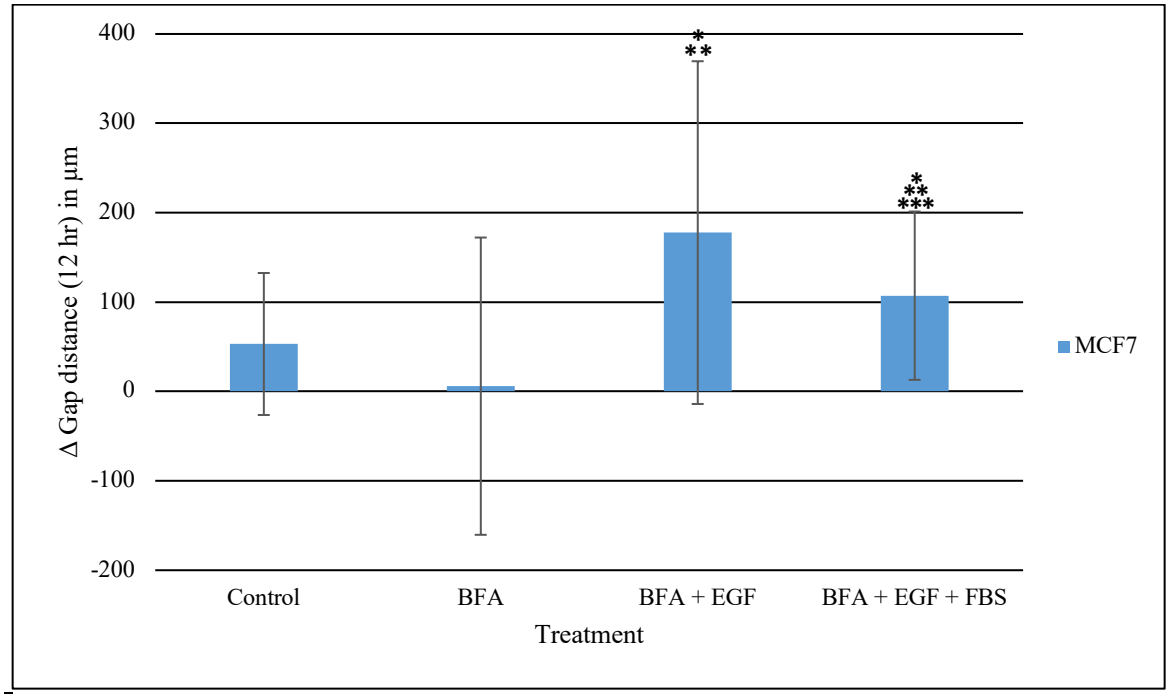

Figure 15. Golgi-disrupted MCF7 cell migration rate, with or without supplementation of EGF or FBS. Average (MCF7 Control n=40, ± STD; MCF7 BFA Present n=45, ± STD; MCF7 BFA and EGF Present n=45, ± STD; MCF7 BFA, EGF and FBS Present n=60, ± STD; Control vs. BFA: p=0.0572; Control vs BFA and EGF: p=0.0004; Control vs BFA, EGF and FBS: p=0.0145; BFA vs. BFA and EGF: p<0.0001; BFA vs. BFA, EGF and FBS: p=0.0007; BFA and EGF vs. BFA, EGF and FBS: p=0.0302) change in gap distance for control and treated cells after 12 hours. Experiments were conducted after FBS starvation, with or without the presence of additional EGF (10 ng/mL), BFA (50 ng/mL) and FBS (10%) during wound healing. Asterisk (*) represents significance compared to the control. Double asterisks (**) represent significance compared to BFA treatment. Triple asterisks (***) represent significance compared to BFA and EGF treatment.

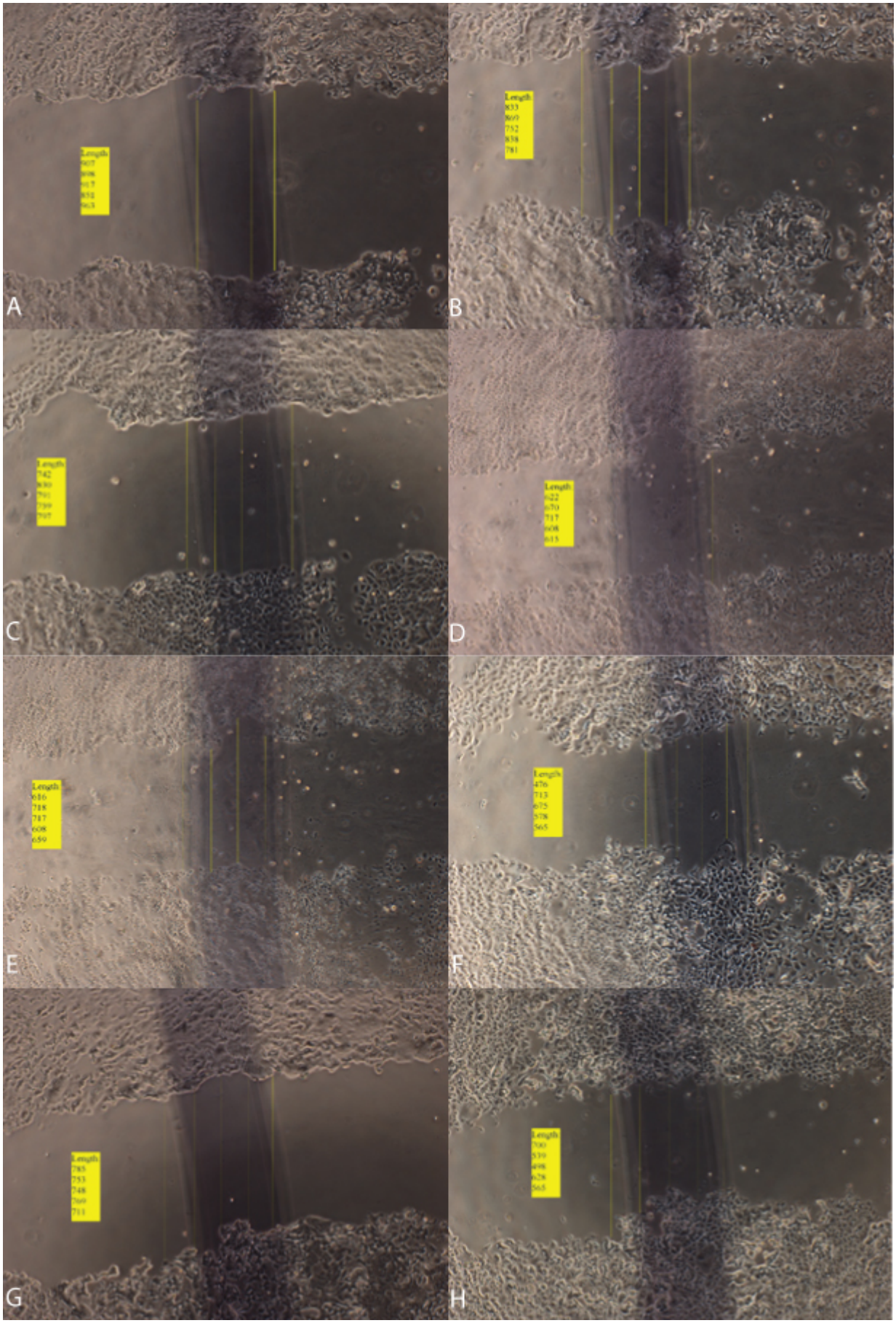
A
B
C
D
E
F
G
H

Figure 16. Images of Golgi-disrupted MCF7 scratch wound assay and associated scratch width measurements. Images were collected with bright-field microscopy using a 4x objective. A) Scratch wound assay using MCF7 cells, immediately after scratch. Experiments were conducted after FBS starvation. Scratch width measurements (μm) are reported in the yellow key. B) Scratch wound assay using MCF7 cells, 12 hours after scratching. Experiments were conducted after FBS starvation. Scratch width measurements (μm) are reported in the yellow key. C) Scratch wound assay using MCF7 cells, immediately after scratch. Experiments were conducted after FBS starvation, with supplemental BFA (50 ng/mL) after starving. Scratch width measurements (μm) are reported in the yellow key. D) Scratch wound assay using MCF7 cells, 12 hours after scratching. Experiments were conducted after FBS starvation, with supplemental BFA (50 ng/mL) after starving. Scratch width measurements (μm) are reported in the yellow key. E) Scratch wound assay using MCF7 cells, immediately after scratch. Experiments were conducted after FBS starvation, with supplemental BFA (50 ng/mL) and EGF (10 ng/mL) after starving. Scratch width measurements (μm) are reported in the yellow key. F) Scratch wound assay using MCF7 cells, 12 hours after scratching. Experiments were conducted after FBS starvation, with supplemental BFA (50 ng/mL) and EGF (10 ng/mL) after starving. Scratch width measurements (μm) are reported in the yellow key. G) Scratch wound assay using MCF7 cells, immediately after scratch. Experiments were conducted after FBS starvation, with supplemental BFA (50 ng/mL), EGF (10 ng/mL) and FBS (10%) after starving. Scratch width measurements (μm) are reported in the yellow key. H) Scratch wound assay using MCF7 cells, 12 hours after scratching. Experiments were conducted after FBS starvation, with supplemental BFA (50 ng/mL), EGF (10 ng/mL) and FBS (10%) after starving. Scratch width measurements (μm) are reported in the yellow key.

After a 12 hour period, the morphology of MCF7 cells is altered when BFA is present (Figure 17B, Table 6). Compared to the control treatment, cells supplemented with only BFA begin to lose the epithelial shape that they typically possess, and instead gain long cellular extensions (Figure 17B). The same is true for cells treated with BFA and EGF, however these cells have a higher number of long, thin protrusions on average (Figure 17C). Finally, the addition of FBS, as well as the previous two reagents, appears to restore the majority of the cells back to the control morphology (Figure 17D, Table 6).

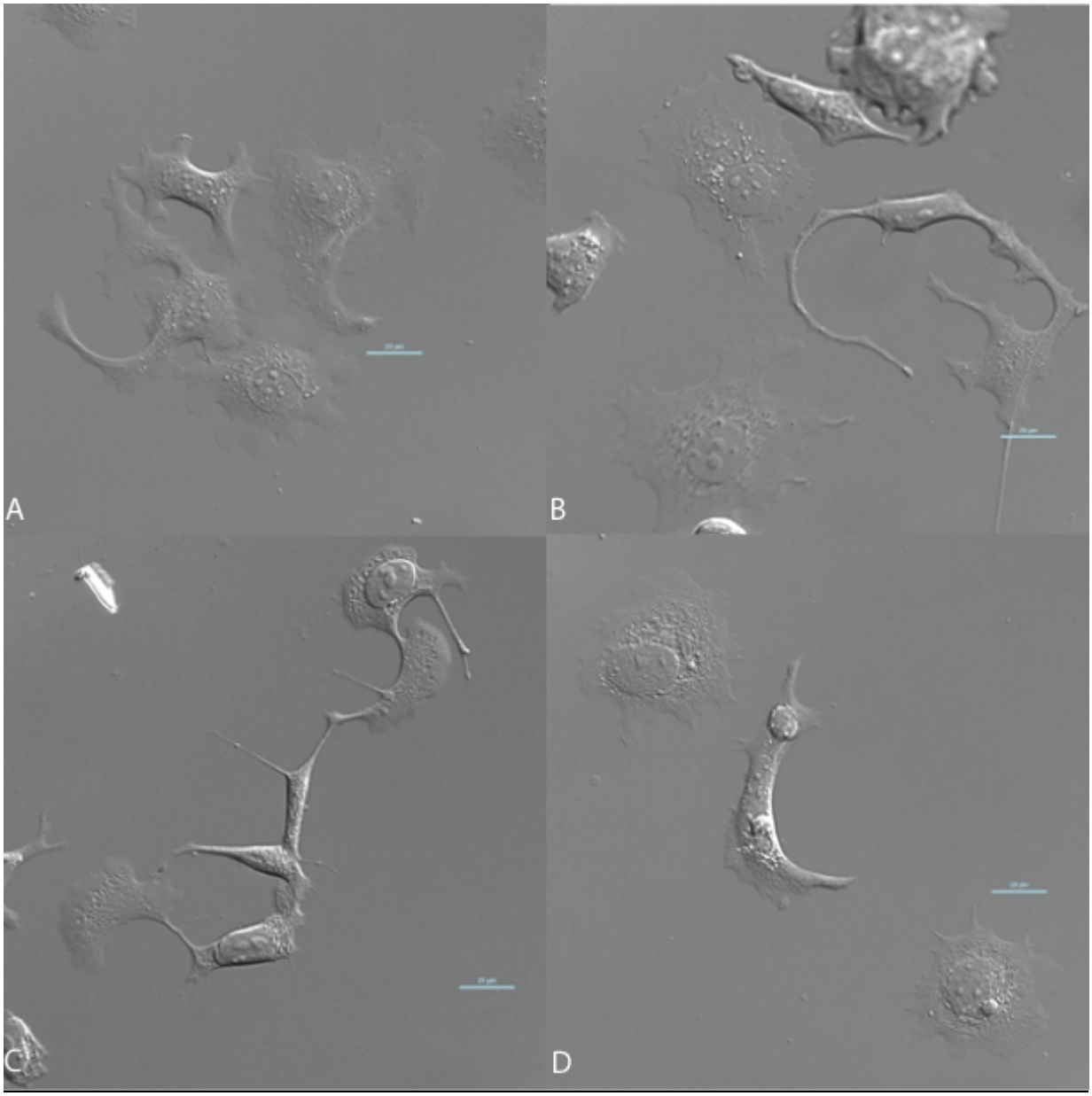

Figure 17. Golgi-disrupted morphology of the MCF7 cell type, in the presence or absence of EGF and FBS. Images were collected with DIC microscopy using a 40x objective. Scale bar is representative of 10 µm. Figure is representative of 10 fields of view. A) Morphology of MCF7 cell after 12 hours of treatment. Experiments were conducted after FBS starvation. B) Morphology of MCF7 cell after 12 hours of treatment. Experiments were conducted after FBS starvation, with supplemental BFA (50 ng/mL) after starving. C) Morphology of MCF7 cell after 12 hours of treatment. Experiments were conducted after FBS starvation, with supplemental BFA (50 ng/mL) and EGF (10 ng/mL) after starving. D) Morphology of MCF7 cell after 12 hours of treatment. Experiments were conducted after FBS starvation, with supplemental BFA (50 ng/mL), EGF (10 ng/mL) and FBS (10%) after starving.

Table 6. Morphology of Golgi-disrupted MCF7 cells, with or without EGF (10 ng/mL), BFA (50 ng/mL) or FBS (10%), observed from 10 fields of view with DIC microscopy using a 40x objective.

Cell Type	Treatment	Cell Morphology	# of Cells
MCF7	Control	Epithelial Mesenchymal	71 16
	BFA	Epithelial Mesenchymal	32 40
	BFA + EGF	Epithelial Mesenchymal	48 33
	BFA + EGF + FBS	Epithelial Mesenchymal	53 16

Analysis of immunofluorescence staining of the MCF7 reveals that the Golgi is in fact more dispersed with BFA treatment (Figures 18A, B; Table 7). The GM130 is more diffuse than in the control conditions. It appears that the addition of EGF results in a more compact organization of the Golgi at the nucleus, however the microtubules of these same cells are severely stunted (Figure 18C; Table 7).

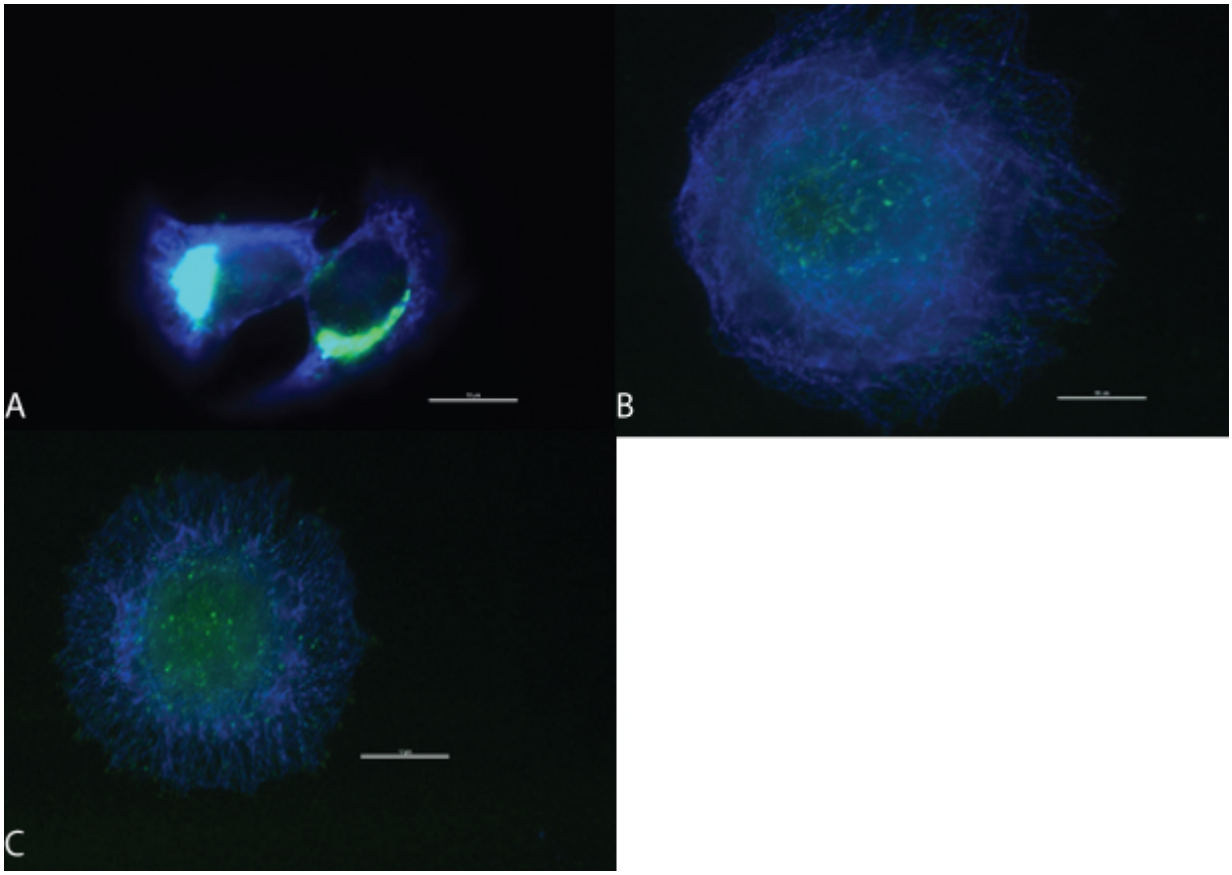

Figure 18. Immunofluorescence of GM130 (green) and α-tubulin (blue) of Golgi-disrupted MCF7 cells. Images were collected with multi-channel fluorescence microscopy using a 60x objective. Scale bar is representative of 10 µm. Figure is representative of 10 fields of view. A) Organization of the Golgi and microtubules within the MCF7 cell at 12 hours after treatment. Experiments were conducted after FBS starvation. B) Organization of the Golgi and microtubules within the MCF7 cell at 12 hours after treatment. Experiments were conducted after FBS starvation, with supplemental BFA (50 ng/mL) after starving. C) Organization of the Golgi and microtubules within the MCF7 cell at 12 hours after treatment. Experiments were conducted after FBS starvation, with supplemental BFA (50 ng/mL) and EGF (10 ng/mL) after starving.

Table 7. Organization of the microtubule (MT) and Golgi distribution in Golgi-disrupted MCF7 cells, with or without BFA (50 ng/mL) or EGF (10 ng/mL), observed from 10 fields of view with multi-channel fluorescence microscopy using a 60x objective.

Cell Type	Treatment	MT Organization	# of Cells	Golgi Distribution	# of Cells
MCF7	Control	Heavily Concentrated Diffuse	16 23	Compact Diffuse	33 6
	BFA	Heavily Concentrated Diffuse	22 6	Compact Diffuse	3 25
	BFA + EGF	Heavily Concentrated Diffuse	11 18	Compact Diffuse	10 19

BFA has a robust impact on the migration of the MDA-MB-231 as any treatment containing it caused a significant decrease in migration, as compared to control conditions, after 12 hours, regardless of EGF or FBS presence (Figure 19; BFA: $p<0.0001$, BFA and EGF: $p<0.0001$, BFA, EGF and FBS: $p=0.0087$). Although the addition of EGF and FBS to the BFA treatment did not rescue the migratory behavior to control condition rates, it did produce a significantly larger change in gap distance than solely BFA or BFA and EGF treated cells (Figure 19; BFA: $p<0.0001$, BFA and EGF: $p=0.0004$).

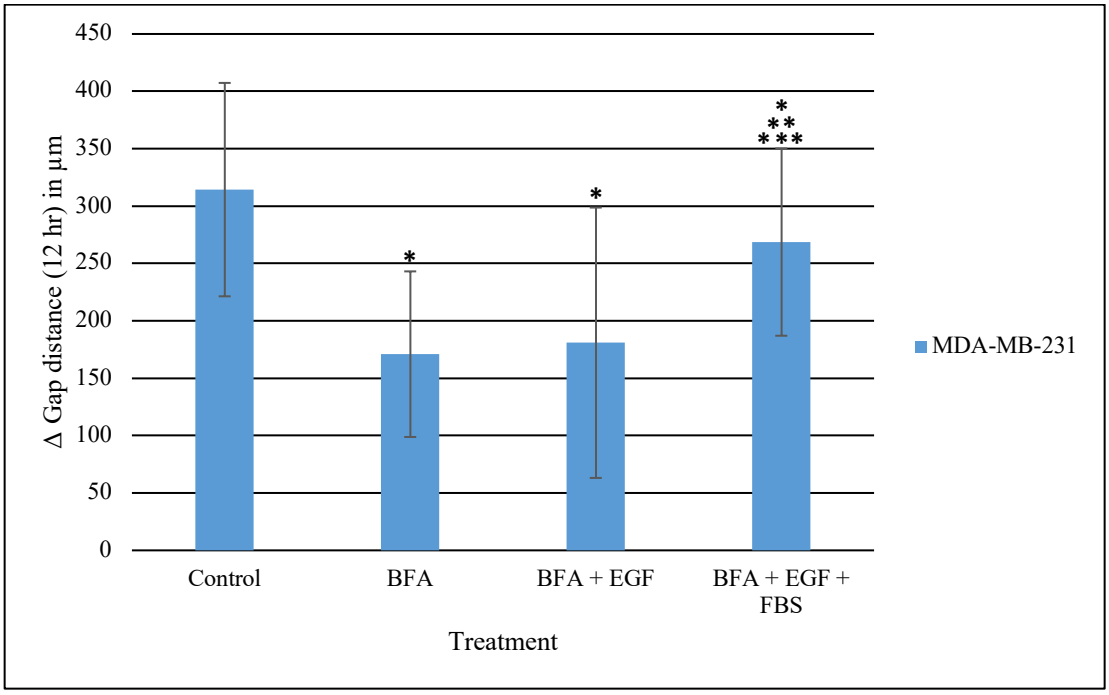

Figure 19. Golgi-disrupted migration of MDA-MB-231 cells, with or without supplementation of EGF or FBS. Average (MDA-MB-231 Control n=60, ± STD; MDA-MB-231 BFA Present n=55, ± STD; MDA-MB-231 BFA and EGF Present n=50, ± STD; MDA-MB-231 BFA, EGF and FBS Present n=45, ± STD; Control vs. BFA: $p<0.0001$; Control vs BFA and EGF: $p<0.0001$; Control vs BFA, EGF and FBS: $p=0.0087$; BFA vs. BFA and EGF: $p=0.8632$; BFA vs. BFA, EGF and FBS: $p<0.0001$; BFA and EGF vs. BFA, EGF and FBS: $p=0.0004$) change in gap distance for control and treated cells after 12 hours. Experiments were conducted after FBS starvation, with or without the presence of additional EGF (10 ng/mL), BFA (50 ng/mL) and/ FBS (10%) during wound healing. Asterisk (*) represents significance compared to the control. Double asterisks (**) represent significance compared to BFA treatment. Triple asterisks (***) represent significance compared to BFA and EGF treatment.

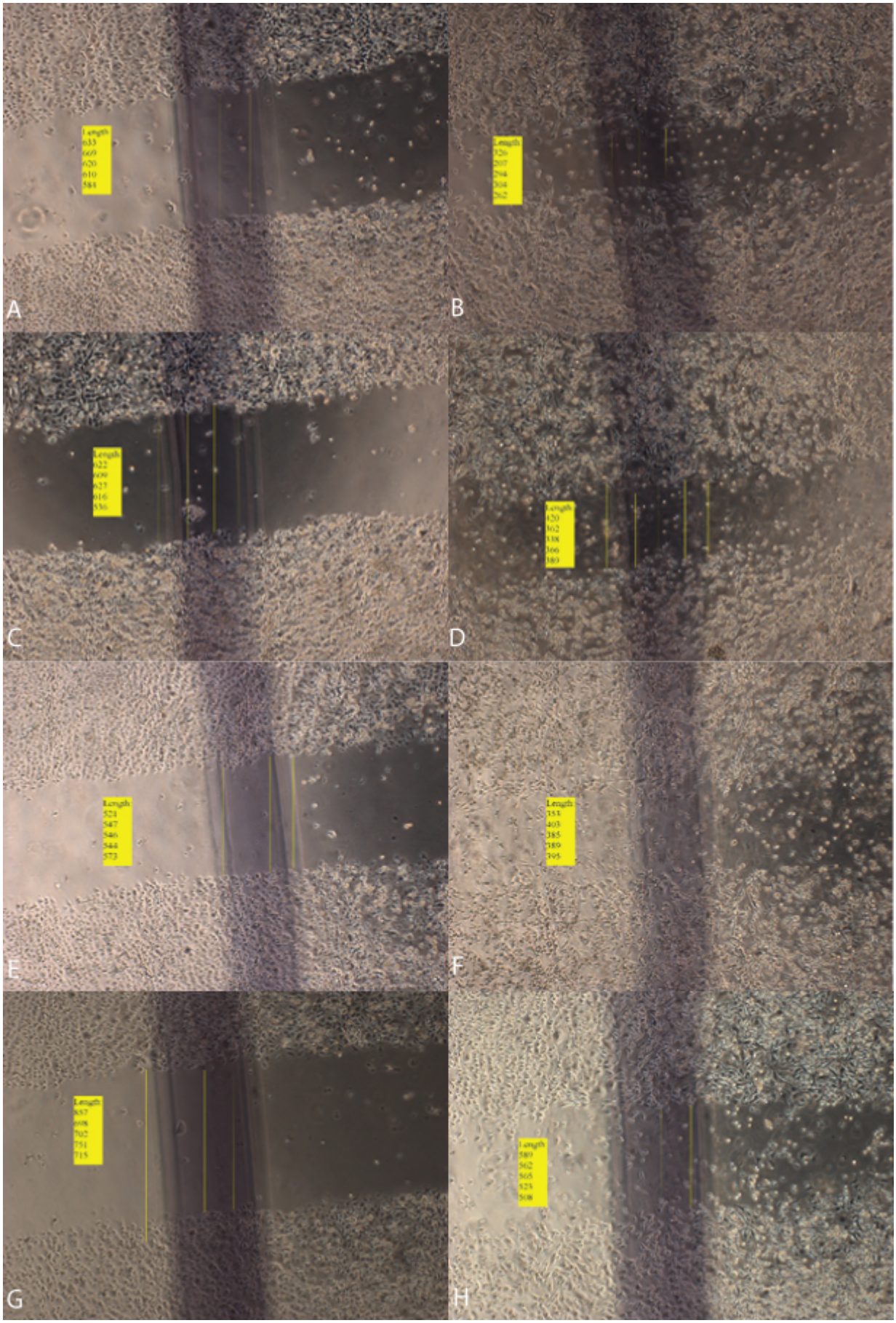
A
B
C
D
E
F
G
H

Figure 20. Images of Golgi-disrupted MDA-MB-231 cell scratch wound assay and associated scratch width measurements. Images were collected with bright-field microscopy using a 4x objective. A) Scratch wound assay using MDA-MB-231 cells, immediately after scratch. Experiments were conducted after FBS starvation. Scratch width measurements (μm) are reported in the yellow key. B) Scratch wound assay using MDA-MB-231 cells, 12 hours after scratching. Experiments were conducted after FBS starvation. Scratch width measurements (μm) are reported in the yellow key. C) Scratch wound assay using MDA-MB-231 cells, immediately after scratch. Experiments were conducted after FBS starvation, with supplemental BFA (50 ng/mL) after starving. Scratch width measurements (μm) are reported in the yellow key. D) Scratch wound assay using MDA-MB-231 cells, 12 hours after scratching. Experiments were conducted after FBS starvation, with supplemental BFA (50 ng/mL) after starving. Scratch width measurements (μm) are reported in the yellow key. E) Scratch wound assay using MDA-MB-231 cells, immediately after scratch. Experiments were conducted after FBS starvation, with supplemental BFA (50 ng/mL) and EGF (10 ng/mL) after starving. Scratch width measurements (μm) are reported in the yellow key. F) Scratch wound assay using MDA-MB-231 cells, 12 hours after scratching. Experiments were conducted after FBS starvation, with supplemental BFA (50 ng/mL) and EGF (10 ng/mL) after starving. Scratch width measurements (μm) are reported in the yellow key. G) Scratch wound assay using MDA-MB-231 cells, immediately after scratch. Experiments were conducted after FBS starvation, with supplemental BFA (50 ng/mL), EGF (10 ng/mL) and FBS (10%) after starving. Scratch width measurements (μm) are reported in the yellow key. H) Scratch wound assay using MDA-MB-231 cells, 12 hours after scratching. Experiments were conducted after FBS starvation, with supplemental BFA (50 ng/mL), EGF (10 ng/mL) and FBS (10%) after starving. Scratch width measurements (μm) are reported in the yellow key.

Just as the morphology of MCF7 cells was impacted by treatment with BFA, so too is the morphology of MDA-MB-231 cells. Treatment with solely BFA causes the cells to begin to round or stunt their protrusions (Figure 21B; Table 8). Interestingly, there is an area of the BFA treated cell, typically located around the nucleus, which appears to be webbed (Figure 21B). This phenomenon is persistent, even when EGF and FBS are added to the cells (Figures 21C, D). Supplementing the cells with FBS prevents the common rounding that is seen in other treatments (Figured 21D; Table 8).

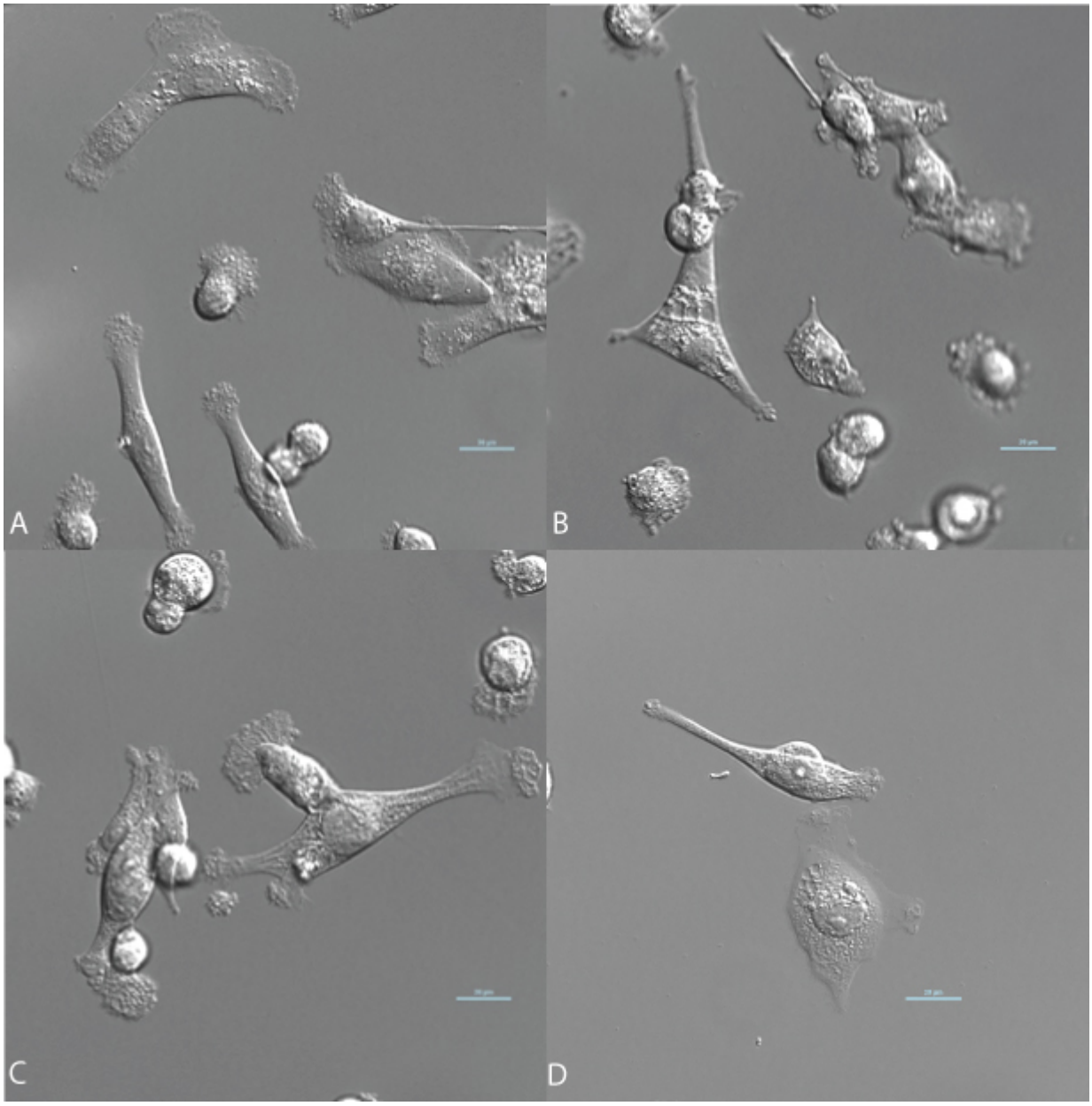

Figure 21. Golgi-disrupted morphology of the MDA-MB-231 cell type, in the presence or absence of EGF and FBS. Images were collected with DIC microscopy using a 40x objective. Scale bar is representative of 10 µm. Figure is representative of 10 fields of view. A) Morphology of MDA-MB-231 cell after 12 hours of treatment. Experiments were conducted after FBS starvation, with no supplemental EGF or FBS after starving. B) Morphology of MDA-MB-231 cell after 12 hours of treatment. Experiments were conducted after FBS starvation, with supplemental BFA (50 ng/mL) given after starving. C) Morphology of MDA-MB-231 cell after 12 hours of treatment. Experiments were conducted after FBS starvation, with supplemental BFA (50 ng/mL) and EGF (10 ng/mL) after starving. D) Morphology of MDA-MB-231 cell after 12 hours of treatment. Experiments were conducted after FBS starvation, with supplemental BFA (50 ng/mL), EGF (10 ng/mL) and FBS (10%) given after starving.

Table 8. Morphology of Golgi-disrupted MDA-MB-231 cells, with and without EGF (10 ng/mL), BFA (50 ng/mL) or FBS (10%), observed from 10 fields of view with DIC microscopy using a 40x objective.

Cell Type	Treatment	Cell Morphology	# of Cells
MDA-MB-231	Control	Epithelial Mesenchymal	17 63
	BFA	Epithelial Mesenchymal	59 15
	BFA + EGF	Epithelial Mesenchymal	35 40
	BFA + EGF + FBS	Epithelial Mesenchymal	12 59

Immunofluorescence imaging of MDA-MB-231 cells may explain the webbed structure seen on the cell. In cells treated with only BFA, the microtubule array is disorganized and appears to be less concentrated in the area that the webbing would appear (Figure 22B; Table 9). This structure appears to be rescued with the addition of EGF, with GM130 collecting especially at the protrusions leading out from the cell (Figure 22C; Table 9).

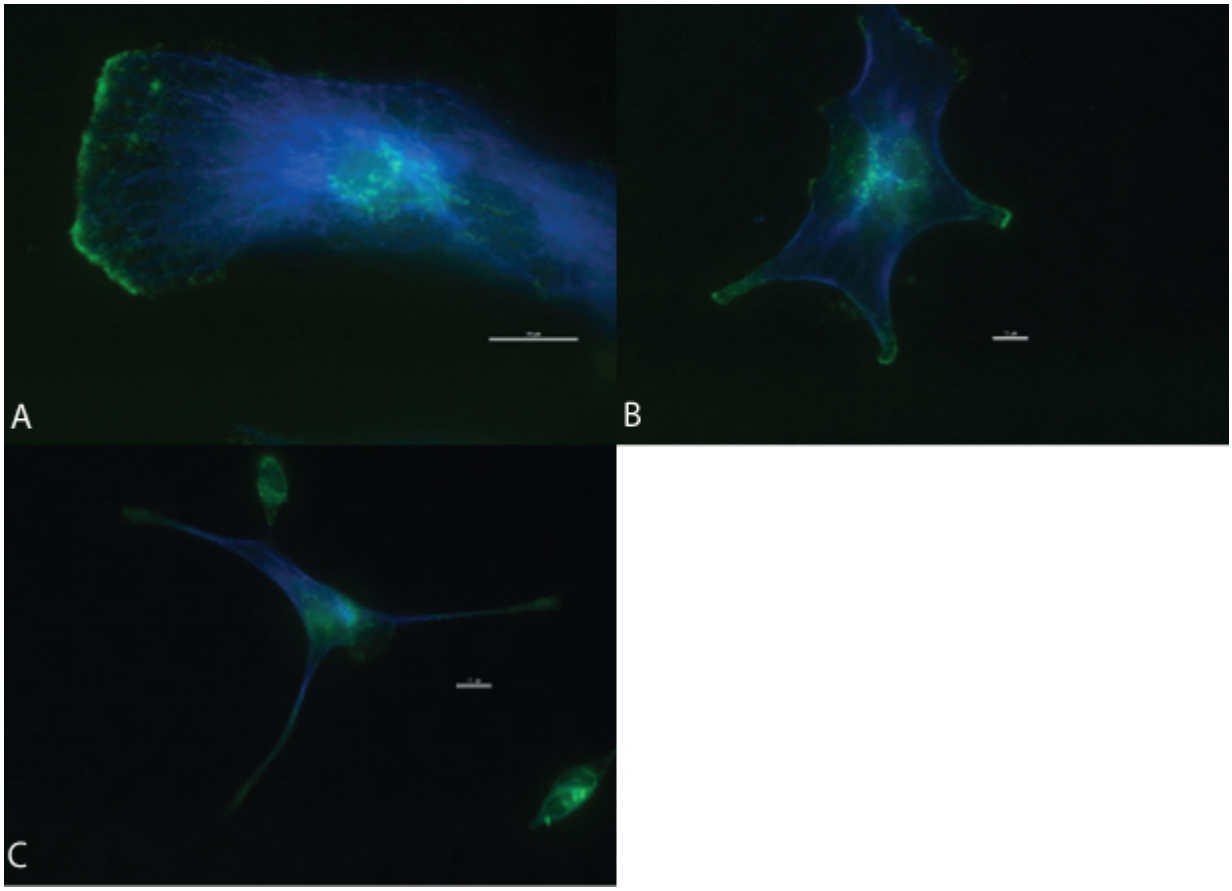

Figure 22. Golgi-disrupted MDA-MB-231 immunofluorescence of GM130 (green) and α-tubulin (blue). Images were collected with multi-channel fluorescence microscopy using a 60x objective. Scale bar is representative of 10 μm. Figure is representative of 10 fields of view. A) Organization of the Golgi and microtubules within the MDA-MB-231 cell at 12 hours after treatment. Experiments were conducted after FBS starvation. B) Organization of the Golgi and microtubules within the MDA-MB-231 cell at 12 hours after treatment. Experiments were conducted after FBS starvation, with supplemental BFA (50 ng/mL) after starving. C) Organization of the Golgi and microtubules within the MDA-MB-231 cell at 12 hours after treatment. Experiments were conducted after FBS starvation, with supplemental BFA (50 ng/mL) and EGF (10 ng/mL) after starving.

Table 9. Organization of the microtubule (MT) and Golgi distribution for Golgi-disrupted MDA-MB-231 cells, with or without BFA (50 ng/mL) or EGF (10 ng/mL), observed from 10 fields of view with multi-channel fluorescence microscopy using a 60x objective.

Cell Type	Treatment	MT Organization	# of Cells	Golgi Distribution	# of Cells
MDA-MB-231	Control	Heavily Concentrated Diffuse	10 24	Compact Diffuse	23 11
	BFA	Heavily Concentrated Diffuse	3 19	Compact Diffuse	5 17
	BFA + EGF	Heavily Concentrated Diffuse	18 9	Compact Diffuse	18 9

Disruption of the Microtubules

Disruption of the microtubules in MCF7 cells, by way of treatment with nocodazole, had no statistically significant effect on the change in gap size after 12 hours, although there appears to be a visible trend (Figure 23; p=0.2583). The addition of EGF and FBS significantly increased the change in gap distance (Figure 23; p=0.0029).

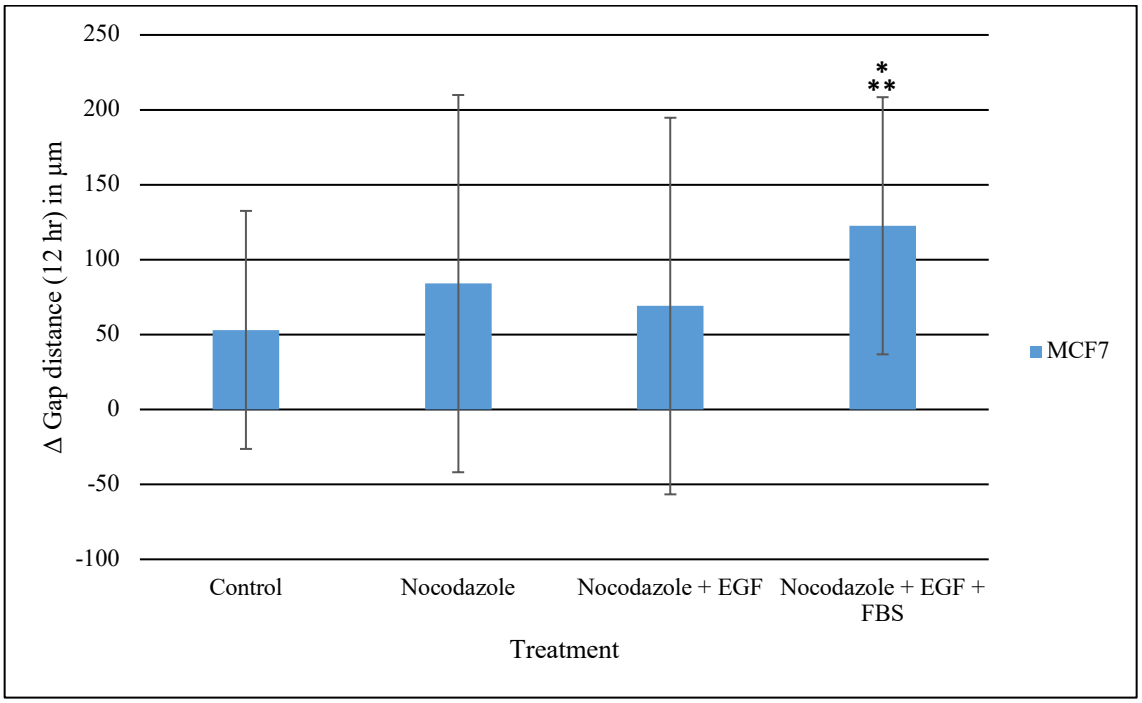

Figure 23. Comparing migration of microtubule-disrupted MCF7 cells, with and without supplementation of EGF and FBS. Average (MCF7 Control n=40, ± STD; MCF7 Nocodazole Present n=55, ± STD; MCF7 Nocodazole and EGF Present n=60, ± STD; MCF7 Nocodazole, EGF and FBS Present n=30, ± STD; Control vs. Nocodazole: p=0.2583; Control vs Nocodazole and EGF: p=0.6577; Control vs Nocodazole, EGF and FBS: p=0.0029; Nocodazole vs. Nocodazole and EGF: p=0.5252; Nocodazole vs. Nocodazole, EGF and FBS: p=0.0986; Nocodazole and EGF vs. Nocodazole, EGF and FBS: p=0.0199) change in gap distance for control and treated cells after 12 hours. Experiments were conducted after FBS starvation, with or without the presence of additional EGF (10 ng/mL), nocodazole (3 µg/mL) and FBS (10%) during wound healing. Asterisk (*) represents significance compared to the control. Double asterisks (**) represent significance compared to nocodazole and EGF treatment.

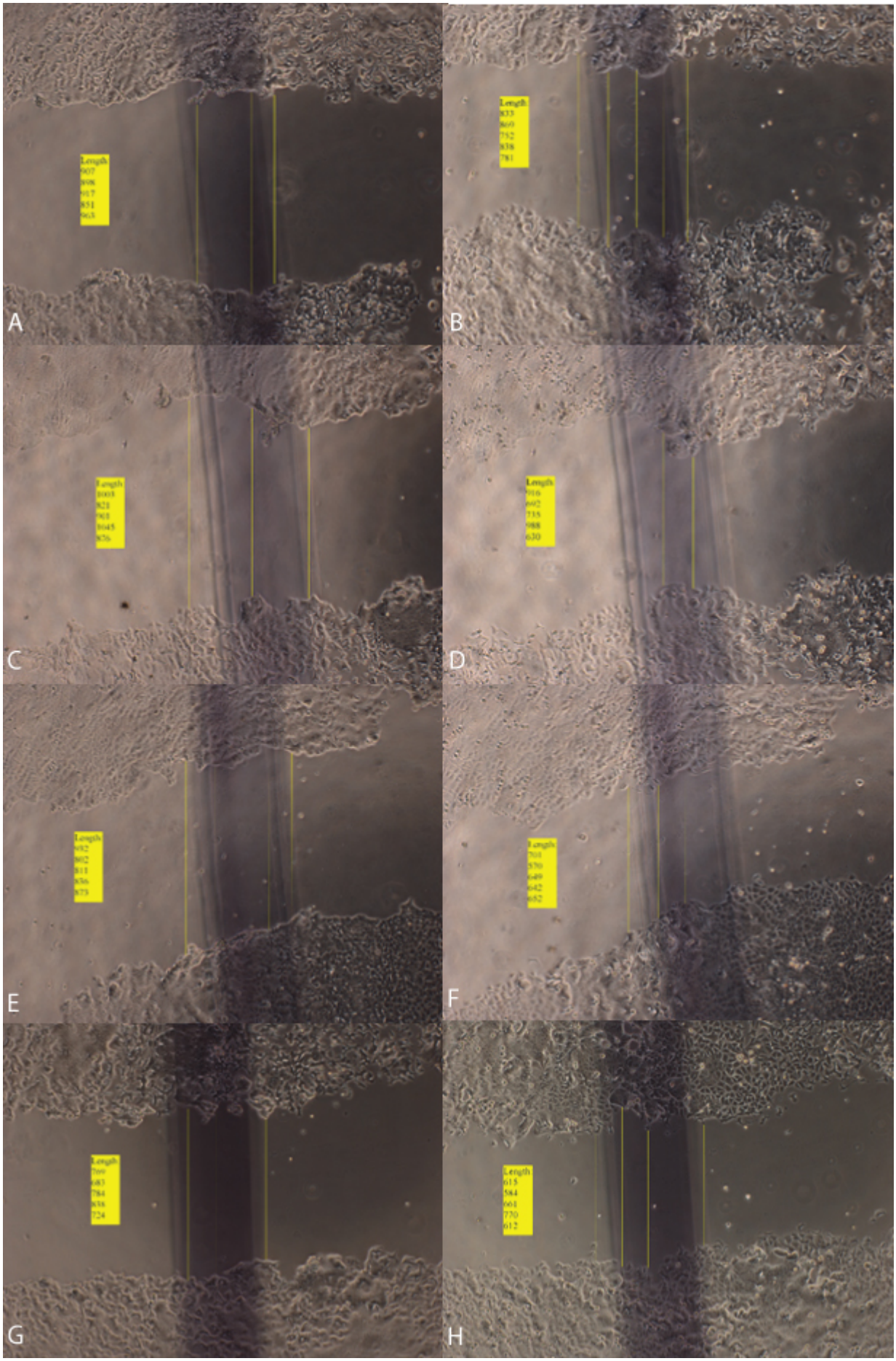
A
B
C
D
E
F
G
H

Figure 24. Images of microtubule-disrupted MCF7 cell scratch wound assay and associated scratch width measurements. Images were collected with bright-field microscopy using a 4x objective. A) Scratch wound assay using MCF7 cells, immediately after scratch. Experiments were conducted after FBS starvation. Scratch width measurements (μm) are reported in the yellow key. B) Scratch wound assay using MCF7 cells, 12 hours after scratching. Experiments were conducted after FBS starvation. Scratch width measurements (μm) are reported in the yellow key. C) Scratch wound assay using MCF7 cells, immediately after scratch. Experiments were conducted after FBS starvation, with supplemental nocodazole (3 μg/mL) after starving. Scratch width measurements (μm) are reported in the yellow key. D) Scratch wound assay using MCF7 cells, 12 hours after scratching. Experiments were conducted after FBS starvation, with supplemental nocodazole (3 μg/mL) after starving. Scratch width measurements (μm) are reported in the yellow key. E) Scratch wound assay using MCF7 cells, immediately after scratch. Experiments were conducted after FBS starvation, with supplemental nocodazole (3 μg/mL) and EGF (10 ng/mL) after starving. Scratch width measurements (μm) are reported in the yellow key. F) Scratch wound assay using MCF7 cells, 12 hours after scratching. Experiments were conducted after FBS starvation, with supplemental nocodazole (3 μg/mL) and EGF (10 ng/mL) after starving. Scratch width measurements (μm) are reported in the yellow key. G) Scratch wound assay using MCF7 cells, immediately after scratch. Experiments were conducted after FBS starvation, with supplemental nocodazole (3 μg/mL), EGF (10 ng/mL) and FBS (10%) after starving. Scratch width measurements (μm) are reported in the yellow key. H) Scratch wound assay using MCF7 cells, 12 hours after scratching. Experiments were conducted after FBS starvation, with supplemental nocodazole (3 μg/mL), EGF (10 ng/mL) and FBS (10%) after starving. Scratch width measurements (μm) are reported in the yellow key.

Comparing the morphology of MCF7 cells with and without treatment, there appear to be no differences. The cells given only nocodazole were more sparsely organized than any of the other treatments (Figure 25B). Interestingly, the morphology of the MCF7 cells treated with nocodazole, EGF and FBS were more mesenchymal than in any of the other conditions (Figure 25D; Table 10).

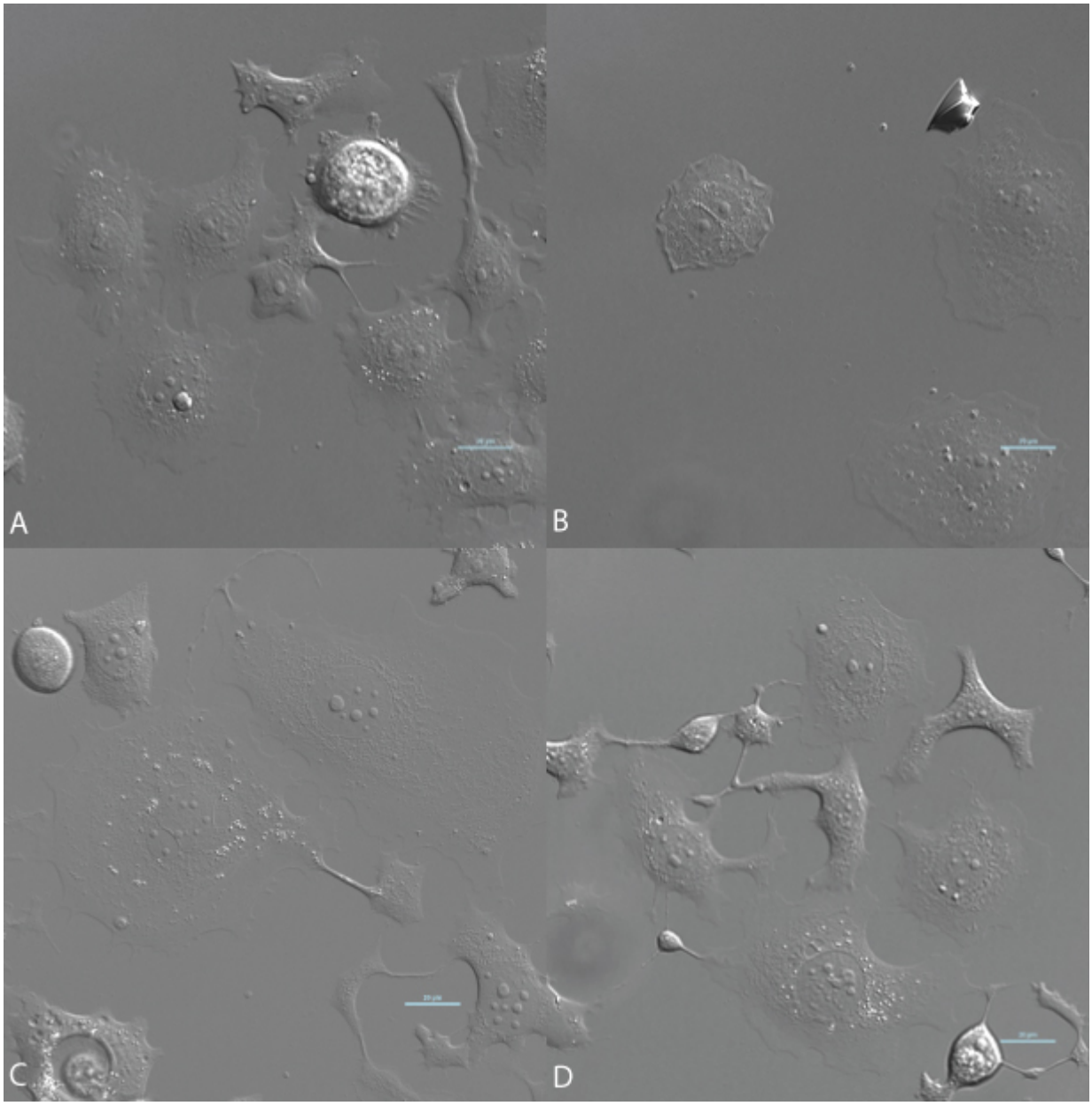

Figure 25. Microtubule-disrupted morphology of the MCF7 cell type, in the presence or absence of EGF and FBS. Images were collected with DIC microscopy using a 40x objective. Scale bar is representative of 10 µm. Figure is representative of 10 fields of view. A) Morphology of MCF7 cell after 12 hours of treatment. Experiments were conducted after FBS starvation. B) Morphology of MCF7 cell after 12 hours of treatment. Experiments were conducted after FBS starvation, with supplemental nocodazole (3 µg/mL) given after starving. C) Morphology of MCF7 cell after 12 hours of treatment. Experiments were conducted after FBS starvation, with supplemental nocodazole (3 µg/mL) and EGF (10 ng/mL) after starving. D) Morphology of MCF7 cell after 12 hours of treatment. Experiments were conducted after FBS starvation, with supplemental nocodazole (3 µg/mL), EGF (10 ng/mL) and FBS (10%) given after starving.

Table 10. Morphology of microtubule-disrupted MCF7 cells, with or without EGF (10 ng/mL), nocodazole (3 μg/mL) or FBS (10%), observed from 10 fields of view with DIC microscopy using a 40x objective.

Cell Type	Treatment	Cell Morphology	# of Cells
MCF7	Control	Epithelial	71
		Mesenchymal	16
	Nocodazole	Epithelial	71
		Mesenchymal	10
	Nocodazole + EGF	Epithelial	63
		Mesenchymal	21
	Nocodazole + EGF + FBS	Epithelial	46
		Mesenchymal	36

Immunofluorescence imaging supports the disruption of the Golgi, as well as the typically organized microtubule array, with the application of nocodazole treatment (Figure 26B; Table 11). Both structures rescued with EGF treatment, however not to the extent which control cells are organized (Figure 26D; Table 11).

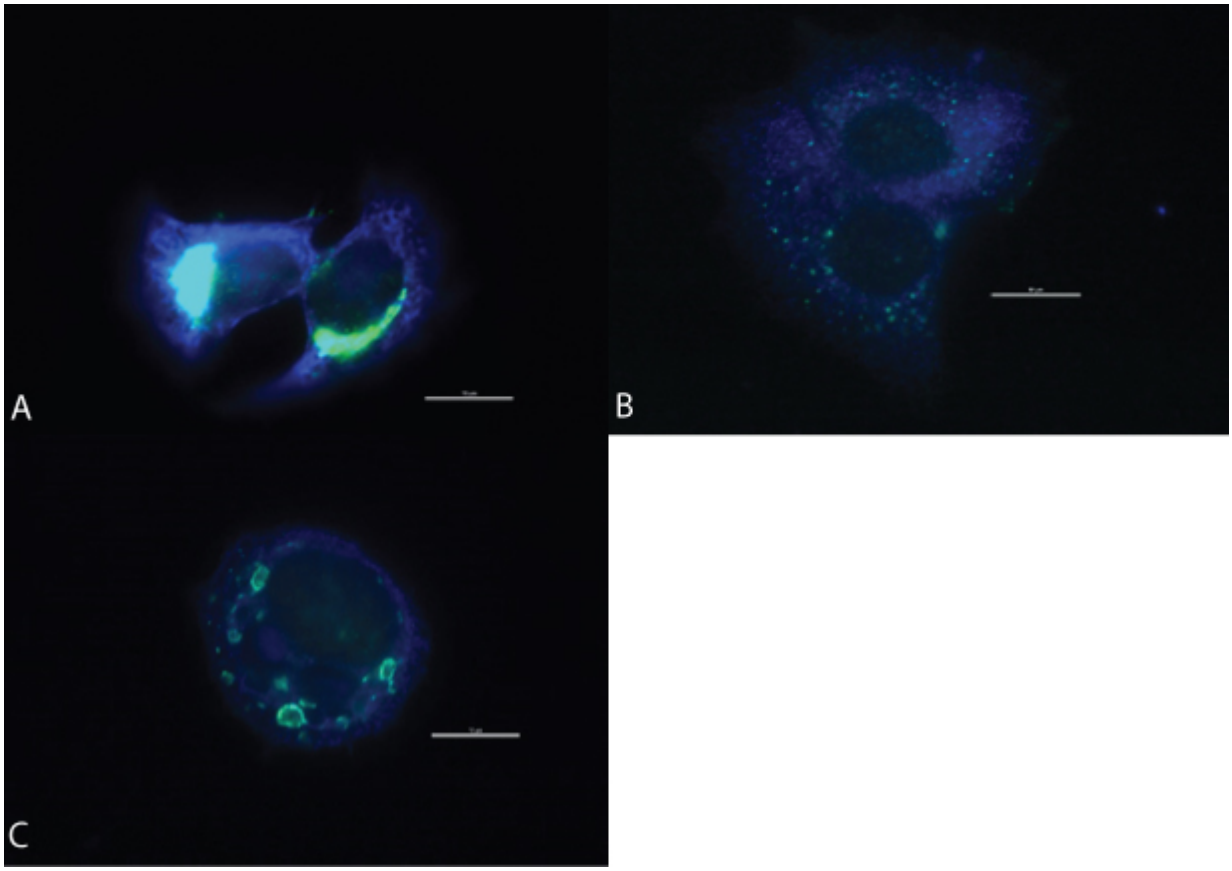

Figure 26. Microtubule-disrupted MCF7 immunofluorescence of GM130 (green) and α-tubulin (blue). Images were collected with multi-channel fluorescence microscopy using a 60x objective. Scale bar is representative of 10 µm. Figure is representative of 10 fields of view. A) Organization of the Golgi and microtubules within the MCF7 cell at 12 hours after treatment. Experiments were conducted after FBS starvation. B) Organization of the Golgi and microtubules within the MCF7 cell at 12 hours after treatment. Experiments were conducted after FBS starvation, with supplemental nocodazole (3 µg/mL) after starving. C) Organization of the Golgi and microtubules within the MCF7 cell at 12 hours after treatment. Experiments were conducted after FBS starvation, with supplemental nocodazole (3 µg/mL) and EGF (10 ng/mL) after starving.

Table 11. Organization of the microtubule (MT) and Golgi distribution for microtubule-disrupted MCF7 cells, with or without nocodazole (3 μg/mL) and EGF (10 ng/mL) observed from 10 fields of view with multi-channel fluorescence microscopy using a 60x objective.

Cell Type	Treatment	MT Organization	# of Cells	Golgi Distribution	# of Cells
MCF7	Control	Heavily Concentrated	16	Compact	33
		Diffuse	23	Diffuse	6
	Nocodazole	Heavily Concentrated	19	Compact	2
		Diffuse	17	Diffuse	34
	Nocodazole + EGF	Heavily Concentrated	15	Compact	20
		Diffuse	18	Diffuse	13

MDA-MB-231 cells were significantly impacted by treatment with nocodazole, with an approximately six-fold reduction in the change in gap distance after 12 hours (Figure 27; $p<0.0001$). Neither the addition of EGF, nor FBS, was able to rescue the cells from the significant reduction in migratory behavior (Figure 27; EGF: $p=0.2681$, EGF and FBS: $p=0.2529$).

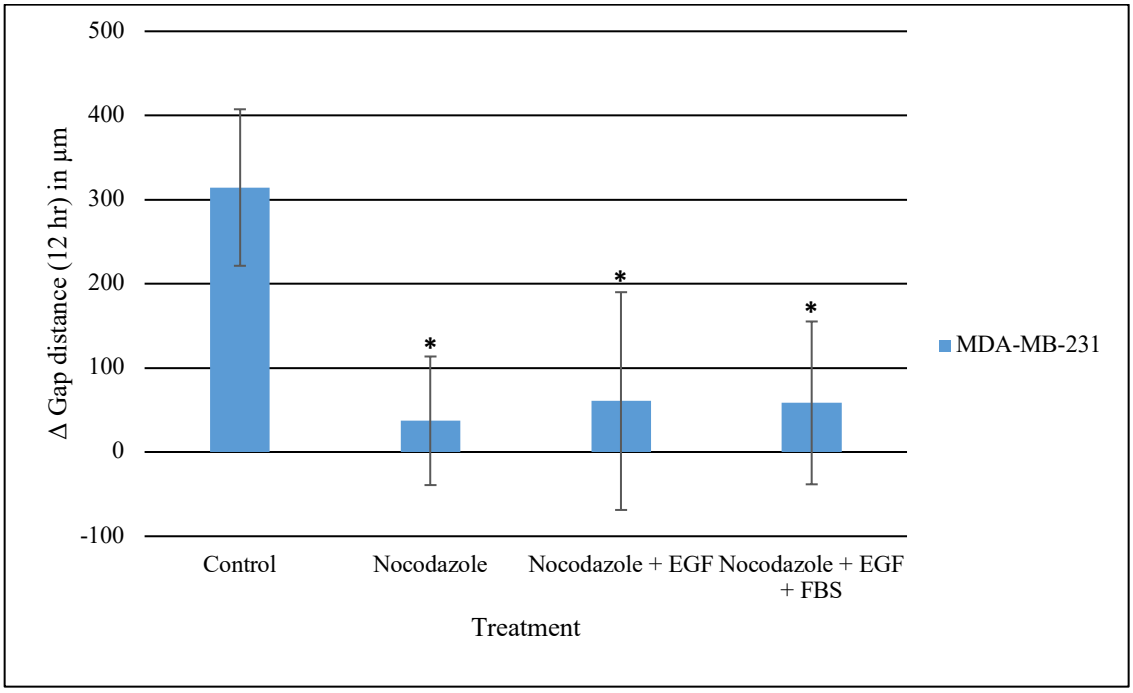

Figure 27. Comparing migration of microtubule-disrupted MDA-MB-231 cells, with and without supplementation of EGF or FBS. Average (MDA-MB-231 Control n=60, ± STD; MDA-MB-231 Nocodazole Present n=55, ± STD; MDA-MB-231 Nocodazole and EGF Present n=50, ± STD; MDA-MB-231 Nocodazole, EGF and FBS Present n=40, ± STD; Control vs. Nocodazole: $p<0.0001$; Control vs Nocodazole and EGF: $p<0.0001$; Control vs Nocodazole, EGF and FBS: $p<0.0001$; Nocodazole vs. Nocodazole and EGF: $p=0.2681$; Nocodazole vs. Nocodazole, EGF and FBS: $p=0.2529$; Nocodazole and EGF vs. Nocodazole, EGF and FBS: $p=0.9279$) change in gap distance for control and treated cells after 12 hours. Experiments were conducted after FBS starvation, with or without the presence of additional EGF (10 ng/mL), nocodazole (3 µg/mL) and FBS (10%) during wound healing. Asterisk (*) represents significance compared to the control.

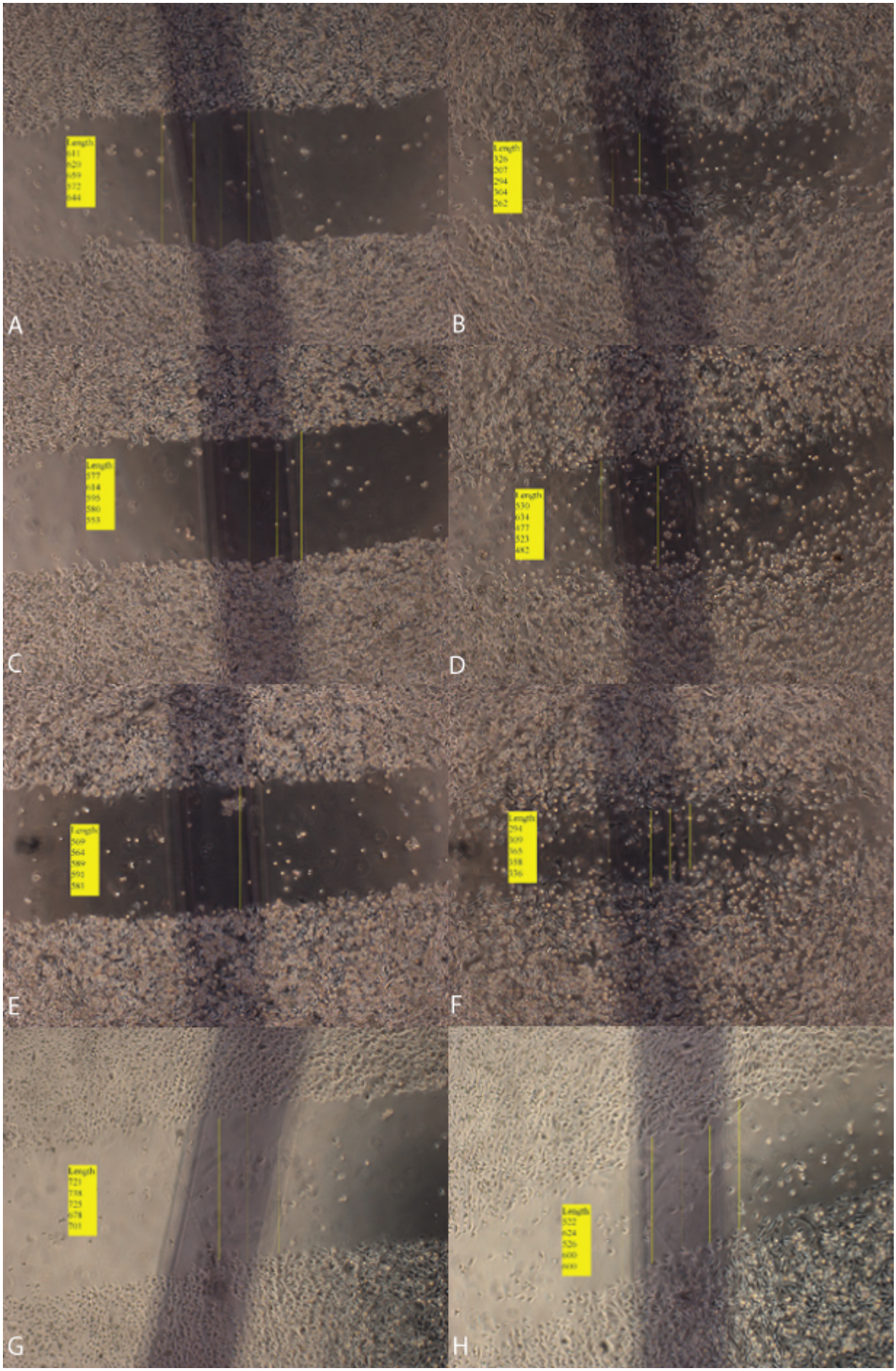
A
B
C
D
E
F
G
H

Figure 28. Images of microtubule-disrupted MDA-MB-231 cell scratch wound assay and associated scratch width measurements. Images were collected with bright-field microscopy using a 4x objective. A) Scratch wound assay using MDA-MB-231 cells, immediately after scratch. Experiments were conducted after FBS starvation. Scratch width measurements (μm) are reported in the yellow key. B) Scratch wound assay using MDA-MB-231 cells, 12 hours after scratching. Experiments were conducted after FBS starvation. Scratch width measurements (μm) are reported in the yellow key. C) Scratch wound assay using MDA-MB-231 cells, immediately after scratch. Experiments were conducted after FBS starvation, with supplemental nocodazole (3 μg/mL) after starving. Scratch width measurements (μm) are reported in the yellow key. D) Scratch wound assay using MDA-MB-231 cells, 12 hours after scratching. Experiments were conducted after FBS starvation, with supplemental nocodazole (3 μg/mL) after starving. Scratch width measurements (μm) are reported in the yellow key. E) Scratch wound assay using MDA-MB-231 cells, immediately after scratch. Experiments were conducted after FBS starvation, with supplemental nocodazole (3 μg/mL) and EGF (10 ng/mL) after starving. Scratch width measurements (μm) are reported in the yellow key. F) Scratch wound assay using MDA-MB-231 cells, 12 hours after scratching. Experiments were conducted after FBS starvation, with supplemental nocodazole (3 μg/mL) and EGF (10 ng/mL) after starving. Scratch width measurements (μm) are reported in the yellow key. G) Scratch wound assay using MDA-MB-231 cells, immediately after scratch. Experiments were conducted after FBS starvation, with supplemental nocodazole (3 μg/mL), EGF (10 ng/mL) and FBS (10%) after starving. Scratch width measurements (μm) are reported in the yellow key. H) Scratch wound assay using MDA-MB-231 cells, 12 hours after scratching. Experiments were conducted after FBS starvation, with supplemental nocodazole (3 μg/mL), EGF (10 ng/mL) and FBS (10%) after starving. Scratch width measurements (μm) are reported in the yellow key.

Morphology of these cells are dramatically changed with nocodazole treatment. All treated cells have significant rounding, losing many mesenchymal features (Figure 29; Table 12). The combination treatment of nocodazole and EGF saved some of the mesenchymal features of these cells but appeared to dwarf the morphology seen in the control MDA-MB-231 cells (Figure 29C, Table 12). Surprisingly, FBS had only a slight rescuing effect on the morphology of the MDA-MB-231 cells (Figure 29D, Table 12).

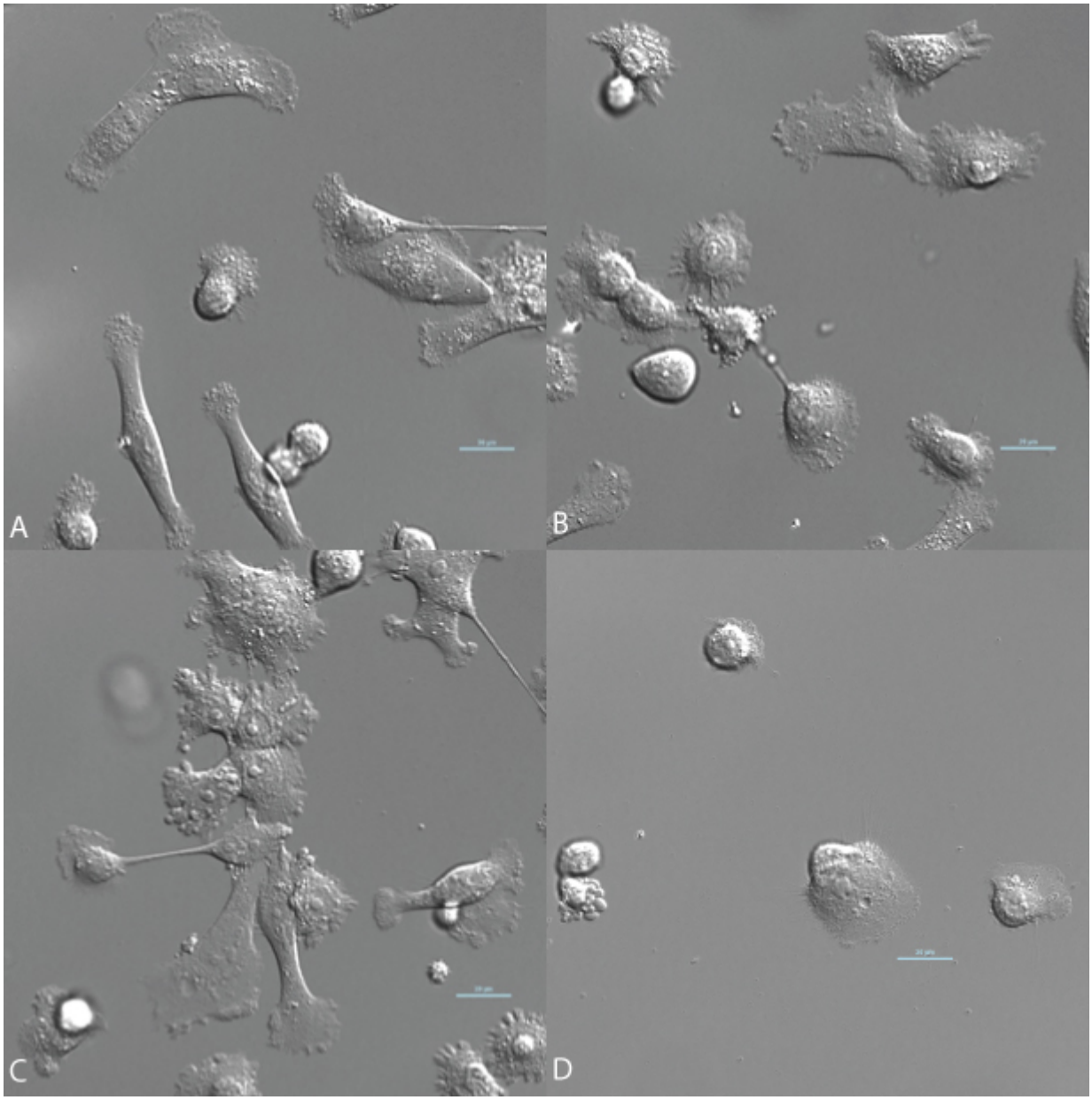

Figure 29. Microtubule-disrupted morphology of the MDA-MB-231 cell type, in the presence or absence of EGF and FBS. Images were collected with DIC microscopy using a 40x objective. Scale bar is representative of 10 µm. Figure is representative of 10 fields of view. A) Morphology of MDA-MB-231 cell after 12 hours of treatment. Experiments were conducted after FBS starvation. B) Morphology of MDA-MB-231 cell after 12 hours of treatment. Experiments were conducted after FBS starvation, with supplemental nocodazole (3 µg/mL) given after starving. C) Morphology of MDA-MB-231 cell after 12 hours of treatment. Experiments were conducted after FBS starvation, with supplemental nocodazole (3 µg/mL) and EGF (10 ng/mL) after starving. D) Morphology of MDA-MB-231 cell after 12 hours of treatment. Experiments were conducted after FBS starvation, with supplemental nocodazole (3 µg/mL), EGF (10 ng/mL) and FBS (10%) given after starving.

Table 12. Morphology of microtubule-disrupted MDA-MB-231 cells, with or without EGF (10 ng/mL), nocodazole (3 μg/mL) or FBS (10%), observed from 10 fields of view with DIC microscopy using a 40x objective.

Cell Type	Treatment	Cell Morphology	# of Cells
MDA-MB-231	Control	Epithelial	17
		Mesenchymal	63
	Nocodazole	Epithelial	50
		Mesenchymal	18
	Nocodazole + EGF	Epithelial	27
		Mesenchymal	44
	Nocodazole + EGF + FBS	Epithelial	48
		Mesenchymal	33

Observation of the microtubules in the immunofluorescence samples of nocodazole treated MDA-MB-231 cells suggests a miniaturization of the arrays, as well as some loss in organization (Figure 30B, Table 13). Interestingly, GM130 in these same cells is less centralized, and expressed around the majority of the perimeter of the cell. More centralized GM130 is observed throughout portions of the cell in the presence of EGF, however this molecule still surrounds the perimeter of the cell (Figure 30C, Table 13).

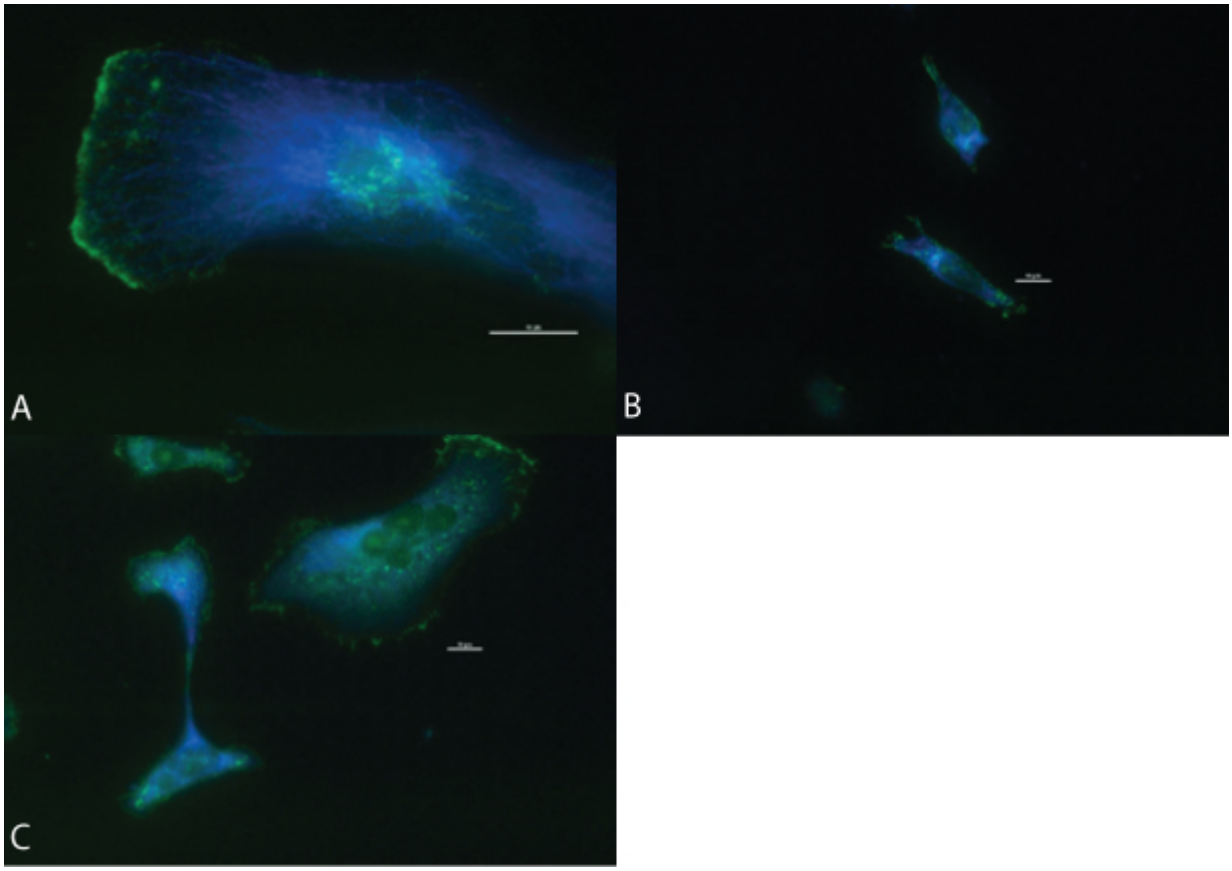

Figure 30. Microtubule-disrupted immunofluorescence in MDA-MB-231 cell of GM130 (green) and α-tubulin (blue). Images were collected with multi-channel fluorescence microscopy using a 60x objective. Scale bar is representative of 10 µm. Figure is representative of 10 fields of view. A) Organization of the Golgi and microtubules within the MDA-MB-231 cell at 12 hours after treatment. Experiments were conducted after FBS starvation. B) Organization of the Golgi and microtubules within the MDA-MB-231 cell at 12 hours after treatment. Experiments were conducted after FBS starvation, with supplemental nocodazole (3 µg/mL) after starving. C) Organization of the Golgi and microtubules within the MDA-MB-231 cell at 12 hours after treatment. Experiments were conducted after FBS starvation, with supplemental nocodazole (3 µg/mL) and EGF (10 ng/mL) after starving.

Table 13. Organization of the microtubule (MT) and Golgi distribution for microtubule-disrupted MDA-MB-231 cells, with or without nocodazole (3 μg/mL) or EGF (10 ng/mL). Immunofluorescence was observed from 10 fields of view with multi-channel fluorescence microscopy using a 60x objective.

Cell Type	Treatment	MT Organization	# of Cells	Golgi Distribution	# of Cells
MDA-MB-231	Control	Heavily Concentrated	10	Compact	23
		Diffuse	24	Diffuse	11
	Nocodazole	Heavily Concentrated	13	Compact	8
		Diffuse	20	Diffuse	25
	Nocodazole + EGF	Heavily Concentrated	20	Compact	10
		Diffuse	5	Diffuse	15

CHAPTER V

Discussion and Conclusions

Discussion

General Observations

Initial testing supported the predicted behavior of the two cancer cell types: the MDA-MB-231 cells migrate more quickly than MCF7 cells (Figure 2). These results were expected as previous work from our lab show that the MDA-MB-231 cell line has a more aggressive basal migratory behavior than the MCF7 cell line in a scratch wound assay (Grady and Lundin-Schiller, personal communication). This same behavior has also been noted in transwell assays (Yokotsuka et al., 2011; Furtado et al., 2012; Hooshmand et al., 2013). Each cell line has a unique morphology: MDA-MB-231 cells have a mesenchymal morphology, while MCF7 cells are epithelial (Figure 4). Immunofluorescence assays indicate a more organized microtubule array in the MDA-MB-231 cells, however the Golgi in these cells has a unique organization, with high concentrations of the GM130 Golgi marker present both perinuclear and at the leading edge (Figure 5). While this Golgi organization was apparent in our hands, other studies do not provide evidence of this occurring during immunofluorescence experiments (Adams et al., 2010; Baschieri et al., 2015). Notably, another Golgi protein marker, Giantin, is organized toward the leading edge, however it is perinuclear (Dubois et al., 2017).

Disruption of the Golgi

Disruption of the Golgi with BFA treatment appears to have a small effect on the rate of migration of MCF7 cells, however it has a significant effect on MDA-MB-231 cells (Figures 15, 19). This BFA-induced reduction in migration was also observed in an earlier study utilizing the MDA-MB-231 cell line (Tseng et al., 2014). A previous study showed that BFA treatment, at a concentration that was greater than ten times that of this study, results in the decrease of motility

in mouse fibroblasts (Bershadsky and Futerman, 1994). The morphology of MCF7 cells do not differ greatly between control and BFA treated cells, however some rounding does occur (Figure 17). Interestingly, just as the migration behavior of the MDA-MB-231 cells is greatly impacted by BFA, so too is the morphology of these cells (Figure 21). Along with morphological changes, the Golgi in each cell type was disrupted after treatment (Figure 22, Table 9). These results are in agreement with those published during the preparation of this manuscript, showing a scattering of the Golgi after BFA treatment in MDA-MB-231 cells (Luchsinger et al., 2018). This disruption has been reported in a number of cell types, with the notable exception of MDCK (Thyberg and Moskalewski, 1992; Reaves and Banting, 1992; van Meer and van't Hof, 1993; Bershadsky and Futerman, 1994). Due to the morphological changes that occur with this treatment, it is likely that the modulation of Golgi-nucleated microtubules, and subsequent Golgi disruption, play a role in the adhesion of these breast cancer cells, especially the MDA-MB-231 cell line.

Disruption of the Microtubules

Disruption of the microtubules with nocodazole has greater impacts on the MDA-MB-231 cell type than the MCF7 cell type. The migration of MCF7 cells is not significantly impacted by the microtubule disruption associated with this treatment (Figure 23). This resistance to nocodazole treatment has also been observed in the adhesion and migration of cells derived from tumor spheroids (Dorie et al., 1986). While others have noted a change in the morphology of leukocytes with nocodazole treatment, this study and another from our lab found that MCF7 cells were resistant to major morphological changes when given nocodazole (Keller et al., 1984; Zahn and Lundin-Schiller, 2016). MDA-MB-231 cell migration is greatly impacted by treatment with nocodazole (Figure 27). This treatment affects microtubules cell-wide, resulting in a much

greater reduction in migratory behavior of these cells, compared to disruption of only the Golgi-nucleated microtubules. There is a visible change in the morphology of the cells, with stunting of cellular protrusions (Figure 29). Similar results have also been observed in fibroblasts, other epithelial cells and vascular endothelial cells (Terasaki et al., 1986). These results suggest potentially related mechanisms which result in the observed adhesion loss of the MDA-MB-231 cells due to nocodazole and BFA treatment.

Rescue

The addition of the chemoattractant EGF impacts the motility of MDA-MB-231 cells and MCF7 cells, this was expected (Figures 13, 14; Zahn and Lundin-Schiller, 2016; Kozlova et al., 2016). The addition of FBS, which contains EGF and other chemoattractants, significantly increases the motility of each cell type (Figures 13, 14). The addition of these chemoattractants increase the migration of MCF7 cells, regardless of treatment with either pharmacological reagent (Figures 15, 23). Interestingly, in these cells there is reorganization of the Golgi and microtubules with EGF treatment, after disruption with BFA (Figure 18). However, because there is no significant change in motility correlated with either microtubule disruption or reorganization, there is no evidence in the current study that microtubules contribute to the directed migration of MCF7 cells.

The efficacy of MDA-MB-231 migratory behavior rescue with chemoattractants differs from the MCF7 cell type. The addition of EGF to MDA-MB-231 cells rescues their migration, while also returning organization to the Golgi and microtubules, after treatment with BFA (Figures 19, 22). This rescue is prevented in cells treated with nocodazole (Figures 27, 30). This suggests that Golgi-nucleated microtubules are involved in the directed migration of MDA-MB-231 cells. However, the inability to rescue migration and organization of the Golgi and

microtubules after nocodazole treatment, combined with an even greater decrease in motility compared to BFA treatment, suggests that the mechanism for directed cell migration in MDA-MB-231 cells likely involves microtubules throughout the cell, not solely those nucleated at the Golgi.

Conclusions

A number of studies have implicated microtubules in the motility of cells (Goslin et al., 1989; Liao et al., 1995; Eddy et al., 2002; Schmoranzer et al., 2003). The results of this study present evidence supporting the hypothesis that a specific subset consisting of Golgi-nucleated microtubules contribute to the directed migration of an aggressive breast cancer cell type. Evidence for this phenomenon exists in other cell types, including other cancer cells (Bershadsky and Futerman, 1994; di Campli et al., 1998). However, this mechanism is not shared by all breast cancer types, as the MCF7 cell migration was unaffected by the loss of organization of these microtubules with BFA treatment. Further, this subset of microtubules is not entirely responsible for directed cell migration in MDA-MB-231 cells, as complete microtubule disassembly decreased migration to an even further extent.

These microtubules may be responsible for the delivery of EGF receptors to the leading edge of the breast cancer cell. Broad disassembly of microtubules has been implicated in the loss of EGF-mediated epithelial migration, as well as polarized trafficking (Eilers et al., 1989; Breitfeld et al., 1990; Nakamura et al., 1991). However, published results show that Golgi-nucleated microtubules are involved in the delivery of the EGF receptor in other cell types, including cancerous cell lines (Gamou and Shimizu, 1988; Gamou et al., 1988; Wang et al., 2010). In our study, supplementation of the cells with EGF rescues the cells from the decreased migration and, to some extent, morphological changes induced by the disruption of Golgi-nucleated microtubules. Another group has noted the rescue of Golgi organization with EGF supplementation (di Campli et al., 1999). It is possible that saturating the cells with EGF utilizes the remaining receptors available to the cell, while disruption of these microtubules prevents the expression of additional EGF receptors at the membrane, as BFA treatment is associated with

retrograde trafficking back to the ER (Lippincott-Schwartz et al., 1990). However, this is also specific to the more aggressive breast cancer cell type, suggesting a difference in the mechanisms involved in EGF receptor transport between the cell types.

It is difficult, with the current results, to determine the molecular mechanisms involved in motility that the Golgi-nucleated microtubules modulate, or for which mechanisms that they may also be utilized in combination with microtubules cell-wide. Microtubules throughout the cell are utilized in the transport of many proteins in a number of cell types, however the transport of EGF receptors has the strongest support in this model (Ojakian and Schwimmer, 1992; Lafont et al., 1994). If this hypothesis is correct, then it is probable that the EGF receptors transported along Golgi-nucleated microtubules to the leading edge are responsible for the activation of FAKs and other molecules involved in interaction of the cell with its surrounding extracellular matrix. Staining for the EGF receptor and FAK in each condition, for each cell type, would provide much greater insight into the actual mechanism through which the Golgi-nucleated microtubules function. Also, models utilizing genetic control over the expression of the many proteins involved in the nucleation of microtubules would be an invaluable tool for studying this process (Stehbens et al., 2014).

Because there is interplay between the different elements of the cytoskeleton and published data implicates EGF in actin organization, it is likely that actin structures are also impacted by these treatments, however these structures were not considered in the current study (Chan et al. 1998). It is important to determine if the results of this study are due solely to modulation of the Golgi and its associated microtubules, or if this is an artifact of changes in other elements of the cytoskeleton. Staining for actin and utilizing compounds which modulate its dynamics would provide evidence to address this concern.

The definitive way to determine that this subset of microtubules provides an important role in cellular migration in highly aggressive breast cancer cells would be to observe and characterize the physical interaction between the components of the Golgi and the microtubule, such as the aforementioned γ-tubulin and AKAP450, during treatment of the cells with compounds which alter directed migration. A study utilizing immunoprecipitation is described in Appendix A for interested readers. However, due to the constraints of this thesis project, a properly working method has yet to be established.

LITERATURE CITED

Adams H, Chen R, Liu Z, Whitehead I (2010). Regulation of breast cancer cell motility by T-cell lymphoma invasion and metastasis-inducing protein. *Breast Cancer Res*, 12(5):R69.

Adams R, Pollard T (1986). Propulsion of organelles isolated from *Acanthamoeba* along actin filaments by myosin-I. *Nature*, 322(6081):754-6.

Adams R, Pollard T (1989). Binding of myosin I to membrane lipids. *Nature*, 340(6234):565-8.

Ades F, Tryfonidis K, Zardavas Z (2017). The past and future of breast cancer treatment—from the papyrus to individualised treatment approaches. e*cancer,* 11:746.

Albrecht-Buehler G (1976). Filopodia of spreading 3T3 cells. Do they have a substrate-exploring function? *J Cell Biol*, 69(2):275-86.

Allen C, Borisy G (1974). Structural polarity and directional growth of microtubules of *Chlamydomonas* flagella. *J Mol Biol*, 90(2):381-402.

Allen J. (2005). New York: Metropolitan Museum of Art; Yale University Press. The art of medicine in ancient Egypt. p. 115.

American Institute for Cancer Research (2007). Washington, DC: American Institute of Cancer Research. Food, nutrition, physical activity and the prevention of cancer: a global perspective.

Anderson R (1977). Actin filaments in normal and migrating corneal epithelial cells. *Invest Ophthalmol Vis Sci*, 16(2):161-6.

Angel A, Farkas J (1974). Regulation of cholesterol storage in adipose tissue. *J Lipid Res,* 15:491-99.

Angelini T, Hannezo E, Trepat X, Fredberg J, Weitz D (2010). Cell migration driven by cooperative substrate deformation patterns. *Phys Rev Lett,* 104.

Arioka M, Hirata A, Takatsuki A, Yamasaki M (1991). Brefeldin A blocks an early stage of protein transport in *Candida albicans*. *J Gen Microbiol*, 137(6):1253-62.

Asch B, Medina D, Brinkley B (1979). Microtubules and actin-containing filaments of normal, preneoplastic, and neoplastic mouse mammary epithelial cells. *Cancer Res*, 39(3):893-907.

Aune D, Chan D, Greenwood D, Vieira A, Rosenblatt D, Vieira R, Norat T (2012). Dietary fiber and breast cancer risk: a systematic review and meta-analysis of prospective studies. *Ann Oncol,* 23(6):1394-402.

Baguley B, Leung E (2011). Breast cancer - carcinogenesis, cell growth and signalling pathways: heterogeneity of phenotype in breast cancer cell lines. Prof. Mehmet Gunduz (Ed.), ISBN: 978-953-307-714-7.

Bannai H, Inoue T, Nakayama T, Hattori M, Mikoshiba K (2004). Kinesin dependent, rapid, bi-directional transport of ER sub-compartment in dendrites of hippocampal neurons. *J Cell Sci*, 117(Pt2):163-75.

Barabutis N, Tsellou E, Schally A, Kouloheri S, Kalofoutis A, Kiaris H (2007). Stimulation of proliferation of MCF-7 breast cancer cells by a transfected splice variant of growth hormone-releasing hormone receptor. *Proc Natl Acad Sci USA,* 104(13):5575-9.

Barnes S, Singletary K, Frey R (2000). Ethanol and acetaldehyde enhance benzo[a]pyrene-DNA abduct formation in human mammary epithelial cells. *Carcinogenesis*, 21:2123-8.

Bartek J, Lukas J (2001). Mammalian G1- and S-phase checkpoints in response to DNA damage. *Curr Opin Cell Biol,* 13(6):738-47.

Baryiko B, Wagner M, Reizes O, Albanesi J (1992). Purification and characterization of a mammalian myosin I. *Proc Natl Acad Sci USA*, 89(2):490-4.

Baschieri F, Allmen E, Legler D, Farhan H (2015). Loss of GM130 in breast cancer cells and its effect on cell migration, invasion and polarity. *Cell Cycle*, 14(8):1139-47.

Baselga J, Tripathy D, Mendelsohn J, Baughman S, Benz C, Dantis L Skarlin N, Seidman A, Hudis C, Moore J, Rosen P, Twaddell T, Henderson I, Norton L (1996). Phase II study of weekly intravenous recombinant humanized anti-p185HER2 monoclonal antibody in patients with HER2/neu-overexpressing metastatic breast cancer. *J Clin Oncol*, 14(3):737-44.

Beatson G (1912). Splenic metastasis in a case of carcinoma of tongue, due probably to vascular dissemination. *Glasgow Med J*, 77(3):161-8.

Berg J, Hutter R (1995). Breast cancer. *Cancer* 1(75): 257-69.

Bernstein L (2002). Epidemiology of endocrine-related risk factors for breast cancer. *J Mammary Gland Biol Neoplasia*, 7:3–15.

Bershadsky A, Futerman A (1994). Disruption of the Golgi apparatus by brefeldin A blocks cell polarization and inhibits directed cell migration. *Proc Natl Acad Sci USA,* 91:5686-9.

Billger M, Bhattacharjee G, Williams Jr. R (1996). Dynamic instability of microtubules assembled from microtubule-associated protein-free tubulin: neither variability of growth and shortening rates nor “rescue” requires microtubule-associated proteins. *Biochemistry*, 35(42):13656-63.

Birkett C, Coulson C, Pogson C, Gull K (1981). Inhibition of secretion of proteins and triacylglycerol from isolated rat hepatocytes mediated by benzimidazole carbamate antimicrotubule agents. *Biochem Pharmacol*, 30(12):1629-33.

Borg A, Sandberg T, Nilsson K, Johannsson O, Klinker M, Måsbäck A, Westerdahl J, Olsson H, Ingvar C (2000). High frequency of multiple melanomas and breast and pancreas carcinomas in CDKN2A mutation-positive melanoma families. *J Natl Cancer Inst,* 92(15):1260-6.

Bose A, Guilherme A, Robida S, Nicoloro S, Zhou Q, Jiang Z, Pomerleau D, Czech M (2002). Glucose transporter recycling in response to insulin is facilitated by myosin Myo1c. *Nature*, 420(6917):821-4.

Boveri T (2008). Concerning the origin of malignant tumours by Theodor Boveri. Translated and annotated by Henry Harris (1914). *J Cell Sci,* 121(Suppl 1):1-84.

Bozzuto G, Condello M, Molínarí A (2015) Migratory behaviour of tumour cells: a scanning electron microscopy study. *Ann Ist Super Sanita,* 51(2):139-47.

Brede C, Fjeldal P, Skjevrak I, Herikstad H (2003). Increased migration levels of bisphenol A from polycarbonate baby bottles after dishwashing, boiling and brushing. *Food Addit Contam,* 20:684-9.

Breitfeld P, McKinnon W, Mostov K (1990). Effect of nocodazole on vesicular traffic to the apical and basolateral surfaces of polarized MDCK cells. *J Cell Biol*, 111(6 Pt 1):2365-73.

Bretscher M, Aguado-Velasco C (1998). Membrane traffic during cell locomotion. *Curr Opin Cell Biol,* 10(4):537-41.

Brooks S, Locke E, Soule H (1973). Estrogen receptor in a human cell line (MCF-7) form breast carcinoma. *J Biol Chem* 248(17):6251-3.

Brunton V, Ozanne B, Paraskeva C, Frame M (1997). A role for epidermal growth factor receptor, c-Src and focal adhesion kinase in an *in vitro* model for the progression of colon cancer. *Oncogene*, 14(3):283-93.

Bryan J (1976). A quantitative analysis of microtubule elongation. *J Cell Biol*, 71(3):749-67.

Brzeska H, Guag J, Remmert K, Chacko S, Korn E (2010). An experimentally based computer search identifies unstructured membrane-binding sites in proteins: application to class I myosins, PAKS and CARMIL. *J Biol Chem*, 285(8)5738-47.

Cailleau R, Olivé M, Cruciger Q (1978). Long-term human breast carcinoma cell lines of metastatic origin: preliminary characterization. *In Vitro,* 14(11):911-5.

Campisi J, Gray H, Pardee A, Dean M, Sonenshein G (1984). Cell-cycle control of *c-myc* but not *c-ras* expression is lost following chemical transformation. *Cell,* 36(2):241-247.

Carlier M, Hill T, Chen Y (1984). Interference of GTP hydrolysis in the mechanism of microtubule assembly: an experimental study. *Proc Natl Acad Sci USA*, 81(3):771-5.

Carlier M, Pantaloni D (1981). Kinetic analysis of guanosine 5'-triphosphate hydrolysis associated with tubulin polymerization. *Biochemistry*, 20(7):1918-24.

Carpenter G, Cohen S (1976). Human epidermal growth factor and the proliferation of human fibroblasts. *J Cell Physiol*, 88(2):227-37.

Caro L, Palade G (1964). Protein synthesis, storage, and discharge in the pancreatic exocrine cell. An autoradiographic study. *J Cell Biol*, 20:473-95.

Cassimeris L, Pryer N, Salmon E (1988). Real-time observation of microtubule dynamic instability in living cells. *J Cell Biol*, 107(6 Pt 1):2223-31.

Celis J, Celis A (1985). Cell cycle-dependent variations in the distribution of the nuclear protein cyclin proliferating cell nuclear antigen in cultured cells: subdivision of S phase. *Proc Natl Acad Sci USA*, 82(10):3262-6.

Chan A, Raft S, Bailly M, Wyckoff J, Segall J, Condeelis J (1998). EGF stimulates an increase in actin nucleation and filament number at the leading edge of the lamellipod in mammary adenocarcinoma cells. *J Cell Sci*, 111(Pt 2):199-211.

Chen J, Russo J (2009). ERα-negative and triple negative breast cancer: molecular features and potential therapeutic approaches. *Biochim Biophys Acta,* 1796(2):162-75.

Cheung H, Terry D (1980). Effects of nocodazole, a new synthetic microtubule inhibitor, on movement and spreading of mouse peritoneal macrophages. *Cell Biol Int Rep*, 4(12):1125-9.

Cid-Arregui A, Parton R, Simons K, Dotti C (1995). Nocodazole-dependent transport, and brefeldin A--sensitive processing and sorting, of newly synthesized membrane proteins in cultured neurons. *J Neurosci*, 15(6):4259-69.

Ciosk R, Zachariae W, Michaelis C, Shevchenko A, Mann M, Nasmyth K (1998). An ESP1/PDS1 complex regulates loss of sister chromatid cohesion at the metaphase to anaphase transition in yeast. *Cell*, 93(6):1067-76.

Claxton L, Woodall Jr. G (2007). A review of the mutagenicity and rodent carcinogenicity of ambient air. *Mutat Res,* 636:36-94.

Cleveland D, Kirschner M, Cowan N (1978). Isolation of separate mRNAs for alpha- and beta tubulin and characterization of the corresponding *in vitro* translation products. *Cell*, 15(3):1021-31.

Cohen S (1965). The stimulation of epidermal proliferation by a specific protein (EGF). *Dev Biol*, 12(3):394-407.

Collaborative Group on Hormonal Factors in Breast Cancer (2012). Menarche, menopause, and breast cancer risk: individual participant meta-analysis, including 118,964 women with breast cancer from 117 epidemiological studies. *Lancet Oncol*, 13:1141–51.

Conney A, Miller E, Miller J (1956). The metabolism of methylated aminoazo dyes. V. Evidence for induction of enzyme synthesis in the rat by 3-methylcholanthrene. *Cancer Res,* 16:450–9.

Cook J, Hewett C, Hieger I (1933). The isolation of a cancer-producing hydrocarbon from coal tar. Parts I, II, and III. *J Chem Soc,* 24:395–405.

Coussens L, Yang-Feng T, Liao Y, Chen E, Gray A, McGrath J, Seeburg P, Libermann T, Schlessinger J, Franke U, Levinson A, Ullrich A (1985). Tyrosine kinase receptor with extensive homology to EGF receptor shares chromosomal location with neu oncogene. *Science*, 230(4730):1132-9.

D'Anselmi F, Masiello M, Cucina A, Proietti S, Dinicola S, Pasqualato A, Ricci G, Dobrowolny G, Catizone A, Palombo A, Bizzarri M (2013) Microenvironment promotes tumor cell reprogramming in human breast cancer cell lines. *PLoS ONE,* 8(12): e83770.

de Brabander M, de May J, Joniau M, Geuens G (1977). Ultrastructural immunocytochemical distribution of tubulin in cultured cells treated with microtubule inhibitors. *Cell Biol Int Rep*, 1(2):177-83.

Delfosse V, Grimaldi M, Pons J, Boulahtouf A, Cavailles V, Labesse G, Bourguet W, Balaguer P (2012). Structural and mechanistic insights into bisphenols action provide guidelines for risk assessment and discovery of bisphenol A substitutes. *Proc Natl Acad Sci USA,* 109(37):14930-5.

Deng Y, Storrie B (1988). Animal cell lysosomes rapidly exchange membrane proteins. *Proc Natl Acad Sci USA*, 85(11):3860-4.

Desai A, Verma S, Mitchison T, Walczak C (1999). Kin I kinesins are microtubule-destabilizing enzymes. *Cell*, 96:69-78.

Desai D, Gu Y, Morgan D (1992). Activation of human cyclin-dependent kinases *in vitro*. *Mol Biol Cell* 3(5):571-825.

di Campli A, Valderrama F, Babià T, De Matteis M, Luini A, Egea G (1998). Morphological changes in the Golgi complex correlate with actin cytoskeleton rearrangements. *Cell Motil Cytoskeleton*, 43(4):334-48.

Doberstein S, Pollard T (1992). Localization and specificity of the phospholipid and actin binding sites on the tail of *Acanthamoeba* myosin IC. *J Cell Biol*, 117(6):1241-9.

Donaldson J, Finazzi D, Klausner R (1992). Brefeldin A inhibits Golgi membrane-catalysed exchange of guanine nucleotide onto ARF protein. *Nature*, 360(6402):350-2.

Donaldson J, Lippincott-Schwartz J, Bloom G, Kris T, Klausner R (1990). Dissociation of a 110 kD peripheral membrane protein from the Golgi apparatus is an early event in brefeldin A action. *J Cell Biol*, 111(6 Pt 1):2295-306

Donato F, Boffetta P, Puoti M (1998). A meta-analysis of epidemiological studies on the combined effect of hepatitis B and C virus infections in causing hepatocellular carcinoma. *Int J Cancer*, 75:347–54.

Dorie M, Kallman R, Coyne A (1986). Effect of cytochalasin B, nocodazole and irradiation on migration and internalization of cells and microspheres in tumor cell spheroids. *Exp Cell Res*, 166(2):370-8.

Downward J, Parker P, Waterfield M (1984). Autophosphorylation sites on the epidermal growth factor receptor. *Nature,* 311:483-5.

Dubois F, Alpha K, Turner C (2017). Paxillin regulates cell polarization and anterograde vesicle trafficking during cell migration. *Mol Biol Cell*, 28(26):3815-31.

Durrbach A, Louvard D, Coudrier E (1996). Actin filaments facilitate two steps of endocytosis. *J Cell Sci*, 109(Pt2):457-65.

Dutta A, Din S, Brill S, Stillman B (1991). Phosphorylation of replication protein A: a role or cdc2 kinase in G1/S regulation. *Cold Spring Harb Symp Quant Biol*, 56:315-24.

Edds K (1977). Dynamic aspects of filopodial formation by reorganization of microfilaments. *J Cell Biol*, 73(2):479-91.

Eddy R, Pierini L, Maxfield F (2002). Microtubule asymmetry during neutrophil polarization and migration. *Mol Biol Cell*, 13(12):4470-83.

Eilers U, Klumperman J, Hauri H (1989). Nocodazole, a microtubule-active drug, interferes with apical protein delivery in cultured intestinal epithelial cells (Caco-2). *J Cell Biol*, 108(1):13-22.

Erickson H (1974). Microtubule surface lattice and subunit structure and observations on reassembly. *J Cell Biol*, 60(1):153-67.

Etienne-Manneville S (2013). Microtubules in cell migration. *Annu Rev Cell Dev Biol*, 29:471-99.

Evans T, Rosenthal E, Youngblom J, Distel D, Hunt T (1983). Cyclin: a protein specified by maternal mRNA in sea urchin eggs that is destroyed at each cleavage division. *Cell*, 33:389-96.

Fang F, Newport J (1991). Evidence that the G1-S and G2-M transitions are controlled by different cdc2 protein in higher eukaryotes. *Cell*, 66(4):731-42.

Fath K, Mamajiwalla S, Burgess D (1993). The cytoskeleton in development of epithelial cell polarity. *J Cell Sci Suppl*, 17:65-73.

Fath K, Trimbur G, Burgess D (1994). Molecular motors are differentially distributed on Golgi membranes from polarized epithelial cells. *J Cell Biol*, 126(3):661-75.

Feit H, Slusarek L, Shelanski M (1971). Heterogeneity of tubulin subunits. *Proc Natl Acad Sci USA*, 68(9):2028-31.

Fey E, Capco D, Krochmalnic G, Penman S (1984). Epithelial structure revealed by chemical dissection and unembedded electron microscopy. *J Cell Biol*, 99(1Pt2):203s-8s.

Fidler I (1989). Origin and biology of cancer metastasis. *Cytometery*, 10:673-80.

Ford D, Easton D, Peto J (1995). Estimates of the gene frequency of *BRCA1* and its contribution to breast and ovarian cancer incidence. *Am J Hum Genet,* 57:1457-62.

Frankel F (1976). Organization and energy-dependent growth of microtubules in cells. *Proc Natl Acad Sci USA*, 73(8):2798-802.

Friedl P, Locker J, Sahai E, Segall JE (2012). Classifying collective cancer cell invasion. *Nat Cell Biol,* 14:777-83.

Fujiwara T, Oda K, Yokota S, Takatsuki A, Ikehara Y (1988). Brefeldin A causes disassembly of the Golgi complex and accumulation of secretory proteins in the endoplasmic reticulum. *J Biol Chem*, 263(34):18545-52.

Furtado C, Marcondes M, Sola-Penna M, Zancan P (2012). Clotrimazole preferentially inhibits human breast cancer cell proliferation, viability and glycolysis. *PLoS One,* 7(2):e30462.

Gamou S, Hirai M, Rikimaru K, Enomoto S, Shimizu N (1988). Biosynthesis of the epidermal growth factor receptor in human squamous cell carcinoma lines: secretion of the truncated receptor is not common to epidermal growth factor receptor-hyperproducing cells. *Cell Struct Funct*, 13(1):25-38.

Gamou S, Shimizu N (1988). Glycosylation of the epidermal growth factor receptor and its relationship to membrane transport and ligand binding. *J Biochem*, 104(3):388-96.

Gard D, Kirschner M (1987). A microtubule-associated protein from *Xenopus* eggs that specifically promotes assembly at the plus-end. *J Cell Biol*, 105(5):2203-15.

Gaudet M, Gapstur S, Sun J, Diver W, Hannah L, Thun M (2013). Active smoking and breast cancer risk: original cohort data and meta-analysis. *J Natl Cancer Inst*, 105:515–25.

Gelbert L, Cai S, Lin X, Sanchez-Martinez C, Del Prado M, Lallena M, Torres R, Ajamie R, Wishart G, Flack R, Neubauer B, Young J, Chan E, Iversen P, Cronier D, Kreklau E, de Dios A (2014). Preclinical characterization of the CDK4/6 inhibitor LY2835219: in-vivo cell cycle-dependent/independent anti-tumor activities alone/in combination with gemcitabine. *Invest New Drugs*, 32(5):825-37.

Gelles J, Landick R (1998). RNA polymerase as a molecular motor. *Cell,* (93)1:13-6.

Gest C, Joimel U, Huang L, Pritchard L, Petit A, Dulong C, Buquet C, Hu C, Mirshahi P, Laurent M, Fauvel-Lafève F, Cazin L, Vannier J, Lu H, Soria J, Li H, Varin R, Soria C (2013). Rac3 induces a molecular pathway triggering breast cancer cell aggressiveness: differences in MDA-MB-231 and MCF-7 breast cancer cell lines. *BMC Cancer,* 13:63.

Gibbons I, Rowe A (1965). Dynein: a protein with adenosine triphosphatase activity from cilia. *Science*, 149(3682):424-6.

Girard F, Strausfeld U, Fernandez A, Lamb N. Cyclin A is required for the onset of DNA replication in mammalian fibroblasts. *Cell*, 67(6):1169-79.

Goodman L, Wintrobe M, Dameshek W, Goodman M, Gilman A, McLennan M (1984). Nitrogen mustard therapy. Use of methyl-bis(beta-chloroethyl)amine hydrochloride and tris(beta-chloroethyl)amine hydrochloride for Hodgkin's disease, lymphosarcoma, leukemia and certain allied and miscellaneous disorders. *JAMA,* 251(17):2255-61.

Gorbsky G, Kallio M, Daum J, Topper L (1999). Protein dynamics at the kinetochore: cell cycle regulation of the metaphase to anaphase transition. *FASEB J*, 13 Suppl 2:S231-4.

Gordon L, Mulligan K, Maxwell-Jones H, Adams M, Walker R, Jones J (2003). Breast cell invasive potential relates to the myoepithelial phenotype. *Int J Cancer,* 106:8-16.

Goslin K, Birgbauer E, Banker G, Solomon F (1989). The role of cytoskeleton in organizing growth cones: a microfilament-associated growth cone component depends upon microtubules for its localization. *J Cell Biol*, 109(4 Pt 1):1621-31.

Gottardis M, Jordan V (1988). Development of Tamoxifen-stimulated growth of MCF-7 tumors in athymic mice after long-term antiestrogen administration. *Cancer Res,* 48:5183-7.

Greene G, Nolan C, Engler J, Jensen E (1980). Monoclonal antibodies to human estrogen receptor. *Proc Natl Acad Sci USA,* 77(9):5115-9.

Gruda M, Kovary K, Metz R, Bravo R (1994). Regulation of Fra-1 and Fra-2 phosphorylation differs during the cell cycle of fibroblasts and phosphorylation in vitro by MAP kinase affects DNA binding activity. *Oncogene,* 9(9):2537-47.

Gu Y, Turck C, Morgan D (1993). Inhibition of CDCK2 activity *in vivo* by an associated 20K regulatory subunit. *Nature*, 366(6456):707-10.

Guilluy C, Swaminathan V, Garcia-Mata R, O'Brien E, Superfine R and Burridge K (2011). The Rho GEFs LARG and GEF-H1 regulate the mechanical response to force on integrins. *Nat Cell Biol*, 13:722-7.

Haimo L, Telzer B, Rosenbaum J (1979). Dynein binds to and crossbridges cytoplasmic microtubules. *Proc Natl Acad Sci USA*, 76(11)5759-63.

Hanahan D, Weinberg R (2011). Hallmarks of cancer: the next generation. *Cell,* 144(5):646-74.

Harada A, Takei Y, Kanai Y, Nonaka S, Hirokawa N (1998). Golgi vesiculation and lysosome dispersion in cells lacking cytoplasmic dynein. *J Cell Biol*, 141(1):51-59.

Harder K, Moller N, Peacock J, Jirik F (1998). Protein-tyrosine phosphatase alpha regulates Src family kinases and alters cell-substratum adhesion. *J Biol Chem*, 273(48):31890-900.

Harris H (1954). Role of chemotaxis in inflammation. *Physiol Rev,* 34:529-62.

Hauck C, Sieg D, Hsia D, Loftus J, Gaarde W, Monia B, Schlaepfer D (2001). Inhibition of focal adhesion kinase expression or activity disrupts epidermal growth factor-stimulated signaling promoting the migration of invasive human carcinoma cells. *Cancer Res*, 61(19):7079-90.

Hayden S, Wolenski J, Mooseker M (1990). Binding of brush border myosin I to phospholipid vesicles. *J Cell Biol*, 111(2):443-51.

HEI Asbestos Literature Review Panel (1991). Cambridge, MA: Asbestos in public and commercial buildings: a literature review and synthesis of current knowledge.

HEI Air Toxics Review Panel (2007). Boston, MA: Mobile-source air toxics: a critical review of the literature on exposure and health effects.

Heidemann S, McIntosh J (1980). Visualization of the structural polarity of microtubules. *Nature*, 286(5772):517-9.

Heldring N, Pike A, Andersson S, Matthews J, Cheng G, Hartman J, Tujague M, Ström A, Treuter E, Warner M, Gustafsson J (2007). Estrogen receptors: how do they signal and what are their targets. *Physiol Rev*, 87(3):905-31.

Hendricks L, McClanahan S, Palade G, Farquhar M (1992). Brefeldin A affects early events but does not affect late events along the exocytic pathway in pancreatic acinar cells. *Proc Natl Acad Sci USA*, 89(15):7242-6.

Herman I, Crisona N, Pollard T (1981). Relation between cell activity and the distribution of cytoplasmic actin and myosin. *J Cell Biol*, 90(1):84-91.

Herrero R, Castellsagué X, Pawlita M et al.; IARC Multicenter Oral Cancer Study Group (2003). Human papillomavirus and oral cancer: the International Agency for Research on Cancer multicenter study. *J Natl Cancer Inst*, 95:1772–83.

Hill T, Carlier M (1983). Steady-state theory of the interference of GTP hydrolysis in the mechanism of microtubule assembly. *Proc Natl Acad Sci*, 80(23):7234-8.

Hitchcock-DeGregori S (1980). Actin assembly. *Nature*, 288(5790):437-8.

Hoebeke J, van Nijen G, de Brabander M (1976). Interaction of oncodazole (R 17934), a new anti-tumoral drug, with rat brain tubulin. *Biochem Biophys Res Commun*, 69(2):319-24.

Holland J (2014). Do infections play a role in breast cancer? Cancer World Report, 2014.

Hollstein M, Sidransky D, Vogelstein B, Harris C (1991). *Science,* 253:49-53.

Hooshmand S, Ghaderi A, Yusoff K, Karraupiah T, Rosli R, Mojtahedi Z (2013). Downregulation of RhoGDIα increased migration and invasion of ER^+ MCF7 and ER^- MDA-MB-231 breast cancer cells. *Cell Adh Migr*, 7(3):297-303.

Horowitz K, Costlow M, McGuire W (1975). MCF-7: a human breast cancer cell line with estrogen, androgen, progesterone, and glucocorticoid receptors. *Steroids,* 26(6):785-95.

Hull B, Staehelin L (1979). The terminal web. A reevaluation of its structure and function. *J Cell Biol*, 81(1):67-82.

Hunter K, Crawford N, Alsarraj J (2008). Mechanisms of metastasis. *Breast Cancer Res*, 10(Supp 1):S2.

Hunziker W, Whitney J, Mellman I (1991). Selective inhibition of transcytosis by brefeldin A in MDCK cells. Cell, 67(3):617-27.

IARC (2002). Lyon: IARC. IARC handbooks of cancer prevention, vol. 6: weight control and physical activity.

IARC (2004). Some drinking-water disinfectants and contaminants, including arsenic. *IARC Monogr Eval Carcinog Risks Hum,* 84:1-477.

IARC (2004). Tobacco smoke and involuntary smoking. *IARC Monogr Eval Carcinog Risks Hum*, 83:1–1438.

IARC (2010). Alcohol consumption and ethyl carbamate. *IARC Monogr Eval Carcinog Risks Hum*, 96:1–1428.

IARC (2013). Diesel and gasoline engine exhausts and some nitroarenes. *IARC Monogr Eval Carcinog Risks Hum,* 105:9–699.

Jackman M, Lindon C, Nigg E, Pines J (2003). Active cyclin B1-Cdk1 first appears on centrosomes in prophase. *Nat Cell Biol,* 5(2):143-8.

Janski N, Masoud K, Batzenschlager M, Herzog E, Evrard J, Houlné G, Bourge M, Chabouté M, Schmit A (2012). The GCP3-interacting proteins GIP1 and GIP2 are required for γ -tubulin complex protein localization, spindle integrity, and chromosomal activity. *Plant Cell*, 24(3):1171-87.

Jeng M, Shupnik M, Bender T, Westin E, Bandyopadhyay D, Kumar R, Masamura S, Santen R (1998). Estrogen receptor expression and function in long-term estrogen-deprived human breast cancer cells. *Endocrinology,* 139(10): 4164-74.

Jensen E (1975). Estrogen receptors in hormone-dependent breast cancers. *Cancer Res,* 35:3362-4.

Johnson M, Maro B (1985). A dissection of the mechanisms generating and stabilizing polarity in mouse 8- and 16-cell blastomeres: the role of cytoskeletal elements. *J Embryol Exp Morphol*, 90:311-34

Johnston J, Sloboda R (1992). A 62-kd protein required for mitotic progression is associated with the mitotic apparatus during M-phase and with the nucleus during interphase. *J Cell Biol*, 119(4):843-54.

Jontes J, Wilson-Kubalek E, Milligan R (1995). A 32 degree tail swing in brush border myosin I on ADP release. *Nature*, 378(6558):751-3.

Joslin E, Opresko L, Well A, Wiley H, Lauffenburger D (2007). EGF-receptor-mediated mammary epithelial cell migration is driven by sustained ERK signaling from autocrine stimulation. *J Cell Sci,* 120:3688-99.

Kaverina I, Straube A (2011). Regulation of cell migration by dynamic microtubules. *Semin Cell Dev Biol*, 22(9):968-74.

Keller H, Naef A, Zimmerman A (1984) Effects of colchicine, vinblastine and nocodazole on polarity, motility, chemotaxis and cAMP levels of human polymorphonuclear leukocytes. *Exp Cell Res*, 153(1):173-85.

Kennaway E (1930). Further experiments on cancer-producing substances. *Biochem J,* 24:497–504.

Keyomarsi K, Pardee A (1993). Redundant cyclin overexpression and gene amplification in breast cancer cells. *Proc Natl Acad Sci USA*, 90(3):1112-6.

Kim B, Pimkhaun H, Chau M, Kim Y, Swartz M, Wu M (2013). Cooperative roles of SDF-1α and EGF gradients on tumor cell migration revealed by a robust 3D microfluidic model. *PLoS One*, 8(7):e68422.

King R, Peters J, Tugendreich A, Rolfe M, Hieter P, Kirschner M (1995). A 20S complex containing CDC27 and CDC16 catalyzes the mitosis-specific conjugation of ubiquitin to cyclin B. *Cell*, 8(2):279-88.

King W, Greene G (1984). Monoclonal antibodies localize oestrogen receptor in the nuclei of target cells. *Nature,* 307(5953):745-7.

Kirschner M (1980). Implications of treadmilling for the stability and polarity of actin and tubulin polymers *in vivo*. *J Cell Biol*, 86(1):330-4.

Kobayashi T (1975). Dephosphorylation of tubulin-bound guanosine triphosphate during microtubule assembly. *J Biochem*, 77(6):1193-7.

Kollman J, Merdes A, Mourey L, Agard D (2011). Microtubule nucleation by γ–tubulin complexes. *Nat Rev Mol Cell Biol*, 12:709-21.

Kozlova N, Samoylenko A, Drobot L, Kietzmann T (2016). Urokinase is a negative modulator of Egf-dependent proliferation and motility in the two breast cancer lines MCF-7 and MDA-MB-231. *Mol Carcinog*, 55(2):170-81.

Krendel M, Zenke F, Bokoch G (2002). Nucleotide exchange factor GEF-H1 mediates cross-talk between microtubules and the actin cytoskeleton. *Nat Cell Biol,* 4(4):294-301.

Kupfer A, Louvard D, Singer S (1982). Polarization of the Golgi apparatus and the microtubule organizing center in cultured fibroblasts at the edge of an experimental wound. *Proc Natl Acad Sci USA*, 79(8):2603-7.

Lachenmeier D, Przybylski M, Rehm J (2012). Comparative risk assessment of carcinogens in alcoholic beverages using the margin of exposure approach. *Int J Cancer*, 131:e995–1003.

Lafont F, Burkhardt J, Simons K (1994). Involvement of microtubule motors in basolateral and apical transport in kidney cells. *Nature*, 372(6508):801-3.

Lakhani S, Reis-Filho J, Fulford L, Penault-Llorca F, van der Vijver M, Parry S, Bishop T, Benitez J, Rivas C, Bignon Y, Chang-Claude J, Hamann U, Cornelisse C, Devilee P, Beckmann M, Nestle-Krämling C, Daly P, Haites N, Varley J, Lalloo F, Evans G, Maugard C, Meijers-Heijboer H, Klijn J, Olah E, Gusterson B, Pilotti S, Radice P, Scherneck S, Sobol H, Jacquemier J, Wagner T, Peto J, Stratton M, McGuffog L, Easton D, Breast Cancer Linkage Consortium (2005). Prediction of *BRCA1* status in patients with breast cancer using estrogen receptor and basal phenotype. *Clin Cancer Res,* 11(14):5175-80.

Lakhtakia, R (2014). A brief history of breast cancer, part 1: surgical domination reinvented. *Sultan Qaboos Univ Med J,* 14(2):e166-9.

Lakhtakia R, Chinoy R (2014). A brief history of breast cancer, part 2: evolution of surgical pathology. *Sultan Qaboos Univ Med J,* 14(3):e319-22.

Langford G (1980). Arrangement of subunits in microtubules with 14 protofilaments. *J Cell Biol*, 87(2 Pt 1):521-6.

Langford G (1995). Actin- and microtubule-dependent organelle motors: interrelationships between the two motility systems. *Curr Opin Cell Biol*, 7(1):82-8.

Lee A, Oesterreich S, Davidson N (2015). MCF-7 cells – changing the course of breast cancer research and care for 45 years. *JNCI J Natl Cancer Inst,* 107(7):1-4.

Lee S, Shu X, Li H, Yang G, Cai H, Wen W, Ji B, Gao J, Goo Y, Zheng W (2009). Adolescent and adult soy food intake and breast cancer risk: results from the Shanghai Women's Health Study. *Am J Clin Nutr,* 89(6):1920-6.

Levenson A, Jordan V (1997). MCF-7: the first hormone-responsive breast cancer cell line. *Cancer Res,* 57(15):3071-8.

Lewtas J (2007). Air pollution combustion emissions: characterization of causative agents and mechanisms associated with cancer, reproductive, and cardiovascular effects. *Mutat Res,* 636:95-133.

Liao G, Nagasaki T, Gunderson G (1995). Low concentrations of nocodazole interfere with fibroblast locomotion without significantly affecting microtubule level: implications for the role of dynamic microtubule in cell locomotion. *J Cell Sci*, 108(Pt 11):3473-83.

Li Y, Wang J, Santen R, Kim T, Park H, Fan P, Yue W (2010). Estrogen stimulation of cell migration involves multiple signaling pathway interactions. *Endocrinology,* 151(11):5146-56.

Linos E, Willett W, Cho E, Colditz G, Frazier L (2008). Red meat consumption during adolescence among premenopausal women and risk of breast cancer. *Cancer Epidemiol Biomarkers Prev,* 17(8):2146-51.

Lippincott-Schwartz J, Donaldson J, Schweizer A, Berger E, Hauri H, Yuan L, Klausner R (1990). Microtubule-dependent retrograde transport of proteins into the ER in the presence of brefeldin A suggests an ER recycling pathway, *Cell*, 60(5):821-36.

Lippincott-Schwartz J, Yuan L, Bonifacino J, Klausner R (1989). Rapid redistribution of Golgi proteins into the ER in cells treated with brefeldin A: evidence for membrane cycling from Golgi to ER. *Cell*, 56(5):801-13.

Lippman M, Bolan G (1975). Oestrogen-responsive human breast cancer in long term tissue culture. *Nature,* 256(5518):592-3.

Liu L, Zhuang W, Wang R, Mukherjee R, Xiao S, Chen Z, Wu X, Zhou Y, Zhang Y (2011). Is dietary fat associated with the risk of colorectal cancer? A meta-analysis of 13 prospective cohort studies. *Eur J Nutr*, 50(3):173-84.

Lo C, Wang H, Dembo M, Wang Y (2000). Cell movement is guided by the rigidity of the substrate. *Biophys J,* 79: 144-52.

Lo S, Janmey P, HardwigJ, Chen L (1994). Interactions of tensin with actin and identification of its three distinct actin-binding domains. *J Cell Biol,* 125:1067-75.

Loo D, Kanner S, Aruffo A (1998). Filamin binds to the cytoplasmic domain of the beta 1-integrin. Identification of amino acids responsible for this interaction. *J Biol Chem,* 273:23304-12.

Loomis D, Grosse Y, Lauby-Secretan B, Ghissassi F, Bouvard V, Benbrahim-Tallaa L, Guha N, Baan R, Mattock H, Straif K (2013). The carcinogenicity of outdoor air pollution. *Lancet Oncol,* 14(13):1262-3.

Louis G, Bloom M, Gatto N, Hogue C, Westreich D, Zhang C (2015). Epidemiology's continuing contribution to public health: the power of "Then and Now". *Am. J. Epidemiol,* 181(8):e1-8.

Low S, Wong S, Tang B, Tan P, Subrmaniam V, Hong W. Inhibition by brefeldin A of protein secretion from the apical cell surface of Madin-Darby canine kidney cells. *J Biol Chem*, 266(27):17729-32.

Lu Z, Jiang G, Blume-Jensen P, Hunter T (2001). Epidermal growth factor-induced tumor cell invasion and metastasis initiated by dephosphorylation and downregulation of focal adhesion kinase. *Mol Cell Biol,* 21(12):4016-31.

Luchsinger C, Aguilar M, Burgos P, Ehrenfeld P, Mardones G (2018). Functional disruption of the Golgi apparatus protein ARF1 sensitizes MDA-MB-231 breast cancer cells to the antitumor drugs Actinomycin D and Vinblastine through ERK and AKT signaling. *PLoS One*, 13(4):e0195401.

MacKie R, Hauschild A, Eggermont A (2009). Epidemiology of invasive cutaneous melanoma. *Ann Oncol,* 20(Supp. 6):vi1-7.

Madden J, Kandalaft S, Bourque R (1972). Modified radical mastectomy. *Ann Surg,* 175(5):624-34.

Magner J, Papgiannes E (1988). Blockade by brefeldin A of intracellular transport of secretory proteins in mouse pituitary cells: effects on the biosynthesis of thyrotropin and free alpha-subunits. *Endocrinology*, 122(3):912-20.

Mareel M, de Brabander M (1978). Effect of microtubule inhibitors on malignant invasion *in vitro*. *J Natl Cancer Inst*, 61(3):787-92.

Mathews M, Bernstein R, Franza B, Garrels J (1984). Identity of the proliferating cell nuclear antigen and cyclin. *Nature*, 309(5966):374-6.

Menko A, Toyama Y, Boettiger D, Holtzer H (1983). Altered cell spreading in cytochalasin B: a possible role for intermediate filaments. *Mol Cell Biol*, 3(1):113-25.

Mezler D, Harries L, Cipelli R, Henley W, Money C, McCormack P, Young A, Guralnik J, Ferrucci L, Bandinelli S, Corsi A, Galloway T (2011). Bisphenol A exposure is associated with *in vivo* estrogenic gene expression in adults. *Environ Health Perspect,* 119:1788-93.

Michaelis C, Ciosk R, Nasmyth K (1997). Cohesins: chromosomal proteins that prevent premature separation of sister chromatids. *Cell*, 91(1):35-45.

Miller E, Miller J (1947). The presence and significance of bound aminoazo dyes in the livers of rats fed *p*-dimethylaminoazobenzene. *Cancer Res,* 7:468–80.

Miller S, Carnell L, Moore H (1992). Post-golgi membrane traffic: brefeldin A inhibit export from distal Golgi compartments to the cell surface but not recycling. *J Cell Biol,* 118(2):267-83.

Mills G, Lu Y, Fang X, Wang H, Eder A, Mao M, Swaby R, Cheng K, Stokoe D, Siminovitch K, Jaffe R, Gray J (2001). The role of genetic abnormalities of PTEN and the phosphatidylinositol 3-kinae pathway in breast and ovarian tumorigenesis, prognosis and therapy. *Semin Oncol,* 28 (5 Supp 16):125-41.

Mingle L, Okuhama N, Shi J, Singer R, Condeelis J, Liu G (2005). Localization of all seven messenger RNAs for the actin-polymerization nucleator Arp2/3 complex in the protrusions of fibroblasts. *J Cell Sci,* 118(Pt 11):2425-33.

Misumi Y, Misumi Y, Miki K, Takatsuki A, Tamura G, Ikehara Y (1986). Novel blockade by brefeldin A of intracellular transport of secretory proteins in cultured rat hepatocytes. *J Biol Chem*, 261(24):11398-403.

Mitchison T, Kirschner M (1984). Dynamic instability of microtubule growth. *Nature,* 312:237-242.

Mooseker M (1976). Brush border motility. Microvillar contraction in triton-treated brush borders isolated from intestinal epithelium. *J Cell Biol*, 71(2):417-33.

Moritz M, Braunfeld M, Sedat J, Alberts B, Agard D (1995). Microtubule nucleation by gamma-tubulin-containing rings in the centrosome. *Nature*, 378(6557):638-40.

Muhua L, Karpova T, Cooper J (1994). A yeast actin-related protein homologous to that in vertebrate dynactin complex is important for spindle orientation and nuclear migration. *Cell*, 78(4):669-79.

Muirhead C, O'Hagan J, Haylock R, Phillipson M, Willcock T, Berridge G, Zhang W (2009). Mortality and cancer incidence following occupational radiation exposure: third analysis of the National Registry for Radiation Workers. *Br J Cancer,* 100:206-12.

Mukherjee D, Zhao J (2013). The role of chemokine receptor CXCR4 in breast cancer metastasis. *Am J Cancer Res*, 3(1):46-57.

Müller A, Homey B, Soto H, Ge N, Catron D, Buchanan M, McClanahan T, Murphy E, Yuan W, Wagner S, Barrera J, Mohar A, Verástegui E, Zlotnik A (2001). Involvement of chemokine receptors in breast cancer metastasis. *Nature,* 410(6824):50-6.

Murphy D, Borisy G (1975). Association of high-molecular-weight proteins with microtubules and their role in microtubule assembly *in vitro*. *Proc Natl Acad Sci*, 72(7):2696-700.

Murphy S, Preble A, Patel U, O'Connell K, Dias D, Moritz M, Agard D, Stults J, Stearns T (2001). GCP5 and GCP6: two new members of the human gamma-tubulin complex. *Mol Biol Cell*, 12(11):3340-52.

Murphy S, Urbani L, Stearns T (1998). The mammalian gamma-tubulin complex contains homologues of the yeast spindle pole body components spc97p and spc98p. *J Cell Biol*, 141(3):663-74.

Nakamura M, Mishima H, Nishida T, Otori T (1991). Requirement of microtubule assembly for initiation of EGF-stimulated corneal epithelial migration. *Jpn J Ophthalmol*, 35(4):377-85.

Nakamura M, Yagi N, Kato T, Fujita S, Kawashima N, Ehrhardt D, Hashimoto T. (2012). *Arabidopsis* GCP3-interacting protein 1/MOZART 1 is an integral component of the γ -tubulin-containing microtubule nucleating complex. *Plant J*, 71(2):216-25.

Nass S, Dickson R (1997). Defining a role for c-myc in breast tumorigenesis. *Breast Cancer Res Treat,* 44:1-22.

National Cancer Institute (2015). SEER: cancer stat facts: female breast cancer. <https://seer.cancer.gov/statfacts/html/breast.html>

National Center for Health Statistics (2017). Health, United States, 2016: With Chartbook on Long-term Trends in Health. Hyattsville, MD.

Nielsen S, Celis A, Ratz G, Celis J (1987). Identification of two human phosphoproteins (dividin and IEF59dl) that are first detected late in G1 near the G1/S transition border of the cell cycle. *Leukemia*, 1(1):69-77.

Nigg E (1995). Cyclin-dependent protein kinases: key regulators of the eukaryotic cell cycle. *Bioessays*, 17:471-80.

Nurse P (1990). Universal control mechanism regulating onset of M-phase. *Nature*, 344:503-8.

Oesterreich S, Zhang P, Guler R, Sun X, Curran E, Welshons W, Osborne C, Lee A (2001). Re-expression of estrogen receptor α in estrogen receptor α -negative MCF-7 Cells restores both estrogen and insulin-like growth factor-mediated signaling and growth. *Cancer Res*, 61:5771-7.

Ojakian G, Schwimmer R (1992). Antimicrotubule drugs inhibit the polarized insertion of an intracellular glycoprotein pool into the apical membrane of Madin-Darby canine kidney (MDCK) cells. *J Cell Sci*, 103(Pt 3):677-87.

Orci L, Tagaya M, Amherdt M, Perrelet A, Donaldson J, Lippincott-SchwartzJ, Klausner R, Rothman J (1991). Brefeldin A, a drug that blocks secretion, prevents the assembly of non-clathrin-coated buds on Golgi cisternae. *Cell*, 64(6):1183-95.

Osborn M, Weber K (1976). Cytoplasmic microtubules in tissue culture cells appear to grow from an organizing structure towards the plasma membrane. *Proc Natl Acad Sci USA*, 73(3):867-71.

Osborne C (1996). Athymic nude mouse model for the study of new antioestrogens in breast cancer. *The Breast,* 5(3):181-5.

Osborne C, Boldt D, Clark G, Trent J (1983). Effects of Tamoxifen in human breast cancer cell cycle kinetics: accumulation of cells in early G_1 phase. *Cancer Res,* 43:3583-5.

Pantaloni D, Carlier M, Coue M, Lal A, Brenner S, Korn E (1984). The critical concentration of actin in the presence of ATP increases with the number concentration of filaments and approaches the critical concentration of actin•ADP. *J Biol Chem*, 259(10):6274-83.

Pantaloni D, Carlier M, Korn E (1985). The interaction between ATP-actin and ADP-actin. A tentative model for actin polymerization. *J Biol Chem*, 260(11):6572-8.

Parsonnet J, Hansen S, Rodriguez L *et al.* (1994). *Helicobacter pylori* infection and gastric lymphoma. *N Engl J Med*, 330:1267–71.

Pavalko F, Otey C, Simon K, Burridge K (1991). Alpha-actinin: a direct link between actin and integrins. *Biochem Soc Trans,* 19:1065-9.

Pearce M, Salotti J, Little M, McHugh K, Lee C, Kim K, Howe N, Ronckers C, Rajaraman P, Craft A, Parker L, González A (2012). Radiation exposure from CT scans in childhood and subsequent risk of leukaemia and brain tumours: a retrospective cohort study. *Lancet,* 380:499-505.

Pelletier G (1974). Autoradiographic studies of synthesis and intracellular migration of glycoproteins in the rat anterior pituitary gland. *J Cell Biol*, 62(1):185-97.

Pérez-Yépez E, Ayala-Sumuano J, Reveles-Espinoza A, Meza I (2012). Selection of a MCF-7 breast cancer cell subpopulation with high sensitivity to IL-1β: characterization of and correlation between morphological and molecular changes leading to increased invasiveness. *Int J Breast Cancer,* 2012:1-12.

Perou C, Sørlie T, Eisen M, van de Rijn M, Jeffrey S, Rees C, Pollack J, Ross D, Johnsen H, Akslen , Fluge O, Pergamenschikov A, Williams C, Zhu S, Lønning P, Børresen-Dale A, Brown P, Botstein D (2000). Molecular portraits of human breast tumours. *Nature,* 406(6797):747-52.

Perrot-Applanat M, Di Bennedetto M (2012). Autocrine functions of VEGF in breast tumor cells: Adhesion, survival, migration and invasion. *Cell Adh Migr,* 6(6):547-53.

Porowska H, Paszkiewicz-Gadek A, Lemancewicz D, Bielawski T, Wo Cyznski S (2008). Effect of brefeldin A on membrane localization of MUC1 mucin and adhesive properties of cancer cells. *Neoplasma*, 55(4):305-11.

Porter K (1964). Cell fine structure and biosynthesis of intracellular macromolecules. *Biophys J*, 4(1 Pt 2):167-96.

Price J, Tiganis T, Agarwal A, Djakiew D, Thompson E (1999). Epidermal growth factor promotes MDA-MB-231 breast cancer cell migration through a phosphatidylinositol 3'-kinase and phospholipase C-dependent mechanism. *Cancer Res,* 59(21):545-8.

Pupo M, Pisano A, Lappano R, Santolla M, de Francesco E, Abonante S, Roasano C, Maggiolini M (2012). Bisphenol A induces gene expression changes and proliferative effects through GPER in breast cancer cells and cancer-associated fibroblasts. *Environ Health Perspect*, 120(8):1177-82.

Rabindran S, Discafani C, Rosfjord E, Baxter M, Floyd M, Golas J, Hallett W, Johnson B, Nilakantan R, Overbeek E, Reich M, Shen R, Shi X, Tsou H, Wang Y, Wissner A (2004). Antitumor activity of HKI-272, an orally active, irreversible inhibitor of the HER-2 tyrosine kinase. *Cancer Res*, 64(11):3958-65.

Ramazzini B (2001). De Morbis Artificum Diatriba (1713). *Am J Public Health,* 91(9):1380-2.

Reaves B, Banting G (1992). Perturbation of the morphology of the trans-Golgi network following Brefeldin A treatment: redistribution of a TGN-specific integral membrane protein, TGN38. *J Cell Biol*, 116(1):85-94.

Reed S, Wittenberg C, Lew D, Dulic V, Henze M (1991). G1 control in yeast and animal cells. *Cold Spring Harb Symp Quant Biol*, 56:61-7.

Reinhart-King CA, Dembo M, Hammer DA (2005). The dynamics and mechanics of endothelial cell spreading. *Biophys J,* 89:676-89.

Renaud F, Rowe A, Gibbons I (1968). Some properties of the protein forming the outer fibers of cilia. *J Cell Biol*, 36(1):79-90.

Richardson H, Wittenberg C, Cross F, Reed S (1989). An essential G1 function for cyclin-like proteins in yeast. *Cell*, 59(6):1127-33.

Rindler M, Ivanov I, Sabatini D (1987). Microtubule-acting drugs lead to the nonpolarized delivery of the influenza hemagglutinin to the cell surface of polarized Madin-Darby canine kidney cells. *J Cell Biol*, 104(2):231-41.

Rivero S, Cardenas J, Bornens M, Rios R (2009). Microtubule nucleation at the *cis*-side of the Golgi apparatus requires AKAP450 and GM130. *EMBO J*, 28:1016-28.

Roca-Cusachs P, Iskratsch T, Sheetz MP (2012). Finding the weakest link – exploring integrin-mediated mechanical molecular pathways. *J Cell Sci,* 125:3025-38.

Roca-Cusachs P, Sunyer R, Trepat X (2013). Mechanical guidance of cell migration: lessons from chemotaxis. *Curr Opin Cell Biol,* 25(5):543-9.

Rodewald R, Newman S, Karnovsky M (1976). Contraction of isolated brush borders form the intestinal epithelium. *J Cell Biol*, 7(3):541-54.

Rogalski A, Bergmann J, Singer S (1984). Effect of microtubule assembly status on the intracellular processing and surface expression of an integral protein of the plasma membrane. *J Cell Biol*, 99(3):1101-9.

Rogalski A, Singer S. Associations of elements of the Golgi apparatus with microtubules. *J Cell Biol*, 99(3):1092-100.

Rondelez Y, Tresset G, Nakashima T, Kato-Yamad Y, Fujita H, Takeuchi S, Noji H (2005). Highly coupled ATP synthesis by F1-ATPase single molecules. *Nature,* 433(7027):773-7.

Rosa P, Barr F, Stinchombe J, Binacchi C, Huttner W (1992). Brefeldin A inhibits the formation of constitutive secretory vesicles and immature secretory granules from the trans-Golgi network. *Eur J Cell Biol*, 59(2):265-74.

Rose S, Pruss R, Herchman H (1975). Initiation of 3T3 fibroblast cell division by epidermal growth factor. *J Cell Physiol*, 86 Suppl 2(3 Pt 3):593-8.

Rosenberg S, Stracher A, Lucas R (1981). Isolation and characterization of actin and actin-binding protein from human platelets. *J Cell Biol*, 91(1):201-11.

Rottner K, Hall A, Small J (1999). Interplay between Rac and Rho in the control of substrate contact dynamics. *Curr Biol,* 9:640.

Russell P, Nurse P (1987). Negative regulation of mitosis by wee1+, a gene encoding a protein kinase homolog. *Cell*, 49(4):559-67.

Sadhu K, Reed S, Richardson H, Russell P (1990). Human homolog of fission yeast cdc25 mitotic inducer is predominantly expressed in G2. *Proc Natl Acad Sci USA*, 87:5193-43.

Samet J, Cohen A (2006). New York, NY: Cancer epidemiology and prevention. p. 355-81.

Schmoranzer J, Kreitzer G, Simon S (2003). Migrating fibroblasts perform polarized, microtubule-dependent exocytosis towards the leading edge. *J Cell Sci*, 116(Pt 22):4513-9.

Scholey J, Porter M, Grissom P, McIntosh J (1985). Identification of kinesin in sea urchin eggs, and evidence for its localization in the mitotic spindle. *Nature*, 318(6045):483-6.

Schulz W, Deng L, Mann M (2005). Phosphotyrosine interactome of the ErbB-receptor kinase family. *Mol Syst Biol,* 1:2005.0008.

Schüz J, Ahlbom A (2008). Exposure to electromagnetic fields and the risk of childhood leukemia: a review. *Radiat Prot Dosimetry,* 132(2):202-11.

Serafini T, Stenbeck G, Brecht A, Lottspeich F, Orci L, Rothman J, Wieland F (1991). A coat subunit of Golgi-derived non-clathrin-coated vesicles with homology to the clathrin -coated vesicle coat protein beta-adaptin. *Nature*, 349(6306):215-20.

Shelanski M, Gaskin F, Cantor C (1973). Microtubule assembly in the absence of added nucleotides. *Proc Natl Acad Sci USA*, 70(3):765-8.

Sieg D, Hauck C, Klingbeil C, Schaefer E, Damsky C, Schlaepfer D (2000). FAK initiates growth-factor and integrin signals to promote cell migration. *Nat Cell Biol*, 2(5):249-56.

Singletary K, Frey R, Yan W (2001). Effect of ethanol on proliferation and estrogen receptor-α expression in human breast cancer cells. *Cancer Lett*, 165:131-7.

Singletary K, Gapstur S (2001). Alcohol and breast cancer: review of epidemiologic and experimental evidence and potential mechanisms. *JAMA*, 286:2143–51.

Singleton V, Bohonos N, Ullstrup A (1958). Decumbin, a new compound from a species of *Penicillium*. *Nature*, 181(4615):1072-3.

Sinha S, Wagner D (1987). Intact microtubules are necessary for complete processing, storage and regulated secretion of von Willebrand factor by endothelial cells. *Eur J Cell Biol*, 43(3):377-83.

Skotheim J, Di Talia S, Siggia E, Cross F (2008). Positive feedback of G1 cyclins ensures coherent cell cycle entry. *Nature,* 454(7202):291-6.

Slamon D, Clark G, Wong S, Levin W, McGuire W (1987). Human breast cancer: correlation of relapse and survival with amplification of the HER-2/neu oncogene. *Science,* 235(4785):177-82.

Slautterback D (1963). Cytoplasmic microtubules. I. hydra. *J Cell Biol*, 18:367-8.

Sloboda R, Dentler W, Rosenbaum J (1976). Microtubule-associated proteins and the stimulation of tubulin assembly *in vitro*. *Biochemistry* 15(20):4497-505.

Sloboda R, Rudolph S, Rosenbaum J, Greengard P (1975). Cyclic AMP-dependent endogenous phosphorylation of a microtubule-associated protein. *Proc Natl Acad Sci USA*, 72(1):177-81.

Small J, Isenberg G, Celis J (1978). Polarity of actin at the leading edge of cultured cells. *Nature*, 272(5654):638-9.

Snyder J, McIntosh J (1975). Initiation and growth of microtubules from mitotic centers in lysed mammalian cells. *J Cell Biol*, 67(3):744-60.

Sørlie T, Perou C, Tibshirani R, Aas T, Geisler S, Johnsen H, Hastie T, Eisen M, van de Rijn M, Jeffrey S, Thorsen T, Quist H, Matese J, Brown P, Botstein D, Lønning P, Børresen-Dale A (2001). Gene expression patterns of breast carcinomas distinguish tumor subclasses with clinical implications. *Proc Natl Acad Sci USA,* 98(19):10869-74.

Soule H, Vazguez J, Long A, Albert S, Brennan M (1973). A human cell line from a pleural effusion derived from a breast carcinoma. *J Natl Cancer Inst,* 51(5):1409-16.

Stearns M, Brown D (1979). Purification of cytoplasmic tubulin and microtubule organizing center proteins functioning in microtubule initiation from the alga *Polytomella*. *Proc Natl Acad Sci USA*, 76(11):5745-9.

Steeg P, Zhou Q (1998). Cyclins and breast cancer. *Breast Cancer Res Treat,* 52:17-28.

Stehbens S, Paszek M, Pemble H, Ettinger A, Gierke S, Wittmann T (2014). CLASPs link focal adhesion-associated microtubule capture to localized exocytosis and adhesion site turnover. *Nat Cell Biol*, 16(6):561-73

Stephens P, Tarpey P, Davies H, Loo P, Greenman C, Wedge D, Nik-Zainal S, Martin S, Varela I, Bignell G, Yates L, Papaemmanuil E, Beare D, Butler A, Cheverton A, Gamble J, Hinton J, Jia M, Jayakumar A, Jones D, Latimer C, Lau K, McLaren S, McBride D, Menzies A, Mudie L, Raine K, Rad R, Chapman M, Teague J, Easton D, Langerød A, OSBREAC, Lee M, Shen C, Tee B, Huimin B, Broeks A, Vargas A, Turashvili G, Martens J, Fatima A, Miron P, Chin S, Thomas G, Boyault S, Mariana O, Lakhani S, Vijver M, van't Veer L, Foekens J, Desmedt C, Sotiriou C, Tutt A, Caldas C, Reis-Filho J, Aparicio S, Salomon A, Børresen-Dale A, Richardson A, Campbell P, Futreal P, Stratton M (2012). The landscape of cancer genes and mutational processes in breast cancer. *Nature,* 486:400-4.

Stern B, Nurse P (1996). A quantitative model for the cdc2 control of S phase and mitosis in fission yeast. *Trends Genet,* 12(9):345-50.

Stewart B, Wild C (Eds) (2014): World Cancer Report. IARC *Press*. Lyon 2014.

Stoddard P, Williams T, Garner E, Baum B (2017). Evolution of polymer formation within the actin superfamily. *Mol Biol Cell*, 28(19):2461-9.

Storme G, Mareel M. Effect of anticancer agents on directional migration of malignant C3H mouse fibroblastic cells *in vitro*. *Cancer Res*, 40(3):943-8.

Subik K, Lee J, Baxter L, Strzepek T, Costello D, Crowley P, Xing L, Hung M, Bonfiglio T, Hicks D, Tang P (2010). The expression patterns of ER, PR, HER2, CK5/6, EGFR, Ki-67 and AR by immunohistochemical analysis in breast cancer cell lines. *Breast Cancer (Auckl),* 4:35-41.

Sutherland R, Green M, Hall R, Reddel R, Taylor I (1983). Tamoxifen induces accumulation of MCF 7 human mammary carcinoma cells in the G0/G1 phase of the cell cycle. *Eur J Cancer Clin Oncol,* 19(5):615-21.

Sweeney E, McDaniel R, Maximov P, Fan P, Jordan C (2012). Models and mechanisms of acquired antihormone resistance in breast cancer: significant clinical progress despite limitations. *Horm Mol Biol Clin Investig,* 9(2):143-63.

Swenson K, Farrell K, Ruderman J (1986). The clam embryo cyclin A induces entry into M phase and the resumption of meiosis in *Xenopus* oocytes. *Cell*, 47(6):861-70.

Takahashi M, Yamagiwa A, Nishimura T, Mukai H, Ono Y (2002). Centrosomal proteins CG-NAP and Kendrin provide microtubule nucleation sites by anchoring γ–tubulin ring complex. *Mol Biol Cell*, 13:3235-45.

Tambe D (2011). Collective cell guidance by cooperative intracellular forces. *Nat Mater,* 10:469-75.

Tanaka E, Ho T, Kirschner M (1995). The role of microtubule dynamics in growth cone motility and axonal growth. *J Cell Biol*, 128(1-2):139-55.

Tate S, Cai S, AjamieR, Burke T, Beckmann R, Chan E, de Dois A, Wishart G, Gelbert L, Cronier D (2014). Semi-mechanistic pharmacokinetic/pharmacodynamic modeling of the antitumor activity of LY2835219, a new cyclin-dependent kinase 4/6 inhibitor, in mice bearing human tumor xenografts. *Clin Cancer Res*, 20(14):3763-74.

Taylor D, Condeelis J, Moore P, Allen R (1973). The contractile basis of amoeboid movement. I. The chemical control of motility in isolated cytoplasm. *J Cell Biol*, 59(2 Pt 1):378-94.

Terasaki M, Chen L, Fujiwara K (1986). Microtubules and the endoplasmic reticulum are highly interdependent structures. *J Cell Biol*, 103(4):1557-68.

Thyberg J, Moskalewski S (1992). Reorganization of the Golgi complex in association with mitosis: redistribution of mannosidase II to the endoplasmic reticulum and effects of brefeldin A. *J Submicrosc Cytol Pathol*, 24(4):495-508.

Tilney L, Gibbins J (1969). Microtubules and filaments in the filopodia of the secondary mesenchyme cells of *Arbacia punctulata* and *Echinarachius parma*. *J Cell Sci*, 5(1):195-210.

Tomar A, Schlaepfer D (2009). Focal adhesion kinase: switching between GAPs and GEFs in the regulation of cell motility. *Curr Opin Cell Biol,* 27:676-83.

Tryfonidis K, Zardavas D, Katzenellenbogen B, Piccart M (2016). Endocrine treatment in breast cancer: Cure, resistance and beyond. *Cancer Treat Rev,* 50:68-81.

Tseng C, Hong Y, Chang H, Yu T, Hung T, Hou M, Yuan S, Cho C, Liu C, Chiu C, Huang C (2014). Brefeldin A reduces anchorage-independent survival, cancer stem cell potential and migration of MDA-MB-231 human breast cancer cells. *Molecules*, 19(11):17464-77.

Uhlmann F, Lottspeich F, Nasmyth K (1999). Sister-chromatid separation at anaphase onset is promoted by cleavage of the cohesion subunit Scc1. *Nature*, 400(6739):37-42.

Uhlmann F, Wernic D, Poupart M, Koonin E, Nasmyth K (2000). Cleavage of cohesion by the CD clan protease separin triggers anaphase in yeast. *Cell*, 103(3):375-86.

Ulmer J, Palade G (1989). Targeting and processing of glycophorins in murine erythroleukemia cells: use of brefeldin A as a perturbant of intracellular traffic. *Proc Natl Acad Sci USA*, 86(18):6992-6.

Vale R (2003).The molecular motor toolbox for intracellular transport. *Cell,* 112:467-80.

Vale R, Hotani H (1988). Formation of membrane networks *in vitro* by kinesin-driven microtubule movement. *J Cell Biol*, 107(6 Pt1):2233-41.

Vale R, Reese T, Sheetz M (1985). Identification of a novel force-generating protein, kinesin, involved in microtubule-based motility. *Cell*, 42(1):39-50.

Vale R, Schnapp B, Mitchison T, Steuer E, Reese T, Sheetz M (1985). Different axoplasmic proteins generate movement in opposite directions along microtubules *in vitro*. *Cell*, 43(3 Pt2):623-32.

van den Heuvel S, Harlow E (1993). Distinct roles for cyclin-dependent kinases in cell cycle control. *Science*, 262(5142):2050-4.

van Meer G, van't Hof W (1993). Epithelial sphingolipid sorting is insensitive to reorganization of the Golgi by nocodazole, but is abolished by monesin in MDCK cells and by brefeldin A in Caco-2 cells. *J Cell Sci*, 104(Pt 3):833-42.

Vasquez R, Gard D, Cassimeris L (1994). XMAP from *Xenopus* eggs promotes rapid plus end assembly of microtubules and rapid microtubule polymer turnover. *J Cell Biol*, 127(4):985-93.

Veigel C, Coluccio L, Jontes J, Sparrow J, Milligan R, Molloy J (1999). The motor protein myosin-I produces its working stroke in two steps. *Nature*, 398(6727):530-3.

Voldborg B, Damstrup L, Spang-Thomsen M, Poulsen H (1997). Epidermal growth factor receptor (EGFR) and EGFR mutations, function and possible role in clinical trials. *Ann Oncol*, 8:1197-206.

Waizenegger I, Hauf S, Meinke A, Peters J (2000). Two distinct pathways remove mammalian cohesion from chromosome arms in prophase and from centromeres in anaphase. *Cell*, 103(3):399-410.

Walczak C, Mitchison T, Desai A (1996). XKCM1: a *Xenopus* kinesin-related protein that regulates microtubule dynamics during mitotic spindle assembly. *Cell*, 84:37-47.

Wang Y (1985). Exchange of actin subunits at the leading edge of living fibroblasts: possible role of treadmilling. *J Cell Biol*, 101(2):597-602.

Wang Y, Wang H, Yamaguchi H, Lee HH, Lee HJ, Hung M (2010). COPI-mediated retrograde trafficking from the Golgi to the ER regulates EGFR nuclear transport. *Biochem Biophys Res Commun*, 399(4):498-504.

Ward H (1973). Anti-oestrogen Therapy for Breast Cancer: A Trial of Tamoxifen at Two Dose Levels. *Br Med J,* 1:13-4.

Warfield R, Bouck G (1974). Microtubule-macrotubule transitions: intermediates after exposure to the mitotic inhibitor vinblastine. *Science*, 186(4170):1219-21.

Wassberg C, Thörn M, Yuen J, Hakulinen T, Ringborg U (1999). Cancer risk in patients with earlier diagnosis of cutaneous melanoma in situ. *Int J Cancer,* 83(3):314-7.

Wehland J, Henkart M, Klausner R, Sandoval I (1983). Role of microtubules in the distribution of the Golgi apparatus: effect of taxol and microinjected anti-alpha-tubulin antibodies. *Proc Natl Acad Sci USA*, 80(14):4286-90.

Wellings S, Jensen H, Marcum R (1975). An atlas of subgross pathology of the human breast with special reference to possible precancerous lesions. *J Natl Cancer Inst,* 55:231-73.

Wessells N, Spooner B, Ash J, Bradley M, Luduena M, Taylor E, Wrenn J, Yamada K (1971). Microfilaments in cellular and developmental processes. *Science*, (171)3967:135-43.

Whiteman D, Watt P, Purdie D, Hughes M, Hayward N, Green A (2003). Melanocytic nevi, solar keratosis, and divergent pathways to cutaneous melanoma. *J Natl Cancer Inst,* 95(11):806-12.

Wickerham D, O'Connell M, Costantino J, Cronin W, Paik S, Geyer Jr. C, Ganz P, Petrelli N, Mamounas E, Julian T, Wolmark N (2008). The half century of clinical trials of the National Surgical Adjuvant Breast and Bowel Project. *Semin Oncol,* 35(5):522-9.

Wiley H, Woolf M, Opresko L, Burke P, Will B, Morgan J, Lauffenburger D (1998). Removal of the membrane-anchoring domain of epidermal growth factor leads to intracrine signaling and disruption of mammary epithelial cell organization. *J Cell Biol,* 143(5):1317-28.

Wittenberg C, Reed S (1988). Control of the yeast cell cycle is associated with assembly/disassembly of the cdc28 protein kinase complex. *Cell*, 54(7):1061-72.

Wooster R, Neuhausen S, Mangion J, Quirk Y, Ford D, Collings N, Nguyen K, Seal S, Tran T, Averill D (1994). Localization of a breast cancer susceptibility gene, BRCA2, to chromosome 13q12-13. *Science,* 265(5181):2088-90.

World Health Organization (2017) Cancer. <http://www.who.int/cancer/en/>

Xia W, Mullin R, Keith B, Liu L, Ma H, Rusnak D, Owens G, Alligood K, Spector N (2002). Anti-tumor activity of GW572016: a dual tyrosine kinase inhibitor blocks EGF activations of EGFR/erB2 and downstream Erk1/2 and AKT pathways. *Oncogene*, 21(41):6255-63.

Xiang X, Beckwith S, Morris N (1994). Cytoplasmic dynein is involved in nuclear migration in *Aspergillus nidulans*. *Proc Natl Acad Sci USA*, 91(6):2100-4.

Xiong Y, Hannon G, Zhang H, Casso D, Kobayashi R, Beach D (1993). p21 is a universal inhibitor of cyclin kinases. *Nature*, 366(6456):701-4.

Yamagiwa K, Ichikawa K (1918). Experimental study of the pathogenesis of carcinoma. *J Cancer Res,* 3:1–21.

Yarden Y, Schlessinger J (1987). Epidermal growth factor induces rapid, reversible aggregation of the purified epidermal growth factor receptor. *Biochemistry*, 26(5):1443-51.

Yokotsuka M, Iwaya K, Saito T, Pandiella A, Tsuboi R, Kohno N, Matsubara O, Mukai K (2011). Overexpression of HER2 signaling to WAVE2-Arp2/3 complex activates MMP independent migration in breast cancer. *Breast Cancer Res Treat*, 126(2):311-8.

Zahn L, Lundin-Schiller S (2016). Microtubule nucleation at the Golgi in breast cancer cells. Clarksville, TN: Austin Peay State University, Master's Thesis.

Zarich N, Oliva J, Martínez N, Jorge R, Ballester A, Gutiérez-Eisman S, García-Vargas S, Rojas J (2006). Grbs is a negative modulator of the intrinsic Ras-GEF activity of hSOS1. *Mol Biol Cell*, 17(8):3591-3597.

Zhao M (2009). Electrical fields in wound healing – An overriding signal that directs cell migration. *Semin Cell Dev Biol,* 20(6):674-82.

Zheng Y, Wong M, Alberts B, Mitchison T (1995). Nucleation of microtubule assembly by a gamma-tubulin-containing ring complex. *Nature*, 378(6557):578-83.

APPENDIX A: Co-immunoprecipitation Study

Introduction

As described briefly earlier, recent work has suggested that a specific subset of microtubules originate from the Golgi apparatus. One purpose for these microtubules is to stabilize the Golgi structure and orient it near the ER. Another role for these microtubules is in directed cell migration because they have the ability to polarize, as discussed earlier in the thesis. Both signaling molecules and proteins required for cellular interaction with the extra cellular matrix at the leading edge are transported along these microtubules.

The main model for Golgi nucleated microtubule work is the human retinal epithelium cell line. The role of these microtubules in breast cancer cell lines remains relatively unexplored. Earlier work from our lab by Laura Zahn sought to determine if microtubule nucleation at the Golgi occurred at different rates in cells with different migratory behaviors. The MCF7 and MDA-MB-231 cell lines were chosen for this work. Historical evidence, as well as more recent work from our lab by Clare Grady and work done in this thesis, support that MDA-MB-231 cells are more invasive than MCF7 cells. The difference in these migratory behaviors is associated with a variation in cellular morphology. MDA-MB-231 cells are mesenchymal, with higher α-tubulin expression than the epithelial MCF7 cells.

Laura Zahn's work supported the hypothesis that more microtubule nucleation was associated with the more migratory, MDA-MB-231 cell line. Also, cells stimulated with epidermal growth factor were associated with increased microtubule nucleation at the Golgi, as compared to non-stimulated cells. An important component of the molecular mechanism of microtubule nucleation at the Golgi is the recruitment of the γ-tubulin ring complex, a microtubule template structure, and associated anchoring proteins. One of these anchoring

proteins is AKAP450, which interacts with GM130, a Golgi peripheral protein. AKAP450 acts as an anchor, hypothesized to bind with the γ-tubulin subunit of the γ-tubulin ring complex, as well as other γ-tubulin ring complex binding proteins, CDK5RAP2 and myomegalin. Recent results from work done in the Akhmanova lab suggest that AKAP450 is vital for cell invasiveness. AKAP450 knock down retinal epithelium cells experienced greatly diminished migratory behavior, as compared to those cells with functioning AKAP450 protein.

Hypothesis

Evidence supports the necessity of AKAP450 for microtubule nucleation at the Golgi, as discussed in the last subsection. There is also evidence that this protein is also required for migration in at least one cell line. Because of the hypothesized importance of this protein in each of these activities, it is an interesting candidate for study.

The goal of this study was to test the hypothesis for which support was observed in earlier work from our lab. The intimate nature of AKAP450 with microtubules make it a potentially useful immune-marker for Golgi nucleated microtubules. The general hypothesis of this study was the same, Golgi nucleated microtubules appear at a higher concentration in a more migratory cell. However, immunoprecipitation was the method chosen for the study. To identify Golgi nucleated microtubules specifically, AKAP450 would be immunoprecipitated from the cells of interest. Those proteins involved at the Golgi would likely physically interact with GM130. Co-immunoprecipitation using GM130 would be used to separate Golgi-located AKAP450s from others. These proteins would serve as a molecular proxy for Golgi nucleated microtubules. The major prediction for this study was that more invasive cell lines, or those supplemented with growth factors, such as epidermal growth factor, would have increased microtubule nucleation at the Golgi. In this study, these would be represented by AKAP450 bound to GM130, which could be quantified using a protein assay.

Materials and Methods

Cell Culture

Cell culture conditions for this study were the same as those from the thesis. EGF treatment concentration of epidermal growth factor also matched the thesis work, at 10 ng/mL.

Cell Lysis

Cells were lysed to access the proteins of interest, located near the membrane of the Golgi. Cell pellets were suspended in PBS to wash any trypsin or media from the cells. Cells were centrifuged again at 1000 x *g* for 5 minutes, to form a cell pellet. After draining the PBS, ice-cold, non-denaturing lysis buffer (IP lysis/wash buffer: 25mM tris, 150 mM NaCl, 1mM EDTA, 1% NP-40, 5% glycerol, pH 7.4; ThermoFisher Scientific, catalog #88805) was added to the conical (300 µL/ $5x10^6$ cells). A protease and phosphatase inhibitor cocktail was added to the lysis buffer to prevent proteolytic activity during lysis (Halt protease and phosphatase inhibitor cocktail: 1mM HCl 4-(2-Aminoethyl)-benzenesulfonyl fluoride (AEBSF), 800 nM aprotinin, 50 µM bestatin, 15 µM E64, 20 µM leupeptin, 10 µM pepstatin A; ThermoFisher Scientific, catalog #78440). After the cell pellet was suspended in the lysis buffer, the solution was transferred to a 1.5 mL microcentrifuge tube and incubated for 5 minutes with periodic mixing. After incubation, aliquots were taken for protein quantification and total cell lysate examination. The remaining contents were centrifuged at 13,000 x *g* to separate the cellular debris from the soluble fraction.

Lowry Assay

After lysis, protein concentration determinations had to be quantified using the Lowry assay. A standard curve was created by reading the A_{750} of diluted BSA standards at concentrations of 0, 20, 40, 60, 80 and 100 µg/mL in triplicate. The solutions were made at a volume of 250 µL, with 750 µL of Lowry solution added to each and incubated for 10 minutes at

room temperature. The Lowry solution consisted of three solutions at a ratio of 100:1:1: A (NaOH and Na_2CO3), B ($CuSO_4 \cdot 5H_2O$) and C (sodium tartrate • $2H_2O$). Finally, 75 µL of yellow folin solution (1:1 yellow folin: ultrapure water) was added to the sample/ Lowry solution and incubated for 45 minutes at room temperature. The mean absorbance value of the 0 µg/mL (solely comprised of cell lysis buffer) was subtracted from each of these, to account for any effect the cell lysis buffer diluent had on absorbance. The mean absorbance value for each concentration was plotted against the concentration of each diluted standard. The resulting linear equation for the standard curve was recorded. The spectrophotometer was blanked with H_2O for standard curve determination.

To determine the protein concentration of lysates, 5µL of sample was diluted in 245 µL of ultrapure water. The samples were quantified at a stock, 1:10 and 1:20 concentration. 750 µL of Lowry solution was added to each lysate sample and incubated for 10 minutes at room temperature. After this incubation period, 75 µL of yellow folin solution was added to each sample/Lowry solution and incubated at room temperature for 45 minutes. The spectrophotometer was blanked with cell lysis buffer. All calculated concentrations were multiplied by 4 to give concentrations per milliliter.

Immunoprecipitation

Cell lysate fractions were immunoprecipitated to purify the proteins of interest. Before immunoprecipitation was performed, the 1° antibody against the protein of interest was crosslinked to protein G bound to magnetic beads (Pierce protein A/G magnetic beads; ThermoFisher Scientific, catalog #88805). To bind the antibody to the beads, 25 µL of magnetic beads were washed with 500 µL of 1X modified coupling buffer (Coupling Buffer: 150mM NaCl, pH 7.2; ThermoFisher Scientific, catalog #88805), then incubated for 15 minutes at room temperature with a 100 µL, 5 µg 1° antibody solution consisting of coupling buffer and IP lysis/wash buffer. The bead solution was gently vortexed every 5 minutes to keep the beads in suspension. The beads were then washed twice with 100 µL of coupling buffer to remove unbound antibody. Finally, bound antibodies were covalently cross-linked to the protein G of the magnetic beads through the use of disuccinimidyl suberate (DSS; ThermoFisher Scientific, catalog #88805) as follows: The DSS was mixed with dimethyl sulfoxide (DMSO), Coupling Buffer, and ultrapure water to a working concentration of 20 µM. This solution was added at a 10X concentration to the magnetic beads and incubated for 30 minutes at room temperature. After incubation and removal of the DSS solution, elution buffer (elution buffer: glycine, pH 2; ThermoFisher Scientific, catalog #88805) was added to the beads for 5 minutes at room temperature and mixed on a rotating platform to remove non-crosslinked antibody and quench the reaction. Then, the beads were washed with 100 µL of elution buffer. Finally, the beads were rinsed twice in 200 µL of ice-cold IP lysis/ wash buffer.

To complete the immunoprecipitation, 500 µL lysate fraction was added to the microcentrifuge tube containing the crosslinked magnetic beads and mixed for 1 hour at room temperature. Following incubation, beads were pulled down with a hand-held magnet and supernatants containing any unbound antigen were saved for later analysis. The beads were then

washed with 500 µL of IP lysis/wash buffer, followed by 500 µL of ultrapure water. To purify the proteins of interest from the antibodies, the bead solution was incubated with 100 µl elution buffer for 5 minutes at room temperature on a rotator. The newly isolated antigen and accompanying proteins of interest were neutralized with 10 µL neutralization buffer (neutralization buffer; ThermoFisher Scientific, catalog #88805). These samples were then separated by SDS-PAGE (sodium dodecylsulfate-polyacrilamide gel electrophoresis) for Western blots.

Dot Blot

Dot blots are used to identify successful antigen-antibody interaction, as well as to determine the most efficient concentration of antibody for antigen detection. Two (2) µL of cell lysate (1µg of total protein) was pipetted onto a nitrocellulose membrane and allowed to dry for 30 minutes at room temperature. Non-specific sites on the membrane were blocked by incubation in 10 mL blocking solution (5% dried milk, in tris-buffered saline with 0.1% Tween-20, TBS-T). After this incubation period, membranes were rinsed with TBS-T for 15 minutes, then incubated overnight at 4 °C with 5 µg of 1° antibody diluted in 10 mL of blocking buffer (1% BSA diluted in TBS-T) or with 5 µg non-immune serum. Following 1° antibody incubation, the membrane was rinsed again for 15 minutes using TBS-T and then incubated in 0.5 µg of 2° antibody, raised against the 1° antibody, conjugated with horse-radish peroxidase (HRP), and diluted in 10 mL of blocking buffer, for 1 hour at room temperature. Following this incubation, the membrane was rinsed with TBS-T for 10 minutes and then tris-buffered saline (TBS) for 5 minutes. After rinsing, the membrane was incubated with a 10 mL 3,3'-diaminobenzidine tetrahydrochloride solution (10% DAB and 90% hydrogen peroxide) for approximately 30 minutes at room temperature, providing a colorimetric change as the substrate precipitated the HRP bound to the

antibody complex of the protein of interest. This change accompanies successful identification of the protein of interest or those which co-localize with it.

To create an antibody titer to determine efficient antibody concentrations required for antigen/1° antibody binding, a dot blot utilizing serial dilutions of 1° and 2° antibody concentration, in blocking buffer, is performed. Those dots with a more drastic colorimetric change are indicative of more efficient binding.

SDS-PAGE

The SDS-PAGE technique is an effective way to separate proteins through a polyacrylamide gel based on size. Proteins were separated using a Bio-Rad Mini-PROTEAN Tetra Cell system. The polyacrylamide gel was made of a 4% stacking gel and a 10% separating gel. The separating layer was comprised of 47.8% H_2O, 10% acrylamide stock, 25% tris base (1.5mM, pH 8.8), 0.1% SDS, 0.1% APS and 0.2% TEMED. The stacking gel was comprised of 72.8% H_2O, 5% acrylamide stock, 12.5% tris base (0.5M, pH6.8), 25 µL 10% SDS, 25 µL 10% APS and 5 µL TEMED. Reagents were combined and the separating gel solution pipetted into the casting frame. Butanol was dropped across the top of the solution to ensure even dispersal. The solution polymerized for approximately 30 minutes and rinsed with H_2O to remove any residual butanol. The stacking gel solution was then pipetted evenly across the top of the polymerized separating gel. After the casting frame was filled, a comb was added to create the necessary wells.

A Laemmli buffer (1.15 mL glycerol, 100 µL 2-mercaptoethanol, 0.2 g 10% SDS, 0.001 g bromophenol blue, 1.25 mL 4x stacking gel solution) was required for the proteins to denature and traverse the gel based solely on size. Laemmli buffer was mixed at a 1:1 ratio with sample, and the resultant solution was boiled at 95°C for 5 minutes.

The running chamber was filled with 1x SDS-PAGE running buffer (3.025 g tris-base, 14.4 g glycine, 1 g SDS, diluted to 1 L with H_2O). Twenty (20) µL of 1:1 sample/ Laemmli buffer was loaded into wells, with Laemmli buffer loaded into any wells not containing sample to ensure even travel of the dye front. A reference ladder (iBright prestained protein ladder; ThermoFisher Scientific, catalog #LC5615) was loaded into the far-left lane in each gel. Electrophoresis was performed at 70 volts for 30 minutes while the samples migrated through the stacking gel. Once all samples were even within the stacking the gel, the voltage was increased to 130. Samples migrated through the gel until the dye front ran off of the gel.

Coomassie Staining

Once proteins have migrated throughout the gel, a staining dye can be used to visualize the separated proteins as bands located throughout the gel. Once samples had migrated through the gel, the gels were rinsed with H_2O and incubated in Coomassie brilliant blue staining solution (0.25 g Coomassie brilliant blue R-250, 90% 1:1 methanol:H_2O, 10% glacial acetic acid) for 30 minutes at room temperature. Following staining, the gels were rinsed with water and incubated in destaining solution (40% methanol, 10% acetic acid, 50% H_2O) for 10 minutes. The staining solution was then drained, and fresh destaining solution was added. Gels were incubated for 30 more minutes in the fresh destaining solution. Finally, the gels were left in H_2O until complete destaining occurred.

Western Blot

The Western blot is a commonly used technique that allows for the biochemical identification of separated proteins. This is accomplished through the electrophoretic transfer of the separated proteins in the SDS-PAGE acrylamide gel to a nitrocellulose membrane and subsequent immuno-reaction. This technique is useful to confirm successful

immunoprecipitation, as well as confirm co-immunoprecipitation of other proteins with a sample that has been purified through immunoprecipitation.

Unlike the process used to stain and identify the protein bands present on the gels immediately after SDS-PAGE, the gels were instead equilibrated in transfer buffer (25mM tris, pH 8.3, 192 mM glycine and 20% methanol) after migration, until the Mini Trans-Blot Electrophoretic Transfer Cell system was assembled. To prepare the system, a sandwich consisting of a transfer cassette, fiber pad, filter paper, nitrocellulose membrane, previously run gel, second filter paper and second fiber pad were assembled. This completed sandwich was placed into a cassette holder and lowered into the transfer chamber. An ice pack, magnetic spin bar and transfer buffer were added to the chamber. Electrophoretic transfer was performed at 100V for 60 minutes, until transfer to the membrane was complete.

After the transfer, a number of proteins were located on the membrane, including those proteins of interest. To successfully identify the presence of these proteins, a colorimetric, immunoprecipitation reaction was performed. After the transfer period, the membrane was removed from the cassette and incubated in blocking solution at room temperature for 30 minutes to prevent non-specific binding of the 1° antibody to any part of the membrane that did not have bound protein. After blocking, the membrane was rinsed with TBS-T for 15 minutes and then incubated overnight at 4 °C with 5 µg of 1° antibody, raised against the protein of interest or those hypothesized to co-localize with the protein of interest, diluted in 10 mL of blocking buffer. Following the first antibody incubation period, the membrane was rinsed again with TBS-T for 15 minutes and incubated for one hour at room temperature with 1 µg of 2° antibody, raised against the 1° antibody, diluted in 10 mL of blocking buffer. Finally, the membrane was rinsed with TBS-T for 10 minutes, followed by a rinse with TBS for 5 more

minutes. After the remaining rinses, the membrane was incubated with DAB substrate for approximately 30 minutes at room temperature while the colorimetric reaction developed.

Results

Results were inconsistent throughout this study. Early results suggested successful activity of the antibodies used in this study, especially using dot blots. However, this may have been due to improper blocking or rinsing, allowing extra primary antibody to remain behind to non-specifically interact with the secondary antibody. Lysing of the cells did provide access to the inside of the cell, as evident by SDS-PAGE results. However, no successful immunoprecipitation has been performed to separate the proteins of interest from all other cellular debris.

Discussion

A member of the Kaverina lab provided some advice, explaining that these proteins in particular are largely inaccessible to exogenous proteins unless antibodies are made specifically with a truncated region of interest. Finding evidence of increased AKAP450 and GM130 interaction in the MDA-MB-231 cell line or in EGF treated cells would support the current hypothesis, using biochemical evidence to implicate Golgi nucleated microtubules in directed cell migration. This interaction is hypothesized to be crucial for microtubule nucleation at the Golgi. Currently, troubleshooting is required to advance the project further in the future.